

Lipschitz Regularized Generative Adversarial Nets

Zhiming Zhou

HEYOHAIZHOU@GMAIL.COM

Department of Computer Science, School of Information Management and Engineering

Shanghai University of Finance and Economics

100 Wudong Road, Yangpu District, Shanghai 200433, China

Zhihua Zhang

ZHZHANG@MATH.PKU.EDU.CN

Department of Probability and Statistics, School of Mathematical Sciences

Peking University

5 Yiheyuan Road, Haidian District, Beijing 100871, China

Abstract

In this paper, we show that Generative Adversarial Networks (GANs) without regularization in the discriminative function space commonly suffer from an issue that the gradients from the discriminator can be uninformative to guide the generator. However, interestingly, we find that Lipschitz regularization in the discriminative function space can generally resolve the gradient uninformativeness issue and guarantee the GANs' convergence. We hence provide a thoroughgoing theoretical and empirical study upon Lipschitz regularization and Lipschitz regularized GANs. We thereby achieve consistently superior performance over WGANs with theoretical justification. And then, to make the understanding of the training instability of GANs more comprehensive, we further provide a systematic study on the gradient issues of traditional GANs and their practical behaviors, with unregularized GANs as their representative, from which we venture a conjecture on the mechanisms of how traditional GANs work in practice and find a fundamental cause of mode collapse, i.e., the locality of their gradient information. Finally, we study the differentiation properties of GANs with the help of envelope theorem and realize that the current GANs is essentially a sample-based framework and the information interchange between the generator and the discriminator must be passed via the gradients of the discriminative function with respect to generated samples, because the discriminator takes a sample as input.

Keywords: Lipschitz regularization, generative adversarial networks, training instability, convergence issue, gradient information

1. Introduction

Generative Adversarial Networks (GANs, Goodfellow et al. 2014), as one of the most promising generative models, has been successfully applied in various related tasks. However, GANs is also well-known for its difficulties in training (Goodfellow, 2016). The common issues include training instability, mode collapse, low sample quality, etc. The underlying obstacles, though have been heavily studied (Arjovsky and Bottou, 2017; Mescheder et al., 2017, 2018; Metz et al., 2017; Unterthiner et al., 2018), are still not fully understood.

The objective of GANs is usually defined as a distance metric between the target (real) distribution \mathcal{P}_t and the generation (fake) distribution \mathcal{P}_g formed by generated samples,

which implies that $\mathcal{P}_g = \mathcal{P}_t$ is the unique global optimum. The training instability issue of traditional GANs has been considered stems from the illness of the distance metric (Arjovsky and Bottou, 2017), e.g., the distance between \mathcal{P}_g and \mathcal{P}_t keeps constant when their supports are disjoint. Arjovsky et al. (2017) accordingly suggested using the Wasserstein distance as a preferable distance metric, which can properly measure the distance between two distributions no matter whether their supports are disjoint.

In this paper, we propose to study the training instability of GANs from the perspective of the optimal discriminative function f^* . By inspecting f^* and its gradient with respect to generated samples, the understanding of GANs's training can be much more clear. The reason is that we now take the G-D structure of GANs into account, i.e., the generator and discriminator structure, and we are inspecting the samples, i.e., x instead of the densities $\mathcal{P}_g(x)$, and the gradients that the generator receives from the discriminator with respect to the samples to be updated, i.e., $\nabla_x f^*(x)$. That is inspecting the connecting point of the generator and the discriminator. In this sense, GANs works as follows. G models the samples to be updated and updates them accordingly, while D, whose behavior is theoretically defined by f^* and practically affected by the training details, tells the generator how these samples should be updated via its gradient with respect to these samples.

We demonstrate that the theoretical convergence of GANs heavily depends on the regularization in the discriminative function space, i.e., whether there is a regularization in the discriminator and what regularization it is. We find that if there is no regularization in the discriminative function space, the GANs generally does not guarantee its convergence and provably suffers from a gradient uninformativeness issue, which means in many cases that have been proved to commonly exist, the gradient that the generator receives from the optimal discriminator does not tell any information of the target distribution. We also find that this gradient uninformativeness issue is nontrivial, not any single simple regularization in the discriminative function space can resolve it.

However, interestingly, we find that Lipschitz regularization can generally resolve the gradient uninformativeness issue and guarantee the GANs' convergence. We provide a sufficient condition for the construction of these GANs, which we believe is very close to the necessary condition for GANs whose discriminator takes a single sample as input. The condition turns out to cover most popular choices of GANs objective and hence explain how Lipschitz regularization works when combined with these GANs.

We provide detailed analysis upon why Lipschitz regularization can generally resolve the gradient uninformativeness issue and show that Lipschitz regularization makes the gradients of the optimal discriminative function with respect to generated samples point directly towards real samples, i.e., samples in target distributions. We demonstrate the existence and uniqueness of the optimal discriminative function for GANs under Lipschitz regularization, and prove that there is only a single Nash equilibrium between the generator and the optimal discriminative function, and show that otherwise, the GANs will always move samples from locations where there is too much to locations where there is too less.

The above leads to the Lipschitz regularized GANs, a GANs family, shortened as LGANs. In trying to attain the optimal discriminative function, with which we can then verify its theoretical properties, we find various underlying issues in the current implementations of

Lipschitz regularization. We hence provide a serious study on the implementation of Lipschitz regularization, and thereby propose two revised versions with theoretical justification. We then construct several instances of this LGANs family, and empirically verify their theoretical properties, and then show their consistently superior performance over WGANs.

Then, to gain a deeper understanding of the training instability and convergence issue of GANs, we feel it is required to understand how the traditional GANs, especially these unregularized ones, work in practice. We hence provide a systematic study on the gradient issues of these GANs and investigate how they behave in practice, with which we venture a conjecture on how these theoretically not guaranteed GANs work in practice.

In a nutshell, tuning supplies the lack of theory, and common practices (or tricks) lead to simple and smooth discriminative function or avoid the fatal optimal discriminative function, which favors the training and make the training more likely to success, but still being unstable, sensitive to hyper-parameters and network architecture, and hard to use. Besides, we find a fundamental cause of mode collapse, i.e., the locality of their gradients.

Finally, we study the gradient flow between the generator and discriminator in various GANs with the help of the envelope theorem, a classic result on the differentiation properties of an optimization problem, to see what is the indispensable element for convergence guarantee.

With the study of unregularized GANs and the propose compact dual form of Wasserstein distance under the envelope theorem, we realize that the current GANs is essentially a sample-based framework and the information interchange between the generator and discriminator must flow via the gradients of the discriminative function with respect to generated samples.

And given the previous analysis of the issues of traditional GANs and the effect of Lipschitz regularization in GANs, we believe that f -divergence or these distance metrics induced by unregularized GANs are not favorable distance metrics for GANs, given its sample-based nature, and optimal transport based distance metrics or these distance metrics induced by Lipschitz regularization are more compatible with the current GANs framework.

The remainder of this paper is organized as follows. In Section 2, we provide some preliminaries that will be used in this paper. In Section 3, we study the gradient uninformativeness issue in detail. In Section 4, we present the Lipschitz regularized GANs and their theoretical properties. In Section 5, we study the implementation of Lipschitz regularization. In Section 6, we provide the empirical analysis of the Lipschitz regularized GANs. In Section 7, we study the gradient issues of traditional GANs and how they work in practice. In Section 8, we study the essence of convergence of GANs via the lens of envelope theorem. Finally, we discuss related work in Section 9 and conclude the paper in Section 10.

2. Preliminaries

In this section, we first introduce some notions that will be used in this paper including Lipschitz continuity and Wasserstein distance. And then we present a generalized formulation for GANs whose discriminator has a single input sample, and lastly introduce the key research object of this paper, i.e., the gradients that the generator receives from the discriminator with respect to generated samples.

2.1 Lipschitz Continuity and Lipschitz Constant

Given two metric spaces (X, d_X) and (Y, d_Y) , a function $f: X \rightarrow Y$ is said to be (k -)Lipschitz continuous, if there exists a constant $k \geq 0$ such that

$$d_Y(f(x_1), f(x_2)) \leq k \cdot d_X(x_1, x_2), \forall x_1, x_2 \in X. \quad (1)$$

In this paper and most existing GANs papers, like WGANs (Arjovsky et al., 2017), the metrics d_X and d_Y are by default Euclidean distance or norm¹, which we denote by $\|\cdot\|$.

The smallest constant k is called the Lipschitz constant of f , which we denote by $k(f)$.

2.2 Wasserstein Distance and its Dual Forms, and an Important Proposition

The first-order Wasserstein distance W_1 between two probability distributions is defined as

$$W_1(\mathcal{P}_g, \mathcal{P}_t) = \inf_{\pi \in \Pi(\mathcal{P}_g, \mathcal{P}_t)} \mathbb{E}_{(x,y) \sim \pi} [d(x, y)], \quad (2)$$

where $\Pi(\mathcal{P}_g, \mathcal{P}_t)$ denotes the set of all probability measures with marginals \mathcal{P}_g and \mathcal{P}_t . It can be interpreted as the minimum cost of transporting the distribution \mathcal{P}_g to the distribution \mathcal{P}_t . We use π^* to denote the optimal transport plan, and let \mathcal{S}_g and \mathcal{S}_t denote the supports of \mathcal{P}_g and \mathcal{P}_t , respectively.

The Kantorovich-Rubinstein (KR) duality (Villani, 2008) provides a way of more efficient computing of Wasserstein distance. The duality states that

$$\begin{aligned} W_1(\mathcal{P}_g, \mathcal{P}_t) &= \sup_f \mathbb{E}_{x \sim \mathcal{P}_g} [f(x)] - \mathbb{E}_{x \sim \mathcal{P}_t} [f(x)], \\ &\text{s.t. } f(x) - f(y) \leq d(x, y), \forall x, \forall y. \end{aligned} \quad (3)$$

The constraint in Eq. (3) implies that f is Lipschitz continuous with $k(f) \leq 1$.

Interestingly, we find a more compact dual form of the Wasserstein distance. That is,

$$\begin{aligned} W_1(\mathcal{P}_g, \mathcal{P}_t) &= \sup_f \mathbb{E}_{x \sim \mathcal{P}_g} [f(x)] - \mathbb{E}_{x \sim \mathcal{P}_t} [f(x)], \\ &\text{s.t. } f(x) - f(y) \leq d(x, y), \forall x \in \mathcal{S}_g, \forall y \in \mathcal{S}_t. \end{aligned} \quad (4)$$

This new dual form relaxes the Lipschitz continuity condition from over the entire space to respectively over their supports. The proof for this dual form is given in Appendix A.1.

As shown by WGANs-GP (Gulrajani et al., 2017), the gradient of the optimal discriminative function in the KR dual form of the Wasserstein distance has the following property:

Proposition 1 *Let π^* be the optimal transport plan in Eq. (2) and $x_t = tx + (1-t)y$ with $0 \leq t \leq 1$. If the optimal discriminative function f^* in Eq. (3) is differentiable and $\pi^*(x, x) = 0$ for all x , then it holds that*

$$\mathbb{P}_{(x,y) \sim \pi^*} [\nabla_{x_t} f^*(x_t) = \frac{y-x}{\|y-x\|}] = 1. \quad (5)$$

1. When switching to other norms, the property of the gradients will get changed. Different norms will induce different gradients with different properties. See Appendix A.5 for some basic arguments on this.

| | ϕ | φ | \mathcal{F} | $f^*(x)$ |
|----------------------------|--|--------------------|---|--|
| Original GANs | $-\log(\sigma(-x))$ | $-\log(\sigma(x))$ | Free | $\log \frac{\mathcal{P}_t(x)}{\mathcal{P}_g(x)}$ |
| Least-Squares GANs | $(x - \alpha)^2$ | $(x - \beta)^2$ | Free | $\frac{\alpha \cdot \mathcal{P}_g(x) + \beta \cdot \mathcal{P}_t(x)}{\mathcal{P}_t(x) + \mathcal{P}_g(x)}$ |
| μ -Fisher GANs | x | $-x$ | $\mathbb{E}_{x \sim \mu} f(x) ^2 \leq 1$ | $\frac{\mathcal{P}_t(x) - \mathcal{P}_g(x)}{\mathcal{F}_\mu(\mathcal{P}_t, \mathcal{P}_g) \cdot \mu(x)}$ |
| Wasserstein GANs | x | $-x$ | $k(f) \leq 1$ | N/A |
| Lipschitz Regularized GANs | any ϕ and φ satisfying Eq. (12) | | $k(f)$ regularized | N/A |

Table 1: The comparison of different objectives of GANs.

This proposition indicates: (i) for each generated sample x , there exists a real sample y such that $\nabla_{x_t} f^*(x_t) = \frac{y-x}{\|y-x\|}$ for all linear interpolations x_t between x and y , which also means the gradient at any interpolation x_t is pointing towards the real sample y ; (ii) these (x, y) pairs match the optimal coupling π^* , i.e., the direction of $\nabla_{x_t} f^*(x_t)$ indicates the optimal transport; (iii) it also implies that WGANs does not suffer from the gradient vanishing.

2.3 Generalized Formulation of Generative Adversarial Nets

Typically, GANs, whose discriminator has a single input sample, can be formulated as

$$\begin{aligned} \min_{f \in \mathcal{F}} J_D &= \mathbb{E}_{z \sim \mathcal{P}_z} [\phi(f(g(z)))] + \mathbb{E}_{x \sim \mathcal{P}_t} [\varphi(f(x))], \\ \min_{g \in \mathcal{G}} J_G &= \mathbb{E}_{z \sim \mathcal{P}_z} [\psi(f(g(z)))] \end{aligned} \quad (6)$$

where \mathcal{P}_z is the source distribution of the generator in \mathbb{R}^m and \mathcal{P}_t is the target (real) distribution in \mathbb{R}^n . The generative function $g: \mathbb{R}^m \rightarrow \mathbb{R}^n$ learns to output samples that share the same dimension as samples in \mathcal{P}_t , while the discriminative function $f: \mathbb{R}^n \rightarrow \mathbb{R}$ learns to output a score indicating the authenticity of a given sample. \mathcal{F} and \mathcal{G} denote the discriminative and generative function spaces, respectively. $\phi, \varphi, \psi: \mathbb{R} \rightarrow \mathbb{R}$ are the loss metrics². We denote the implicit distribution of the generated samples by \mathcal{P}_g . We use f^* to denote the optimal discriminative function, i.e., $f^* = \arg \min_{f \in \mathcal{F}} J_D$.

We list the choices of ϕ, φ and \mathcal{F} of some representative GANs in Table 1. Without loss of generality, the basic common pattern of these GANs is that the discriminator forces $f(x)$ to be small for generated samples, while forces $f(x)$ to be large for real samples. Different choices of ϕ, φ , and \mathcal{F} , if valid, lead to different distance metrics and hence, in a sense, different GANs. Typically, ψ is chosen to be the negative of ϕ , forming a minimax formulation. We introduce a free ψ to make the framework more general.

For subsequent needs, we let

$$\begin{aligned} \mathring{J}_D(x) &= \mathcal{P}_g(x)\phi(f(x)) + \mathcal{P}_t(x)\varphi(f(x)), \\ \mathring{J}_G(x) &= \psi(f(x)). \end{aligned} \quad (7)$$

It has $J_D = \int \mathring{J}_D(x) dx$ and $J_G = \int \mathcal{P}_g(x) \mathring{J}_G(x) dx$.

2. By *loss metric*, we refer to the function ϕ, φ, ψ , or their combination. And when referring to the entire J_D or J_G or the one with the regularizations in \mathcal{F} or \mathcal{G} , we will use the word *objective*.

2.4 The Gradient that the Generator Receives and Gradient Vanish

In these GANs, the gradient that the generator receives from the discriminator with respect to a generated sample $x \in \mathcal{S}_g$ is

$$\nabla_x \hat{J}_G(x) = \nabla_x \psi(f(x)) = \nabla_{f(x)} \psi(f(x)) \cdot \nabla_x f(x), \quad (8)$$

where the first term $\nabla_{f(x)} \psi(f(x))$ is a scalar, and the second term $\nabla_x f(x)$ is a vector with the same dimension as x , which indicates the direction that the generator should follow for optimizing the generated sample x .

The gradient vanishing issue has been considered as a key phenomenon that indicates the existence of training issues in GANs. For original GANs, when the discriminator is trained to optimum, $\nabla_{f(x)} \psi(f(x))$ tends to become zero. Goodfellow et al. (2014) addressed this issue by using an alternative loss metric for the generator. Actually, only the scalar $\nabla_{f(x)} \psi(f(x))$ is changed. The Least-Squares GANs (Mao et al., 2017), which aims at addressing the gradient vanishing issue, also focused on $\nabla_{f(x)} \psi(f(x))$. And we can actually show that Least-Squares GANs may still suffer from gradient vanishing, due to the zeroness of $\nabla_x f(x)$.

Arjovsky and Bottou (2017) provided a new perspective for understanding the gradient vanishing. They argued that \mathcal{S}_g and \mathcal{S}_t are usually disjoint and the gradient vanishing stems from the illness of traditional distance metrics, i.e., the distance between \mathcal{P}_g and \mathcal{P}_t remains constant when they are disjoint. The Wasserstein distance was thus proposed by Arjovsky et al. (2017) as an alternative distance metric, which can properly measure the distance between two distributions no matter whether their supports are disjoint or not.

3. The Gradient Uninformativeness

In this paper, we will pay our main attention to the gradient direction, which turns out is more interesting and more important than the gradient scale. We will consider the optimal discriminative function $f^*(x)$ and its gradient $\nabla_x f^*(x)$. $\nabla_x f^*(x)$ means along which the generator will be told by the well-optimized discriminator to update the generated sample x .

We show that for many distance metrics and hence many GANs, such a gradient may fail to bring any useful information about \mathcal{P}_t . Consequently, \mathcal{P}_g is not guaranteed to converge to \mathcal{P}_t . We name this phenomenon as the *gradient uninformativeness* and argue that it is a fundamental cause of nonconvergence and instability in the training of traditional GANs³.

The gradient uninformativeness is substantially different from the gradient vanishing. The gradient vanishing is about the scalar term $\nabla_{f(x)} \psi(f(x))$ or the overall scale of $\nabla_x \hat{J}_G(x)$, while the gradient uninformativeness is about the direction of $\nabla_x \hat{J}_G(x)$, which is entirely defined by $\nabla_x f^*(x)$. The two issues are orthogonal, though they sometimes exist simultaneously.

Next, we discuss the gradient uninformativeness in the taxonomy of the regularization in the discriminative function space \mathcal{F} . We will show that: (i) for unregularized GANs, gradient uninformativeness commonly exists; (ii) for GANs with regularization, such an issue may still exist; (iii) with Lipschitz regularization, the issue generally does not exist.

3. By traditional GANs, we refer to original GANs, Least-Squares GANs and so on. We will later give a precise definition of traditional GANs in Section 7, where we study how these GANs work in practice.

3.1 Unregularized GANs: Gradient Uninformativeness Commonly Exists

For many GANs, there is no regularization in the discriminative function space \mathcal{F} . Typical instances include f -divergence based GANs, such as the original GANs (Goodfellow et al., 2014), Least-Squares GANs (Mao et al., 2017).

In these GANs, the value of the optimal discriminative function at each point, i.e., $f^*(x)$, is independent of other points and only reflects the local densities $\mathcal{P}_g(x)$ and $\mathcal{P}_t(x)$:

$$f^*(x) = \arg \min_{f(x) \in \mathbb{R}} \mathcal{P}_g(x)\phi(f(x)) + \mathcal{P}_t(x)\varphi(f(x)), \quad \forall x. \quad (9)$$

Given that $f^*(x)$ only reflects the local densities $\mathcal{P}_g(x)$ and $\mathcal{P}_t(x)$, for each generated sample x , which is not surrounded by real samples (there exists $\epsilon > 0$ such that for all y with $0 < \|y - x\| < \epsilon$, it holds that $y \notin \mathcal{S}_t$), $f^*(x)$ in the surroundings of x would contain no information about \mathcal{P}_t .

Thus, $\nabla_x f^*(x)$, the gradient that the generator receives from the optimal discriminative function for updating this sample, does not reflect any information about \mathcal{P}_t . Hence, there is no guarantee upon whether the generator can update the sample towards getting closer to the target distribution, nor the overall convergence.

Typical situation is that \mathcal{S}_g and \mathcal{S}_t are disjoint, which is common in practice according to Arjovsky and Bottou (2017). That is, gradient uninformativeness commonly exists in unregularized GANs.

To further distinguish the gradient uninformativeness from the gradient vanishing, we consider an ideal case: \mathcal{S}_g and \mathcal{S}_t are totally overlapped and both consist of n discrete points, but their probability masses over these points are different. Check Eq. (9) in this case and you will find that $\nabla_x f^*(x)$ for each generated sample is still uninformative, because there is no real sample around. But the gradient does not vanish and is actually being undefined⁴.

3.2 Regularized GANs: Gradient Uninformativeness May Still Exist

There also exists some GANs that impose regularization in the discriminative function space \mathcal{F} . Typical instances are the Integral Probability Metric (IPM) based GANs (Mroueh and Sercu, 2017; Mroueh et al., 2018; Bellemare et al., 2017) and the Wasserstein GANs (Arjovsky et al., 2017). We next show that GANs with regularization in the discriminative function space might also suffer from the gradient uninformativeness.

The optimal discriminative function of μ -Fisher IPM $\mathcal{F}_\mu(\mathcal{P}_g, \mathcal{P}_t)$, i.e., $f^*(x)$ of the generalized objective of the Fisher GANs (Mroueh et al., 2018), has the following form:

$$f^*(x) = \frac{1}{\mathcal{F}_\mu(\mathcal{P}_g, \mathcal{P}_t)} \frac{\mathcal{P}_g(x) - \mathcal{P}_t(x)}{\mu(x)}, \quad (10)$$

where μ is a distribution whose support covers \mathcal{S}_g and \mathcal{S}_t . $\frac{1}{\mathcal{F}_\mu(\mathcal{P}_g, \mathcal{P}_t)}$ is a constant. It can be observed that μ -Fisher IPM also defines $f^*(x)$ at each point according to the local densities and does not reflect information of other locations. Similar as above, we can conclude that for each generated sample that is not surrounded by real samples, $\nabla_x f^*(x)$ is uninformative.

4. See Section 7 and Section 8 for a deeper understanding of this issue

4. Lipschitz Regularized GANs

Lipschitz continuity regularization has recently become popular in GANs. It was observed that introducing Lipschitz continuity as a regularization in the discriminator leads to improved stability and sample quality (Arjovsky et al., 2017; Gulrajani et al., 2017; Fedus et al., 2018; Miyato et al., 2018; Karras et al., 2018; Zhang et al., 2019).

In this section, we investigate the generalized formulation of GANs with Lipschitz continuity regularization, where the Lipschitz constant of the discriminative function is penalized via a quadratic loss, to theoretically analyze the properties of such GANs.

In particular, we define the Lipschitz regularized Generative Adversarial Nets (LGANs) as:

$$\begin{aligned} & \min_{f \in \mathcal{F}} \mathbb{E}_{z \sim \mathcal{P}_z} [\phi(f(g(z)))] + \mathbb{E}_{x \sim \mathcal{P}_t} [\varphi(f(x))] + \frac{\rho}{2} \cdot k(f)^2, \\ & \min_{g \in \mathcal{G}} \mathbb{E}_{z \sim \mathcal{P}_z} [\psi(f(g(z)))]. \end{aligned} \quad (11)$$

We will show that, if $\rho > 0$ and once the following condition holds, the above defined LGANs can generally resolve the gradient uninformativeness issue and guarantee the convergence.

$$\begin{cases} \phi'(x) > 0, \phi''(x) \geq 0, \\ \varphi'(x) < 0, \varphi''(x) \geq 0, \\ \exists a, \phi'(a) + \varphi'(a) = 0. \end{cases} \quad (12)$$

This condition for the loss metrics ϕ and φ is a sufficient condition for desired properties, and it is actually very mild and should be very close to the necessary condition.

Requiring ϕ to be increasing means that the discriminator will need to force small $f(x)$ for generated samples. Requiring φ to be decreasing, meaning that the discriminator will need to force large $f(x)$ for real samples. The other constraints are included because, otherwise, this problem is not guaranteed to have a solution.

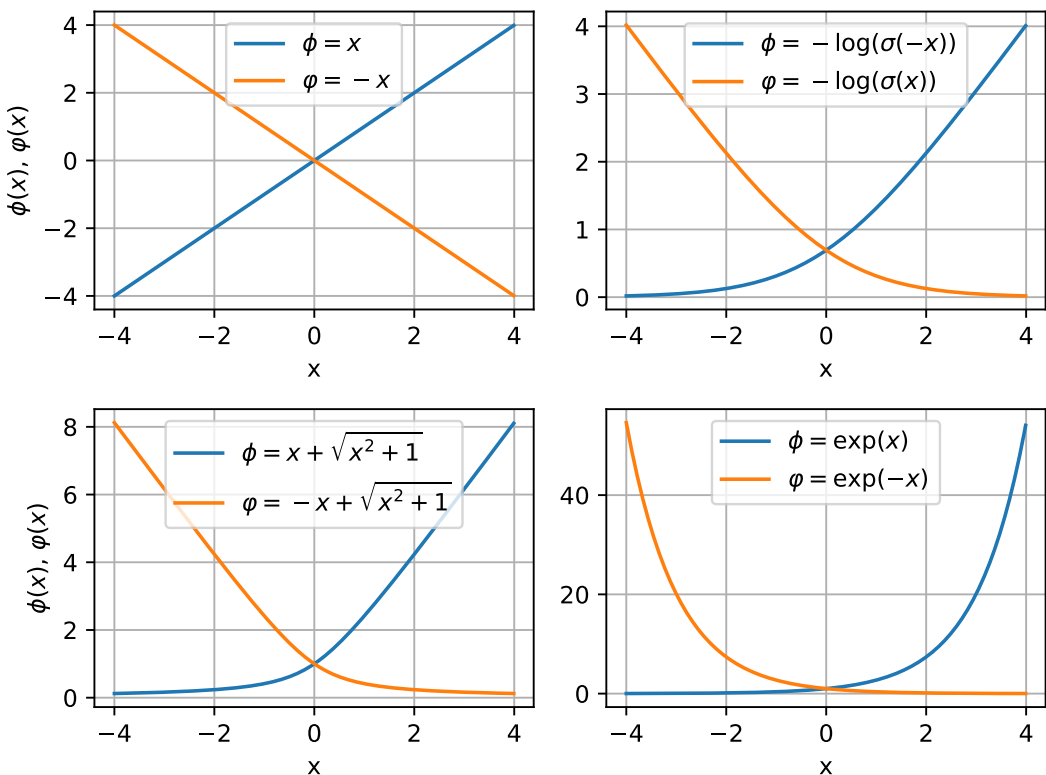
To devise a loss in LGANs, it is practical to let ϕ be an increasing function with non-decreasing derivatives, and then simply set $\phi(x) = \varphi(-x)$ would be sufficient.

Note that in WGANs, the loss metric $\phi(x) = \varphi(-x) = x$ is used, which satisfies Eq. (12). There are many other instances satisfy Eq. (12), such as $\phi(x) = \varphi(-x) = -\log(\sigma(-x))$, $\phi(x) = \varphi(-x) = x + \sqrt{x^2 + 1}$ and $\phi(x) = \varphi(-x) = \exp(x)$.

Note that rescaling and offsetting along the axes are trivial operation to found more ϕ and φ within a function class, and linear combination of two or more ϕ or φ from different function classes also keep satisfying Eq. (12). We illustrate some of these loss metrics in Figure 1.

Meanwhile, there also exists loss metrics used in GANs that do not satisfy Eq. (12), e.g., the quadratic loss (Mao et al., 2017) and the hinge loss (Zhao et al., 2017; Lim and Ye, 2017; Miyato et al., 2018). Nevertheless, we will study them in experiments (See Section 6).

Note that $\phi(x) = \varphi(-x) = -\log(\sigma(-x))$ corresponds to the loss metric of original GANs. As we have shown, the original GANs suffers from the gradient uninformativeness issue. However, as we will show next, when imposing the Lipschitz regularization, the resulting model as a specific instance of LGANs, behaves very well.

Figure 1: Various ϕ and φ that satisfies Eq. (12).

4.1 Theoretical Analysis of Lipschitz Regularized GANs

We now present the theoretical analysis of LGANs. The intention of the analysis is two folds. The first is to verify that the formulation is a valid one. The second is to understand how the gradient uninformativeness issue is resolved. All proofs are deferred to Appendix A.

For the first fold, we will demonstrate the existence and uniqueness of the optimal discriminative function for GANs under Lipschitz regularization. And then we will prove that there is only a single Nash equilibrium between the generator and the optimal discriminative function, and show that, otherwise, the GANs will always move samples from locations where has too much to locations where has too less.

For the second fold, we will, all along the way, provide detailed analysis upon why Lipschitz regularization can generally resolve the gradient uninformativeness issue, and at last show that Lipschitz regularization makes the gradients of the optimal discriminative function with respect to generated samples point directly towards real samples, i.e., samples in target distributions, hence, in a sense, being extremely informative.

4.1.1 EXISTENCE AND UNIQUENESS OF THE OPTIMAL DISCRIMINATIVE FUNCTION

First, we consider the existence and uniqueness of the optimal discriminative function.

Theorem 2 *Under Assumption (12), the optimal discriminative function f^* of Eq. (11) exists. And, if ϕ or φ is strictly convex, it is unique.*

Note that LGANs with the WGANs loss metric, i.e., $\phi(x) = \varphi(-x) = x$ which does not satisfy the condition that ϕ or φ is strictly convex, the solution of Eq. (11), i.e., the optimal discriminative function f^* , still exists but is not unique. Specifically, if f^* is an optimal solution, then $f^* + \alpha$ for any $\alpha \in \mathbb{R}$ is also an optimal solution. And this is actually the only special case. For all other instances that satisfy the condition, ϕ or φ is strictly convex.

4.1.2 UNIQUE NASH EQUILIBRIUM AND THE EXISTENCE OF BOUNDING RELATIONSHIPS

The following theorems can be regarded as a generalization of Proposition 1 of WGANs-GP to LGANs, with more detailed analysis of bounding relationships and equilibrium.

Theorem 3 *Under Assumption (12), we have the optimal discriminative function f^* exists. If we further assume f^* is smooth, we have:*

- (a) *For all $x \in \mathcal{S}_g \cup \mathcal{S}_t$, if it holds that $\nabla_{f^*(x)} \hat{J}_D(x) \neq 0$, then there exists $y \in \mathcal{S}_g \cup \mathcal{S}_t$ with $y \neq x$ such that $|f^*(y) - f^*(x)| = k(f^*) \cdot \|y - x\|$;*
- (b) *For all $x \in \mathcal{S}_g \cup \mathcal{S}_t - \mathcal{S}_g \cap \mathcal{S}_t$, there exists $y \in \mathcal{S}_g \cup \mathcal{S}_t$ with $y \neq x$ such that $|f^*(y) - f^*(x)| = k(f^*) \cdot \|y - x\|$;*
- (c) *If $\mathcal{S}_g = \mathcal{S}_t$ and $\mathcal{P}_g \neq \mathcal{P}_t$, then there exists (x, y) pair in $\mathcal{S}_g \cup \mathcal{S}_t$ with $y \neq x$ such that $|f^*(y) - f^*(x)| = k(f^*) \cdot \|y - x\|$ and $\nabla_{f^*(x)} \hat{J}_D(x) \neq 0$;*
- (d) *There is a unique Nash equilibrium between \mathcal{P}_g and f^* , where $\mathcal{P}_g = \mathcal{P}_t$ and $k(f^*) = 0$.*

This theorem states the basic properties of LGANs, including: (i) the existence of unique Nash equilibrium, where $\mathcal{P}_g = \mathcal{P}_t$ and $k(f^*) = 0$; (ii) the existence of *bounding relationships* in the optimal discriminative function, i.e., $\exists y \neq x$ such that $|f^*(y) - f^*(x)| = k(f^*) \cdot \|y - x\|$. The former ensures that the objective is a well-defined distance metric, and the latter, as we will show next, eliminates the gradient uninformative issue.

It is worth noticing that the penalizing $k(f)$, instead of simply restricting the maximum of $k(f)$ as in WGANs, is, in fact, necessary for Property-(c) and Property-(d). It is due to the existence of cases where $\nabla_{f^*(x)} \mathring{J}_D(x) = 0$ for some x with $\mathcal{P}_g(x) \neq \mathcal{P}_t(x)$, when the loss metric is not $\phi(x) = \varphi(-x) = x$, i.e., when the loss metric is strictly convex.

Minimizing $k(f)$, in any case, guarantees that the only Nash equilibrium is achieved when $\mathcal{P}_g = \mathcal{P}_t$. With the WGANs loss metric, minimizing $k(f)$ is not necessary. However, if $k(f)$ is not minimized towards zero, $\nabla_x f^*(x)$ is not guaranteed to be zero (Mescheder et al., 2018) at the convergence state $\mathcal{P}_g = \mathcal{P}_t$. This implies that minimizing $k(f)$ also benefits WGANs.

4.1.3 THE REFINED PROPERTIES OF BOUNDING RELATIONSHIP

From Theorem 3, we know, as long as \mathcal{P}_g still has not fully converged to \mathcal{P}_t , there must exist point x with $f^*(x)$ being bounded by another point y , such that $|f^*(y) - f^*(x)| = k(f^*) \cdot \|y - x\|$.

We here further clarify that, when there is a bounding relationship, it must involve both real sample(s) and fake sample(s). And surely, because the discriminator forces high values for real samples and low values for generated samples. In a bounding relationship under fully optimized discriminative function, the values of real samples should always be higher.

More formally, we have:

Theorem 4 *Under the conditions in Theorem 3, we have*

- 1) *For any $x \in \mathcal{S}_g$, if $\nabla_{f^*(x)} \mathring{J}_D(x) > 0$, then there must exist some $y \in \mathcal{S}_t$ with $y \neq x$ such that $f^*(y) - f^*(x) = k(f^*) \cdot \|y - x\|$ and $\nabla_{f^*(y)} \mathring{J}_D(y) < 0$;*
- 2) *For any $y \in \mathcal{S}_t$, if $\nabla_{f^*(y)} \mathring{J}_D(y) < 0$, then there must exist some $x \in \mathcal{S}_g$ with $y \neq x$ such that $f^*(y) - f^*(x) = k(f^*) \cdot \|y - x\|$ and $\nabla_{f^*(x)} \mathring{J}_D(x) > 0$.*

The intuition behind the above theorem is that samples from the same distribution, e.g., the generated samples, will not bound each other to violate the optimality of $\mathring{J}_D(x)$. So, when there is strict bounding relationship, i.e., it involves points that hold $\nabla_{f^*(x)} \mathring{J}_D(x) \neq 0$, it must involve both real and generated samples.

It is worth noticing that, if it is the disjoint case, all fake samples hold $\nabla_{f^*(x)} \mathring{J}_D(x) > 0$, while all real samples hold $\nabla_{f^*(y)} \mathring{J}_D(y) < 0$. And for a generated sample $x \in \mathcal{S}_g$, $\nabla_{f^*(x)} \mathring{J}_D(x) > 0$ means $f^*(x)$ can assign a lower value to x so as to better optimize the objective, if it is not bounded by another sample. See lemmas in the proof for more details.

Note that there might exist a chain of bounding relationships that involves a dozen of fake samples and real samples. It can be shown that these points all lie in the same line in the value surface of f^* , i.e., in the space of $(x, f^*(x))$, and bound each other. The bounding

line in the value surface of f^* is the basic building block that connects \mathcal{P}_g and \mathcal{P}_t , and each generated sample with $\nabla_{f^*(x)} \hat{J}_D(x) \neq 0$ lies in at least one of these bounding lines.

4.1.4 THE IMPLICATION OF BOUNDING RELATIONSHIP

Recall that Proposition 1 states $\nabla_{x_t} f^*(x_t) = \frac{y-x}{\|y-x\|}$. We next show that this is actually a direct consequence of the bounding relationship between x and y , i.e., bounding relationship guarantees meaningful $\nabla_x f^*(x)$ for all involved points, making it point towards real samples.

We formally state it as follows:

Theorem 5 *Assume function f is Lipschitz continuous and differentiable, then for all x and y , which satisfy $y \neq x$ and $f(y) - f(x) = k(f) \cdot \|y-x\|$, we have $\nabla_{x_t} f(x_t) = k(f) \cdot \frac{y-x}{\|y-x\|}$ for all $x_t = tx + (1-t)y$ with $0 \leq t \leq 1$.*

In other words, if two points x and y bound each other in terms of $f(y) - f(x) = k(f) \cdot \|y-x\|$, there is a straight line between x and y in the value surface of f . Any point in this straight line holds the maximum gradient slope $k(f)$, and the gradient direction at any point in this straight line is pointing towards the $x \rightarrow y$ direction.

Note that with a deep inspection of the proof of Proposition 1 in Gulrajani et al. (2017) and Theorem 5, we believe the differentiable requirement of f^* is not critical. It does not hold, only when one sample is bounded by multiple bounding lines, i.e., being bounded in different directions, hence forming multiple sub-gradients and being non-differentiable.

4.1.5 SUMMING UP

Combining Theorems 2, 3, 4 and 5, we can conclude that, as long as $\rho > 0$ and the loss metrics ϕ and φ satisfy the condition Eq. (12) and f^* is smooth and differentiable:

- According to Property-(a), when \mathcal{S}_g and \mathcal{S}_t are disjoint, the gradient of the optimal (or practically well-trained) discriminative function for each generated sample $x \in \mathcal{S}_g$, i.e., $\nabla_x f^*(x)$, points towards some real sample $y \in \mathcal{S}_t$, which guarantees that $\nabla_x f^*(x)$ -based generator update would tend to move \mathcal{P}_g towards \mathcal{P}_t at every step.
- In fact, Theorem 3 provides further guarantee on the convergence. Property-(b) implies that, for any generated sample $x \in \mathcal{S}_g$ that does not lie in \mathcal{S}_t , its gradient under optimal discriminative function, i.e., $\nabla_x f^*(x)$, must point towards some real sample $y \in \mathcal{S}_t$.
- And in the fully overlapped case, according to Property-(c), unless $\mathcal{P}_g = \mathcal{P}_t$, there must exist at least one pair of (x, y) in strict bounding relationship and $\nabla_x f^*(x)$ pulls x towards y , and we can actually also claim that it is moving sample from location where it has too much to where it has too less. See lemmas in the proofs for more details.
- Finally, Property-(d) guarantees that the only Nash equilibrium between the generator and discriminator is reached when $\mathcal{P}_g = \mathcal{P}_t$, and it holds that $k(f) = 0$ and hence $\nabla_x f^*(x) = 0$ for all generated samples, which means the training will fully stop.

As we have already seen, the original GANs suffers from the gradient vanishing and the gradient uninformative ness. However, when imposing the Lipschitz regularization in the discriminative function space, the resulting model, as a special case of LGANs, is theoretically sound. In the experiments, we will see that it even outperforms WGANs empirically. This further shows the power of Lipschitz regularization in discriminative function space.

5. Max Gradient Norm Penalty and Augmented Lagrangian

WGANs (Arjovsky et al., 2017) introduces the requirement for Lipschitz regularization in GANs. After that, researchers (Kodali et al., 2017; Fedus et al., 2018; Miyato et al., 2018) also empirically found that Lipschitz regularization is also useful, when combined with other GANs objectives, e.g., the original GANs objective.

Recently, such phenomenon is also theoretically explained (Farnia and Tse, 2018; Zhou et al., 2019a), i.e., combining Lipschitz regularization with common GANs objectives yields a variant distance metrics that are able to provide continuous measure between the real and fake distributions, being similar to the Wasserstein distance.

As it stands, Lipschitz regularization is a promising technique for improving the training of GANs with theoretical guarantee. However, the implementation of Lipschitz regularization remains challenging.

5.1 Existing Lipschitz Regularization Implementations

Quite a few recent works are devoted to investigating the implementation of Lipschitz regularization. The initial attempt in Arjovsky et al. (2017) achieves the Lipschitz regularization via **weight clipping** (WC), i.e., restricting the maximum value of all parameters (also named weights) in the neural network. However, it was later shown to lead to suboptimal solutions (Gulrajani et al., 2017; Petzka et al., 2018).

And corresponding alternative methods were thus proposed for imposing the Lipschitz regularization, named **gradient penalty** (GP) and **Lipschitz penalty** (LP), respectively. The two methods share the same spirit and achieve Lipschitz continuity via penalizing the sample gradients towards a given target value. The target value is usually 1, however, not necessary (Karras et al., 2018; Adler and Lunz, 2018).

They are based on the fact that the Lipschitz constant of a function is equivalent to its max gradient norm (Adler and Lunz, 2018), i.e., the maximum of the norm of its gradients.

Formally, the two methods introduce the following regularization terms, respectively:

$$L_{gp} = \frac{\rho}{2} \cdot \mathbb{E}_{x \sim \mathcal{P}_{\hat{x}}} [(\|\nabla_x f(x)\| - k_0)^2], \quad (13)$$

$$L_{lp} = \frac{\rho}{2} \cdot \mathbb{E}_{x \sim \mathcal{P}_{\hat{x}}} [(\max\{0, \|\nabla_x f(x)\| - k_0\})^2], \quad (14)$$

where $\mathcal{P}_{\hat{x}}$ denotes the sampling distribution, determined by the sample strategy, which is typically random linear interpolation between the real and fake samples.

Petzka et al. (2018) argued that the gradient penalty is less reasonable, because k_0 -Lipschitz does not necessarily imply that the gradient norm at every sample point is k_0 . It is also the reason why they proposed to only penalize gradients whose norm is larger than k_0 .

Apart from those already mentioned, Miyato et al. (2018) provided a new direction for enforcing the Lipschitz continuity, named **spectral normalization** (SN) (Yoshida and Miyato, 2017), which is based on another fact that the Lipschitz constant of a linear function $h(x) = Wx$ is equivalent to the maximum singular value of the weight matrix.

Given the singular value of a weight matrix is (easily) attainable, they proposed to divide the weight of each linear layer of a neural network by its maximum singular value, i.e.,

$$\bar{W}_{SN} = W/\sigma(W), \quad (15)$$

where $\sigma(W)$ denotes the maximum singular value of W . As a result, the Lipschitz constant of every linear layer is fixed as 1. Then if the nonlinearity parts, i.e., activation functions, are also Lipschitz continuous, which is true for common choices like *ReLU* and *tanh*, the resulting model will have an upper bound on the Lipschitz constant.

It is worth noting that the spectral normalization results in a *hard global* restriction on the Lipschitz constant, while gradient penalty and Lipschitz penalty are *soft local* regularizations.

5.2 Analysis on Lipschitz Regularization Implementations and Motivations

Before moving into the detailed discussion of these methods, we would like to provide several important notes in the first place, e.g., the sufficiency of local Lipschitz continuity.

5.2.1 LOCAL LIPSCHITZ REGULARIZATION IS SUFFICIENT

The most common choice of $\mathcal{P}_{\hat{x}}$ in gradient penalty and Lipschitz penalty is the distribution formed by random linear interpolations between the real and fake samples. Currently, why such a choice is valid is still not clear and people tend to believe that it is only a deleterious practical trick (Miyato et al., 2018).

Here, we provide a theoretical justification for such a choice. We will first demonstrate with the Wasserstein distance and then provide arguments to reasonably extend it to LGANs.

To get such a conclusion, we need to delve more deep into the KR duality Eq. (3) and our newly developed compact dual form Eq. (4). For KR duality, x and y are required to sample from the entire sample space, which is hence equivalent to Lipschitz regularization. However, with the compact dual form, we know that x and y are actually only necessarily required to sample from \mathcal{S}_g and \mathcal{S}_t , respectively.

It is worthy noticing that given the constraints in the compact dual form, any other constraints in the KR duality does not affect the final result of $W_1(\mathcal{P}_g, \mathcal{P}_t)$. And more importantly, any f^* in the compact dual form corresponds to (at least) one f^* in the KR duality with the value of f^* on \mathcal{S}_g and \mathcal{S}_t unchanged. Thus, any f^* in the compact dual form Eq. (4) also holds the following key property of Wasserstein distance (Villani, 2008):

Theorem 6 Let π^* be the optimal transport plan in the primal form of Wasserstein distance Eq. (2) and f^* be the optimal discriminative function in the compact dual form Eq. (4). It holds that

$$P_{(x,y)\sim\pi^*}[f^*(x) - f^*(y) = d(x, y)] = 1. \quad (16)$$

Note that the Proposition 1 is based on Eq. (16) and the 1-Lipschitz continuity of f^* . And we can further notice that f^* being locally Lipschitz continuity is sufficient for the proof.

Formally, we have:

Theorem 7 Let $S_{\hat{x}} = \{\hat{x} = x \cdot t + y \cdot (1-t) \mid x \in \mathcal{S}_g, y \in \mathcal{S}_t, t \in [0, 1]\}$ denotes the support of the linear interpolations between \mathcal{P}_g and \mathcal{P}_t . Enforcing the local Lipschitz regularization over $S_{\hat{x}}$ is sufficient to maintain the property of Proposition 1 for Wasserstein distance.

It means the Wasserstein distance and its desired gradient property for GANs keep unchanged, when you drop constraints outside the blending region $S_{\hat{x}}$. Because the blending region has covered the necessity and very parts.

With our analysis upon how Lipschitz regularization works, we can tell these extra constraints, i.e., these outside $S_{\hat{x}}$, are also unnecessary and are indifferent to the forming of bounding relationships. One can imagine the similar holds for Lipschitz regularized GANs.

Note that Theorem 7 also indicates that, for training GANs, restricting the global Lipschitz constant, e.g., spectral normalization, might be unnecessarily too strong. And henceforward, by Lipschitz constant or Lipschitz continuity, we mostly mean that over the local region $S_{\hat{x}}$.

5.2.2 SUPERFLUOUS CONSTRAINTS IN CURRENT LOCAL LIPSCHITZ IMPLEMENTATIONS

We next show that, although imposing local Lipschitz regularization is sufficient, the current implementations of local Lipschitz regularization, i.e., gradient penalty and Lipschitz penalty, contain superfluous constraints and are hence biased.

Gradient penalty and Lipschitz penalty impose the Lipschitz continuity via penalty method. Penalty method is a soft regularization, where the constraint is usually slightly drifted.

And during the training, a penalty based method would provide a dynamic Lipschitz constant, which is usually much larger than the target Lipschitz constant, depending on the weight of the regularization ρ . Likewise, we use the Wasserstein distance as a demonstration.

Let $W_1(\mathcal{P}_g, \mathcal{P}_t, \tilde{k}) = \sup_{k(f) \leq \tilde{k}} \mathbb{E}_{x \sim \mathcal{P}_g}[f(x)] - \mathbb{E}_{x \sim \mathcal{P}_t}[f(x)]$. It holds that $W_1(\mathcal{P}_g, \mathcal{P}_t, \tilde{k}) = \tilde{k} \cdot W_1(\mathcal{P}_g, \mathcal{P}_t)$. Because $W_1(\mathcal{P}_g, \mathcal{P}_t) = \sup_{k(f) \leq \tilde{k}} \mathbb{E}_{x \sim \mathcal{P}_g}[f(x)/\tilde{k}] - \mathbb{E}_{x \sim \mathcal{P}_t}[f(x)/\tilde{k}]$.

Assume we can directly optimize the Lipschitz constant \tilde{k} and consider the following objective:

$$J_{gp}(\tilde{k}) = -W_1(\mathcal{P}_g, \mathcal{P}_t, \tilde{k}) + \frac{\rho}{2} \cdot (\tilde{k} - k_0)^2. \quad (17)$$

Given that \mathcal{P}_g and \mathcal{P}_t is fixed, $W_1(\mathcal{P}_g, \mathcal{P}_t)$ is a constant and we denote it as α . Then, $J_{gp}(\tilde{k})$ is quadratic function $-\alpha \cdot \tilde{k} + \frac{\rho}{2} \cdot (\tilde{k} - k_0)^2$, whose optimum is reached when $\tilde{k}^* = \frac{\alpha}{\rho} + k_0$.

Note that replacing $(\tilde{k} - k_0)^2$ with $\max\{0, \tilde{k} - k_0\}^2$, i.e., analogizing switching from gradient penalty to Lipschitz penalty, will result in the same optimal \tilde{k}^* .

From the above, we can see that⁵, when ρ is small or the distance between \mathcal{P}_g and \mathcal{P}_t is large (i.e., if α is large), the resulting Lipschitz constant can be much larger than k_0 .

Under these circumstances, both gradient penalty and Lipschitz penalty introduce superfluous constraints. Saying the $k_0 = 1$ and the current Lipschitz constant of f is 100, sampled points, whose gradient is larger than k_0 but smaller than 100, are penalized, inadvertently.

We will see in the experiments that these superfluous constraints alter the optimal discriminative function and damage the property of the gradient received by the generator.

Petzka et al. (2018) noted that Lipschitz penalty has a connection to regularized Wasserstein distance. However, regularized Wasserstein distance also alters the property of the optimal discriminative function and leads to blurry π^* (Seguy et al., 2018). That is, their results are not contradictory to our results.

5.3 The Proposed Lipschitz Regularization Implementations

Now we present our proposed methods towards more efficient (i.e., local instead of global) and unbiased (without superfluous constraints) implementation of Lipschitz regularization.

5.3.1 MAX GRADIENT NORM REGULARIZATION WITH PENALTY METHOD

Given that the local Lipschitz continuity over the support of the linear interpolations between the real and fake distributions, i.e., $S_{\hat{x}}$, is sufficient for all desired properties in GANs, we would consider only restricting the Lipschitz constant in such a region.

Similar to gradient penalty, we can regularize the Lipschitz constant via penalty method. But, to avoid the superfluous constraints, we need to only penalize the max gradient norm in $S_{\hat{x}}$, which is equivalent to the Lipschitz constant in the local region of $S_{\hat{x}}$.

The resulting regularization is as follows:

$$L_{maxgp} = \frac{\rho}{2} (\max_{x \sim \mathcal{P}_{\hat{x}}} \|\nabla_x f(x)\|) - k_0)^2. \quad (18)$$

Analogy to Lipschitz penalty, we can also extend the penalty term with $\max\{0, \cdot\}$. However, when only regularizing the max gradient norm, it is less necessary. Because it will only take effect, when the discriminator is underfitting.

Practically, we can either directly use the max gradient norm in a mini-batch, e.g. follow Gulrajani et al. (2017) and sample x as random linear interpolations of the real and fake samples in parallel mini-batches, or further introduce more accurate estimation of $\max_{x \sim \mathcal{P}_{\hat{x}}} \|\nabla_x f(x)\|$ to improve the stability and reduce the bias introduced via batch sampling.

A practical and lightweight method for a more accurate estimation of $\max_{x \sim \mathcal{P}_{\hat{x}}} \|\nabla_x f(x)\|$ is to maintain a buffer B_{\max} that stores these x that achieve the current historical top-k

5. From another perspective, as α goes to zero, i.e., as \mathcal{P}_g converges to \mathcal{P}_t , the optimal Lipschitz constant \tilde{k}^* decreases. And finally, when $\mathcal{P}_g = \mathcal{P}_t$, we have $\alpha = 0$ and the optimal Lipschitz constant $\tilde{k}^* = k_0$.

$\|\nabla_x f(x)\|$, which can be initialized with random samples. During training, use the samples buffered in B_{\max} as part of the batch (or as additional) that estimates the current max gradient norm, and update the B_{\max} after each batch updating of the discriminator.

We have studied these two in experiments. According to our experiments, the historical buffer is usually unnecessary and directly using the max gradient norm in a mini-batch seems good enough, though we do not exclude the possible benefits of historical buffer or other more accurate estimations of max gradient norm or Lipschitz constant.

We suspect that, when the training goes smoothly, the surface of f is also smooth in the sense that the Lipschitz constant in different regions are similar. Hence, a mini-batch estimation could be accurate enough for successful training.

5.3.2 MAX GRADIENT NORM REGULARIZATION WITH AUGMENTED LAGRANGIAN

With the penalty method, the constraint usually cannot be strictly satisfied. The resulting Lipschitz constant, as discussed around Eq. (17), is usually floating / drifted.

In the circumstances of GANs, strictly imposing a given Lipschitz constant might benefit the control of variables in contrast experiments, e.g., when comparing different networks and objectives. Because Lipschitz constant may have a huge impact on the performance.

Also, if one would like to strictly evaluate the Wasserstein distance, a strict restriction of the Lipschitz constant being one would be favorable. Otherwise, it needs to estimate the Lipschitz constant and divide the loss by the estimated Lipschitz constant.

In the situation, where people would like the constraint to be strictly imposed, the augmented Lagrangian is a classic alternative to the penalty method for strict constraint satisfaction. It extends the penalty method by including an extra Lagrange multiplier term.

The regularization term(s) derived from the augmented Lagrangian can be written as follows:

$$L_{maxal} = \lambda_{al} \cdot (\max_{x \sim \mathcal{P}_{\hat{x}}} \|\nabla_x f(x)\| - k_0) + \frac{\rho}{2} \cdot (\max_{x \sim \mathcal{P}_{\hat{x}}} \|\nabla_x f(x)\| - k_0)^2, \quad (19)$$

where λ_{al} is the Lagrange multiplier.

Given that the augmented Lagrangian is a simple extension, and there exists potential benefits, we also investigate the practical performance of augmented Lagrangian in imposing Lipschitz continuity regularization.

5.3.3 FIRST ORDER OPTIMALITY ANALYSIS: PART I, MAXAL PROPERTIES

Some interesting properties of the augmented Lagrangian can be easily derived with its first order optimality analysis. For clarity, we denote $\max_{x \sim \mathcal{P}_{\hat{x}}} \|\nabla_x f(x)\|$ as \tilde{k} . Still, we use the Wasserstein distance for simplicity and demonstration. Let the overall objective be:

$$J_{al}(\tilde{k}) = -W_1(\mathcal{P}_g, \mathcal{P}_t, \tilde{k}) + \lambda_{al} \cdot (\tilde{k} - k_0) + \frac{\rho}{2} \cdot (\tilde{k} - k_0)^2. \quad (20)$$

Similar as previous, because $W_1(\mathcal{P}_g, \mathcal{P}_t, \tilde{k}) = \tilde{k} \cdot W_1(\mathcal{P}_g, \mathcal{P}_t)$ and $W_1(\mathcal{P}_g, \mathcal{P}_t)$ is a constant, we denote $W_1(\mathcal{P}_g, \mathcal{P}_t, \tilde{k})$ as $\alpha \cdot \tilde{k}$. Then, what is optimizing is

$$J_{al}(\tilde{k}) = -\alpha \cdot \tilde{k} + \lambda_{al} \cdot (\tilde{k} - k_0) + \frac{\rho}{2} \cdot (\tilde{k} - k_0)^2. \quad (21)$$

Then, the first order optimality conditions can be written down as follows:

$$\begin{aligned} \frac{\partial J_{al}}{\partial \lambda_{al}} &= \tilde{k} - k_0 = 0, \\ \frac{\partial J_{al}}{\partial \tilde{k}} &= -\alpha + \lambda_{al} + \rho \cdot (\tilde{k} - k_0) = 0. \end{aligned} \quad (22)$$

Thereby, when the augmented Lagrangian converges, $\tilde{k} = k_0$ and $\lambda_{al} = W_1(\mathcal{P}_g, \mathcal{P}_t)$.

Classic results of augmented Lagrangian also involve the choice of ρ , which is out of the scope of the discussion of this paper and hence is not included.

5.3.4 FIRST ORDER OPTIMALITY ANALYSIS: PART II, HOW TO OPTIMIZE MAXAL

Although the following is the traditional result in optimization, we present it here for ease of reference and explain the suggested optimization schema for MaxAL.

To move on, we need to introduce the Lagrange multiplier method and its first order optimality analysis.

The Lagrange multiplier method is also a classical method for constrained optimization. It introduces a Lagrange multiplier into the original optimization problem, i.e.,

$$L_{maxlm} = \lambda_{lm} \cdot (\max_{x \sim \mathcal{P}_{\hat{x}}} \|\nabla_x f(x)\| - k_0), \quad (23)$$

where λ_{lm} is the Lagrange multiplier.

The so-called augmented Lagrangian can also be viewed as an extension of the Lagrange multiplier method, where the quadratic penalty term is regarded as the augmentation.

Considering the optimization problem of

$$J_{lm}(\tilde{k}) = -W_1(\mathcal{P}_g, \mathcal{P}_t, \tilde{k}) + \lambda_{lm} \cdot (\tilde{k} - k_0). \quad (24)$$

The first order optimality condition of the Lagrangian method can be written down as:

$$\begin{aligned} \frac{\partial J_{lm}}{\partial \lambda_{lm}} &= \tilde{k} - k_0 = 0, \\ \frac{\partial J_{lm}}{\partial \tilde{k}} &= -\alpha + \lambda_{lm} = 0. \end{aligned} \quad (25)$$

That is, when the Lagrangian converges, it also holds $\tilde{k} = k_0$ and $\lambda_{lm} = W_1(\mathcal{P}_g, \mathcal{P}_t)$.

The superiority of the augmented Lagrangian over the Lagrangian method can be understood as: with the driven force of the penalty term, it is much easier for the augmented Lagrangian to reach the first order optimality.

Based on the first order optimality conditions of the Lagrange multiplier method and the augmented Lagrangian, we can see that α , which is fixed and being the real target, is equal to $\lambda_{al} + \rho \cdot (\tilde{k} - k_0)$ in augmented Lagrangian. However, in the true, the unregularized, the original objective, λ_{lm} should be equal to α , which means the following should hold:

$$\lambda_{lm} = \lambda_{al} + \rho \cdot (\tilde{k} - k_0). \quad (26)$$

Plus that the augmented Lagrangian can be understood as the Lagrangian method with extra penalty term, which means λ_{al} shall play the role of λ_{lm} . Hence, the common suggestion for the update of λ_{al} in the augmented Lagrangian is using the following update rule:

$$\lambda_{al}^{t+1} = \lambda_{al}^t + \rho \cdot (\tilde{k} - k_0), \quad (27)$$

where t indicates the iteration or timestamp.

Thus, to upgrade from the penalty method to the augmented Lagrangian, one need only introduce the Lagrangian multiplier L_{lm} and add an extra update step for λ_{al} according to Eq. (27) after each iteration of the discriminator.

5.4 Empirical Analysis of Lipschitz Regularization Implementations

In this section, we empirically study the proposed Lipschitz regularization implementations, showing its superiority over existing variants.

We will study the practical behaviors of various implementations of Lipschitz continuity regularization, including spectral normalization (SN), gradient penalty (GP), max gradient norm regularization with penalty method (or simply termed as max gradient norm penalty) (MaxGP), and max gradient norm regularization with augmented Lagrangian (MaxAL). In our experiments, the Lipschitz penalty shares a very similar performance as the gradient penalty, so we take out the Lipschitz penalty for clarity.

We use multilayer perceptrons for all toy experiments and use a Resnet architecture (He et al., 2016) that is similar to the one used in Gulrajani et al. (2017) for all other real data experiments. We use Adam optimizer (Kingma and Ba, 2015) with $\beta_1 = 0$ and $\beta_2 = 0.9$.

Frechet Inception Distance (FID) (Heusel et al., 2017) was used to quantitatively evaluate the resulting models. Another well-known metric is Inception Score (Salimans et al., 2016). However, it is not well explained and the resulting score is highly unstable (Zhou et al., 2018; Borji, 2019). Hence, we here not include the results of Inception Score.

For this part of experiments, we use the WGANs because its theoretical results correspond to optimal transport, which can be more easily understood and checked.

The code for reproducing these results is provided at <https://github.com/ZhimingZhou/MaxGP-MaxAL-for-reproduce>.

5.4.1 TWO DIMENSIONAL TOY DATA

To intuitively study the property of different methods, we first test their performances with simple two dimensional data. In this experiment, we randomly sample two data points in

two dimensional space as \mathcal{P}_g and another two points as \mathcal{P}_t . We fix these two distributions and train a discriminator with different implementations of Lipschitz regularization.

We want to check whether these methods are able to achieve the optimal discriminative function, by verifying the gradients of generated samples, which should follow the Proposition 1 and point towards their target real samples that minimizes the transport cost.

Our first interesting observation is that SN in some cases fails to achieve the optimal discriminative function. As shown in Figure 2, SN quickly converges to a suboptimal solution and sticks there. We currently do not fully understand how such a phenomenon appears. We consider that it might because the global restriction on Lipschitz constant makes the capacity of the discriminator extremely underused such that the optimal discriminative function is not attainable. And we think the probable issues exist in the estimation of maximum singular value, i.e., power iteration, also holds a large portion of the possibility.

We have tried fairly large networks, but it does not help eliminate this issue. We have tried increasing the number of the power iteration that used to acquire the singular value, it does not solve this issue. We have also tried both in-place update of \bar{W}_{SN} and update \bar{W}_{SN} with collection, the issue consistently exists. Training the discriminator for a very long time with a decreasing learning rate also cannot solve this issue and the final result keeps unchanged. We leave further investigation as future work.

In Figure 2, we also noticed that GP leads to an oscillatory discriminator, which evidences that the superfluous constraints affect the optimal discriminator, and it turns out to lead to instability. It seems there is no stable optimum for the discriminative function under GP.

By contrast, we see that MaxGP quickly converges to the optimal discriminator (within 1000 iterations) and stably holds at the optimal state (keep almost unchanged), where the gradients of the generated samples point towards the real samples in an optimal transport manner. It also evidence that the superfluous constraints are harmful from another side.

5.4.2 TOY REAL WORLD DATA

We further compare these methods with real world data. We still want to check whether these methods converge to the optimal discriminative function. However, the real world dataset is too large, and we found practically, the optimal discriminator is almost unachievable. Hence, in this experiment, we use a small subset of the real world dataset, instead. Specifically, we select ten representative CIFAR-10 images as \mathcal{P}_t and use ten random noise as \mathcal{P}_g . Then, same as above, we fix the two distributions and train the discriminator till optimal and check the gradients of the resulting discriminative function of different methods.

For the high dimensional case, visualizing the gradient direction is nontrivial. Hence, we plot the gradient and corresponding increments in Figure 3, where the leftmost in each row is a sample x from \mathcal{P}_g and the second is its gradient $\nabla_x f(x)$. The interiors are $x + \epsilon \cdot \nabla_x f(x)$ with increasing ϵ , and the rightmost is the nearest real sample y from \mathcal{P}_t , i.e., the real sample that is closest to any point in the gradient directed path.

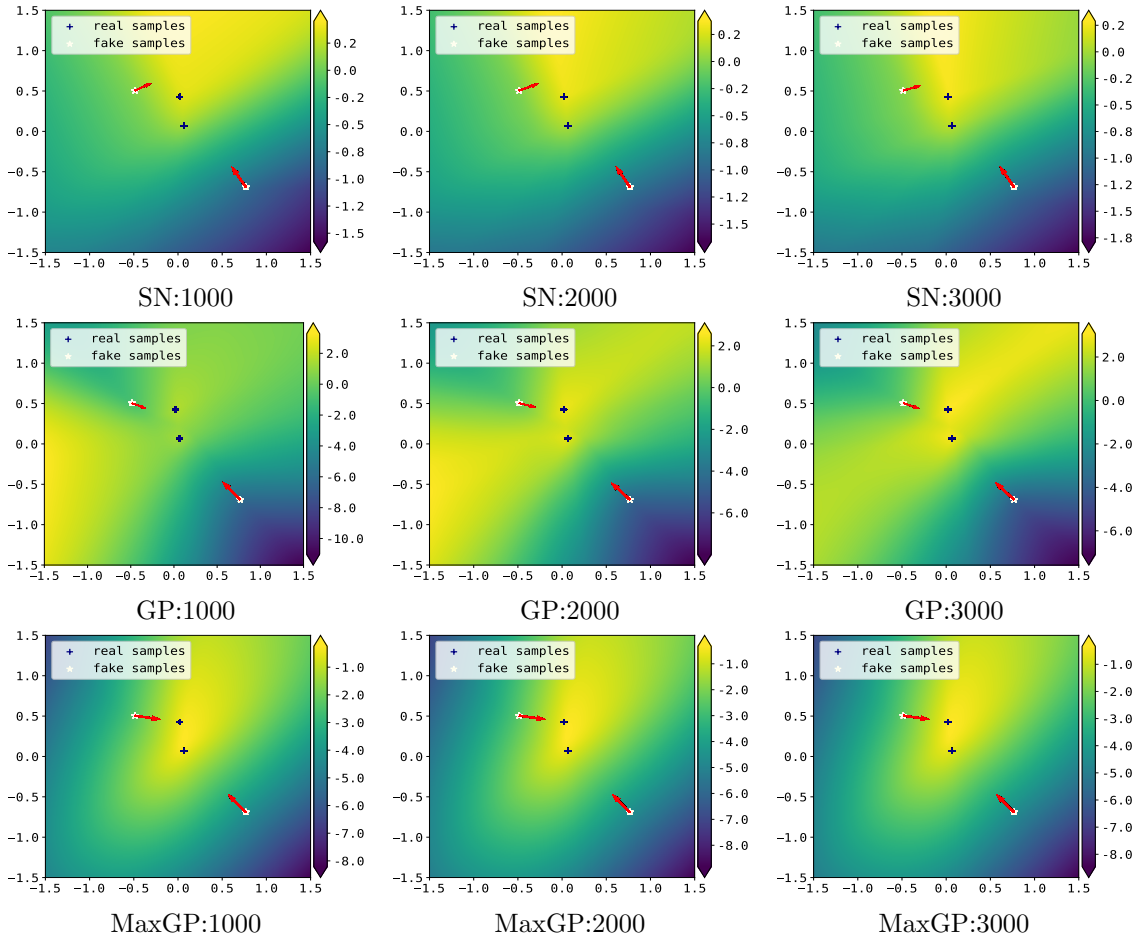


Figure 2: With \mathcal{P}_g and \mathcal{P}_t both being two random sampled points in two dimensional space, we train the discriminator using SN, GP and MaxGP, respectively. The numbers after the name of the methods are the corresponding iteration numbers. The arrows in the figures indicate the gradient scales and directions. From the results, we notice that: (i) SN in this case fails to achieve the optimal discriminator; (ii) the discriminator trained with GP is oscillatory; (iii) MaxGP stably converges to the optimal. Note that the results of SN and MaxGP seem to keep unchanged over iterations. That is because they have already basically converged with 1000 iterations. By contrast, GP keeps oscillatory all the way.

From the results, MaxGP is also able to achieve the optimal discriminative function in the high dimensional case. We see that the gradient $\nabla_x f(x)$ of ten noises in \mathcal{P}_g is pointing towards the ten real images in \mathcal{P}_t , respectively.

However, the resulting gradients of GP do not clearly point towards real samples. The gradient tends to be a blending of several images in the target domain, and it also appears a sort of mode collapse (multiple cats and birds). This experiment once again verifies that these superfluous constraints inadvertently introduced by GP are harmful.

5.4.3 SAMPLE QUALITY ON CIFAR-10

We now test the practical difference, when training a complete GANs model, using these methods to impose Lipschitz regularization. In this experiment, we not only train the model with WGANs loss metric, but also with the hinge loss (Miyato et al., 2018) and original GANs loss metric (Goodfellow et al., 2014), which has also found work well under Lipschitz continuity regularization (Fedus et al., 2018).

The results in terms of training curve of FID are plotted in Figure 5. In Figure 5a, we compare GP, MaxGP and MaxAL with different regularization weights under the WGANs loss metric. We see that the training progresses and final results are quite similar to each other. The visual results are also provided in Figure 4.

As we found in the experiments of toy real world data, given \mathcal{P}_g and \mathcal{P}_t both consist of ten images, the optimal discriminator is already very hard to achieve. Hence, we believe that the reason why these methods do not show obvious differences in these real world applications lies in the optimization level. That is, the attainable result is too far from the optimum, so even whether it is biased or not, the final result appears similar.

We have also checked that, with real world dataset, even the relatively small dataset CIFAR-10 or MNIST, the gradient $\nabla_x f(x)$ of the generated sample is basically nebulous. Maybe the nebulous gradient somehow points towards \mathcal{P}_t (otherwise, how to explain the progress of the training), but being blurry / averaged, and definitely not clearly points towards a certain real sample.

That is, in the current hyper-parameter settings, e.g., DCGAN architecture or shallow Resnet, the optimal discriminative function of WGANs is almost impossible to achieve.

It might also be related to the issues of the optimizer. Amam (Kingma and Ba, 2015), the common-used and somewhat powerful optimizer for GANs, is recently shown to not guarantee the convergence (Reddi et al., 2018; Zhou et al., 2019b; Zou et al., 2019). We are keeping investigating this phenomenon.

In this experiment, we initially use the WGANs loss metric for all methods. However, we found that with the Resnet architecture (Gulrajani et al., 2017), SN fails to converge. The same holds with various small modifications of hyper-parameters. We then notice that in Miyato et al. (2018), when using Resnet architecture, the model with SN is trained using a hinge loss. We therefore also test SN with the hinge loss, and in addition, the original GANs loss metric, which was found to also work well given the Lipschitz regularization.



(a) GP



(b) MaxGP

Figure 3: With \mathcal{P}_g and \mathcal{P}_t being ten fixed noise and real images, respectively, we train discriminator using GP and MaxGP towards optimum. The leftmost in each row is a sample x from \mathcal{P}_g and the second is the gradient $\nabla_x f(x)$. The interiors are $x + \epsilon \cdot \nabla_x f(x)$ with increasing ϵ . The rightmost is the nearest real sample y from \mathcal{P}_t . As we can see, GP fails to achieve the optimal discriminative function, where the gradients of fake samples do not strictly point towards real samples and tend to collapse to a subset of real samples. By contrast, with MaxGP, the gradients of \mathcal{P}_g samples perfectly follow the optimal transport.

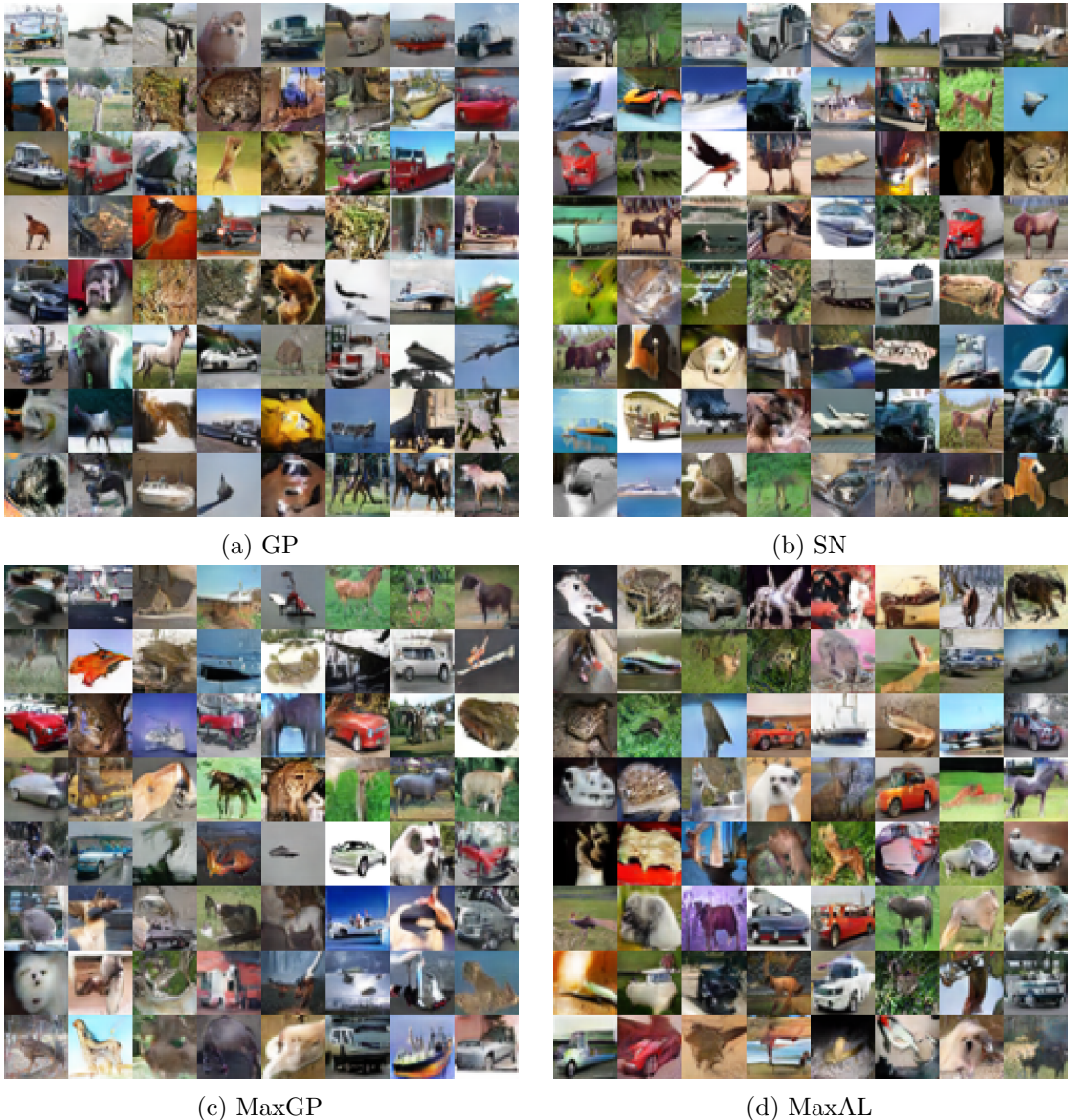


Figure 4: The visual comparison of different implementations of Lipschitz regularization under unsupervised CIFAR-10 generation with the WGANs loss metric. The training with SN diverges, when using WGANs loss metric. Here we plot its result with hinge loss, instead.

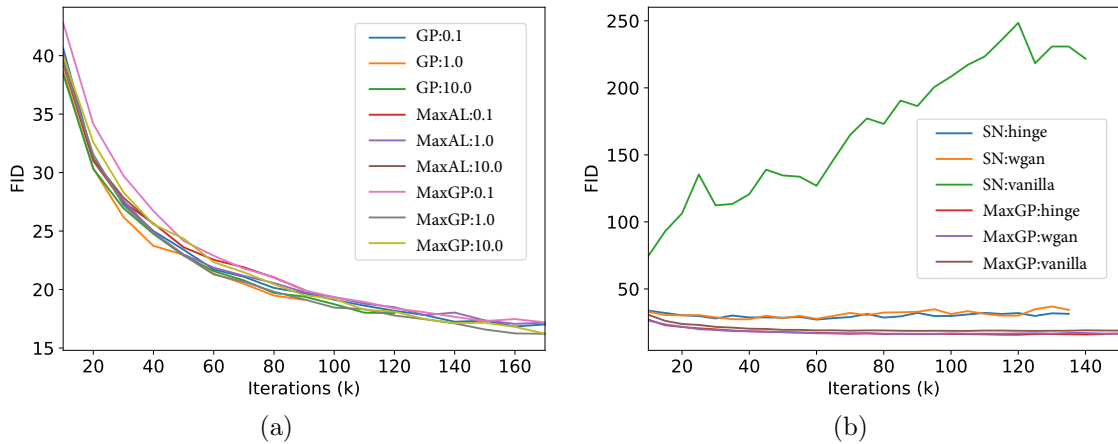


Figure 5: The quantitative comparison of different implementations of Lipschitz regularization under unsupervised CIFAR-10 generation with the WGANs loss metric in terms of FID training curve. The number after the name of the method is the regularization weight ρ and the string after the method name indicates the loss metric it used. GP, MaxGP and MaxAL achieve very similar results, and they are not very sensitive to the regularization weight ρ . The training of SN diverges, when using WGANs loss metric. And even when using the hinge loss or original GANs loss metric, the final results of SN are still apparently worse than MaxGP.

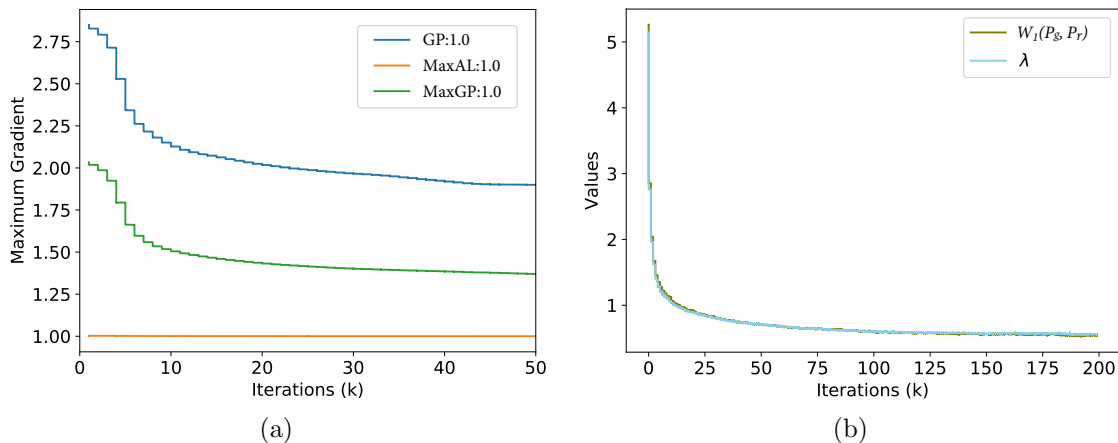


Figure 6: The favorable properties of MaxAL. The number after the name of the method is the regularization weight ρ . With MaxAL, the Lipschitz constant quickly converges to the given target 1. By contrast, the Lipschitz constants achieved by GP and MaxGP are dynamic, which decreases as \mathcal{P}_g converges to \mathcal{P}_t . In addition, the value of the λ is equivalent to the Wasserstein distance.

The results are plotted in Figure 5b. We also include the results of MaxGP with these loss metrics for comparison. As we can see, the result of MaxGP is generally better than SN.

Lastly, we inspect the properties of MaxAL. As shown in Figure 6a, MaxAL is able to quickly restrict the Lipschitz constant to the given target, i.e., 1, and keep the Lipschitz constant fairly stable during the training. By contrast, the Lipschitz constants under GP and MaxGP keep changing, decreasing as \mathcal{P}_g getting closer to \mathcal{P}_t .

Another interesting fact about MaxAL is that, when trained with the WGANs loss metric, the optimal λ is equivalent to $W_1(\mathcal{P}_g, \mathcal{P}_t)$. We verify this fact by plotting these two terms during training together. As shown in Figure 6b, the two lines are basically overlapped.

5.5 Summary on Lipschitz Regularization Implementations

Up to now, we demonstrated that restricting the Lipschitz constant over the support of the interpolations of real and fake samples is sufficient to gain the advantageous gradient properties induced by Lipschitz continuity regularization. It provides theoretical guarantee on the validity of these empirical gradient penalty based methods.

In the meantime, it suggests that global restriction on the Lipschitz constant is unnecessary. Combined with the fact that we found the spectral normalization, the method that provides global restriction on the Lipschitz constant, somehow fails in many practical scenarios. Although the real issues may exist in the estimation of maximum singular value. Given that there is currently no other good alternative to power iteration, we suggest using these methods that regularize local Lipschitz constant in the blending region.

On the other hand, we also observed that the current implementations of local Lipschitz regularization, i.e., gradient penalty and Lipschitz penalty, introduce superfluous constraints to the optimization problem, which evidently alter the optimal discriminative function and impair the favorable gradient properties and lead to sort of instability during training.

We have accordingly proposed revisions to the gradient penalty. Our experiments demonstrated that the proposed MaxGP is able to achieve the optimal discriminative function in an unbiased manner. In addition, we suggested augmented Lagrangian as a simple yet good alternative to the penalty method, which is able to strictly restrict the Lipschitz constant to a given target, resulting in the proposed MaxAL.

6. Empirical Analysis and Verification of Lipschitz Regularized GANs

With both theoretically sound and practically well-behaving MaxGP, we now verify the theoretical properties of LGANs and benchmark various instances of LGANs, and will show its consistently superior performances over WGANs.

To adopt MaxGP for LGANs, we just need to set $k_0 = 0$. In many cases, MaxAL actually can also be used, if preferred. Because if k_0 is small enough and \mathcal{P}_g and \mathcal{P}_t is not close enough, then all required bounding relationships can be established. Or one can consider decreasing k_0 in MaxAL during training if necessary. Penalizing the Lipschitz constant is to ensure the Lipschitz constant is small enough to establish effective bounding relationships

that moves samples from where there is too much to where there is too less, when the two distributions are too close. Nevertheless, the following experiments are based on MaxGP.

The code for reproducing these results is provided at <https://github.com/ZhimingZhou/LGANs-for-reproduce>.

6.1 Verifying $\nabla_x f^*(x)$ in LGANs Points Towards Real Sample

One important theoretical benefit of LGANs is that $\nabla_x f^*(x)$ for each generated sample is guaranteed to point towards some real sample. We here verify the gradient direction of $\nabla_x f^*(x)$ with a set of ϕ and φ that satisfy Eq. (12).

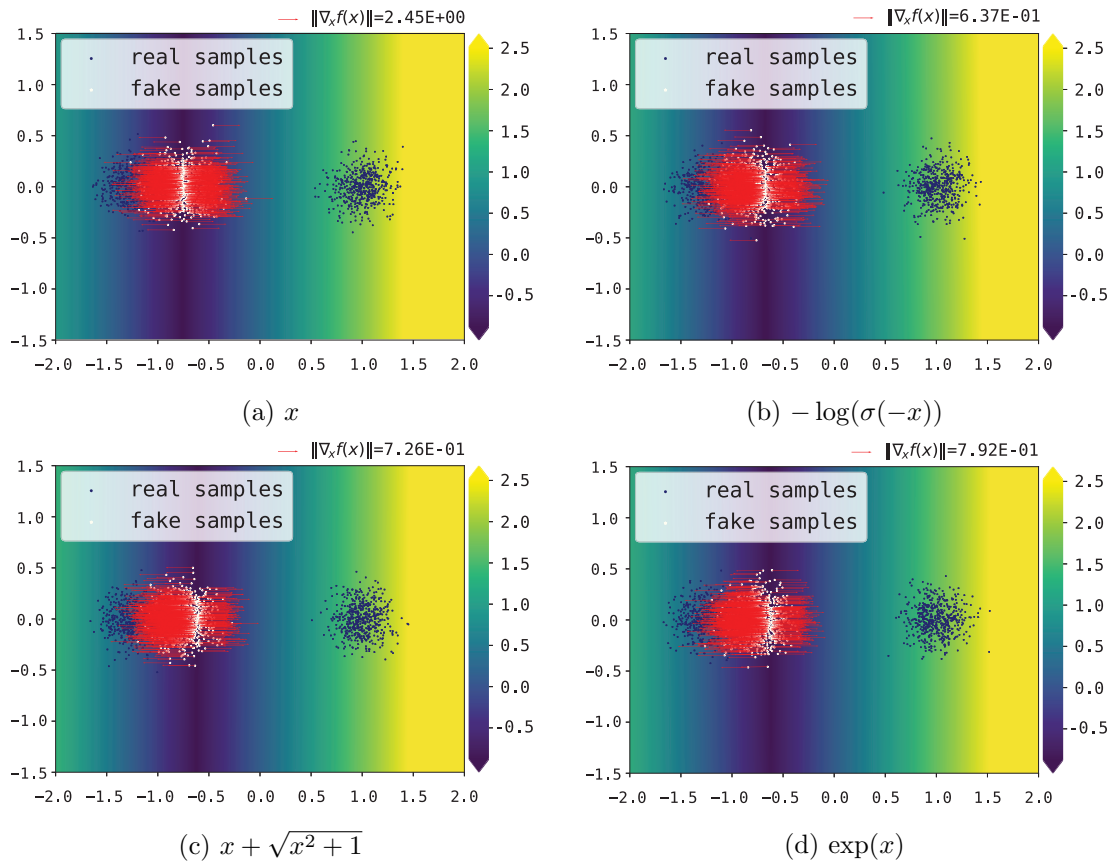
The tested loss metrics include: (a) $\phi(x) = \varphi(-x) = x$; (b) $\phi(x) = \varphi(-x) = -\log(\sigma(-x))$; (c) $\phi(x) = \varphi(-x) = x + \sqrt{x^2 + 1}$; (d) $\phi(x) = \varphi(-x) = \exp(x)$. And they are tested in two scenarios: two dimensional toy data and real world high dimensional data.

In the two dimensional case, \mathcal{P}_t consists of two distant Gaussians and \mathcal{P}_g is fixed as one Gaussian which is close to one of the two real Gaussians, as illustrated in Figure 7. For the latter case, we use the CIFAR-10 training set. To make solving f^* feasible, we use ten CIFAR-10 images as \mathcal{P}_t and ten fixed noise images as \mathcal{P}_g . Note that we fix \mathcal{P}_g on purpose because to verify the direction of $\nabla_x f^*(x)$, learning \mathcal{P}_g is not necessary.

The results are shown in Figures 7 and 8, respectively. In Figure 7, we can easily see that $\nabla_x f^*(x)$ of each generated sample is pointing towards some real sample. Note that the gradients in LGANs do not always follow the optimal transport, which turns out does not necessarily imply a better performance. According to our experiments, LGANs consistently outperforms WGANs and the strict convexity seems to be more important.

For the high dimensional case, visualizing the gradient direction is nontrivial. Hence, we plot the gradient and corresponding increments. In Figure 8, the leftmost in each row is a sample x from \mathcal{P}_g and the second is its gradient $\nabla_x f(x)$. The interiors are $x + \epsilon \cdot \nabla_x f(x)$ with increasing ϵ and the rightmost is the real sample y from \mathcal{P}_t that is nearest to the gradient path. This result visually demonstrates that $\nabla_x f^*(x)$ of generated samples are pointing towards real samples.

Note that the final results of Figure 8 keep almost identical, when varying the loss metrics ϕ and φ in the LGANs family, which we believe is reasonable. Because according to our analysis, when \mathcal{S}_g and \mathcal{S}_t are disjoint, LGANs behaves just like WGANs in the sense that every sample in \mathcal{S}_g must get bounded by a real sample. Given finite and limited samples, it seems unlikely that one sample from \mathcal{P}_g is bounded by two different samples from \mathcal{P}_t . Even if such cases exist, it also does not matter. Just like the continuous case, gradients for generated samples in LGANs do not always follow the optimal transport and may temporally tend to gather samples, but in LGANs, there is an underlying force to avoid mode collapse, i.e., it is always moving samples from where there is too much to where there is too less.

Figure 7: Verifying $\nabla_x f^*(x)$ in LGANs point towards real samples.

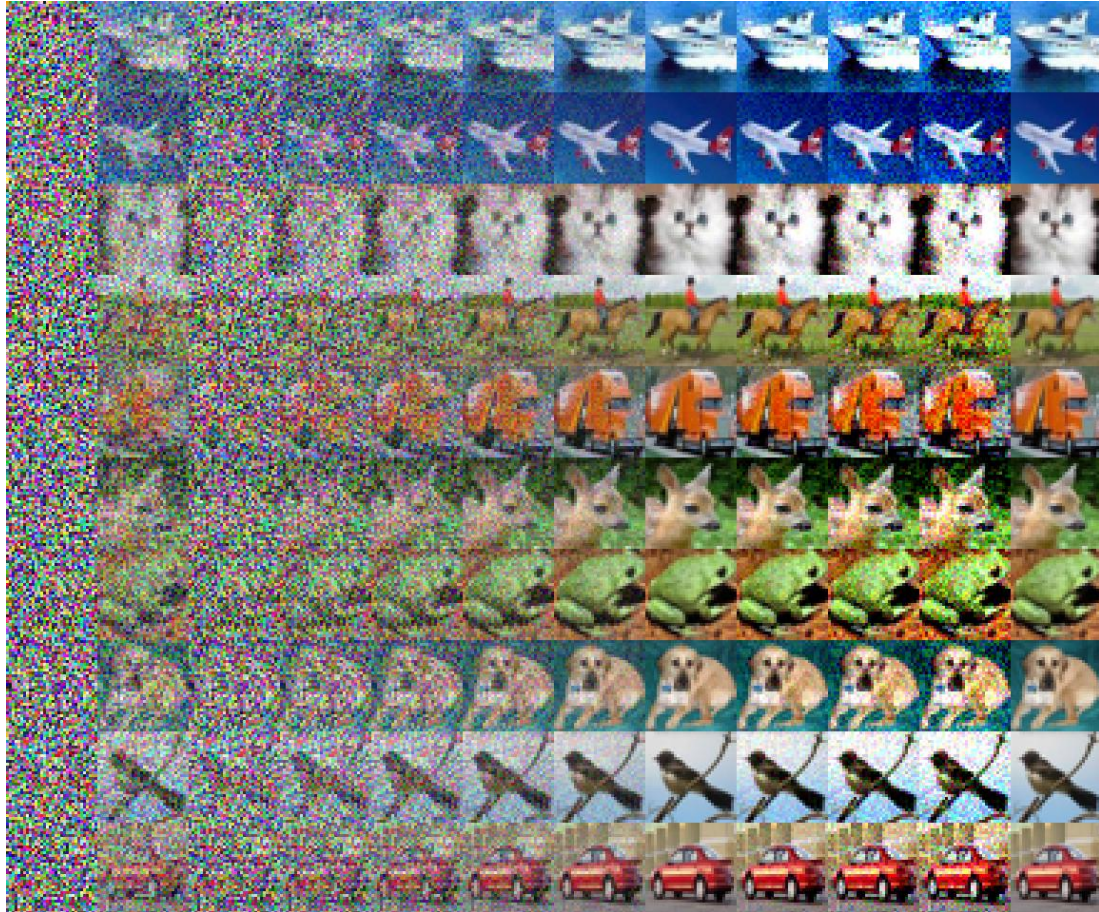


Figure 8: Verifying $\nabla_x f^*(x)$ in LGANs point towards real samples with gradient gradation.

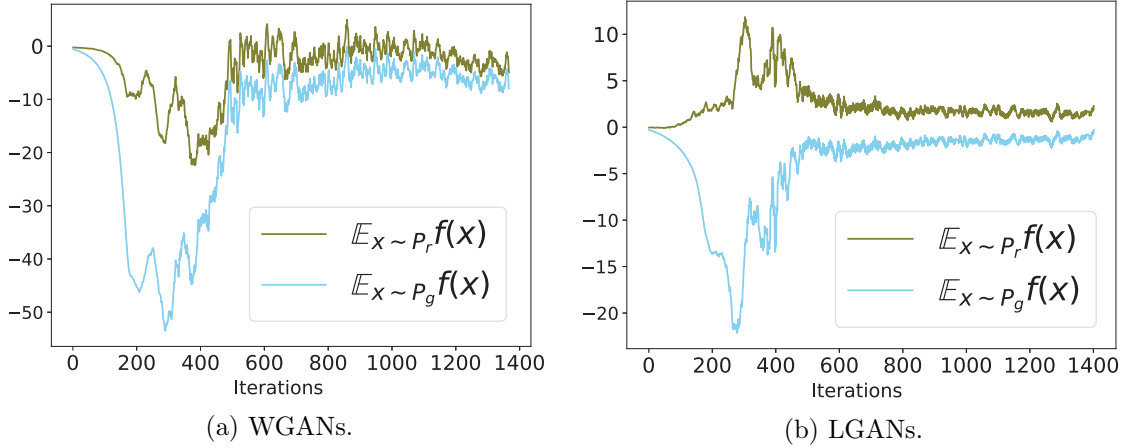


Figure 9: The benefit of the uniqueness of f^* in LGANs. f is more stable during training.

6.2 The Benefit of Uniqueness of f^* in LGANs: Stabilized f .

The loss metric that corresponds to the Wasserstein distance is a very special case that has a solution under Lipschitz regularization. It is the only case where both ϕ and φ have constant derivatives, i.e., both are not strictly convex (otherwise, the uniqueness holds).

As a result, f^* under the Wasserstein distance loss metric has a free offset, i.e., given any optimal discriminative function f^* , $f^* + \alpha$ with any $\alpha \in \mathbb{R}$ is also an optimal. In practice, it behaves as oscillations in $f(x)$ during training.

The oscillations seem to affect the practical performance of WGANs. Karras et al. (2018) and Adler and Lunz (2018) introduced regularization to the discriminative function to prevent $f(x)$ drifting during the training. By contrast, any other instance of LGANs does not have this issue. We illustrate the practical difference in Figure 9.

Note that upon this oscillation effect, WGANs and LGANs with Wasserstein distance loss metric are essentially the same. The difference lies in the resulting value of Lipschitz constant: WGANs force it being or towards one, while LGANs with Wasserstein distance loss metric penalizes it to make it as small as possible.

Nonetheless, the qualitative change happens, when \mathcal{P}_g converges to \mathcal{P}_t . At that time, the training of LGANs will fundamentally stop with wholly zero gradients passing through G-D, i.e., the connecting point of the generator and the discriminator, because $k(f) = 0$. But WGANs, requiring $k(f)$ being one, will keep fluctuating (Mescheder et al., 2018).

6.3 Benchmark with Unsupervised Image Generation

To quantitatively compare the performance of different loss metrics under Lipschitz regularization, we test them with unsupervised image generation tasks.

In this part of experiments, we also include the hinge loss $\phi(x) = \varphi(-x) = \max(0, x + \alpha)$ and quadratic loss (Mao et al., 2017), which do not fit the assumption of strict monotonicity. For the quadratic loss, we set $\phi(x) = \varphi(-x) = (x + \alpha)^2$. We set $\alpha = 1.0$ in all the experiments.

The strict monotonicity assumption of ϕ and φ is critical in Theorem 3 to theoretically guarantee the existence of bounding relationships for *arbitrary datas*. But if we further assume S_g and S_r are limited, it is possible that there exists a suitable ρ , which results in a proper scale of $k(f)$ (see arguments around Eq. 17), such that all real and fake samples lie in a strict monotone region of ϕ and φ . Then, the hinge loss and even the quadratic loss may also work well. For hinge loss, it would mean $2\alpha < k(f) \cdot \|y - x\|$ for all $x \in \mathcal{S}_g$ and $y \in \mathcal{S}_t$.

Our tentative experiments show that the choice of $\psi(x)$ does not play a central role. But in this experiment, we choose to fix the loss metric $\psi(x)$ in J_G as $-x$. The thought behind our current choice of $\psi(x)$ is that: if we choose to use the minimax formulation, though we can get the minimax explanation of what the generator is minimizing, it will have some strange property. That is, when ϕ is strictly convex, then the samples with lower $f(x)$ value will get a smaller gradient scale because it is weighted by $\nabla_{f(x)}\psi(f(x))$; but a lower $f(x)$ value somehow (not strict and not always true) indicates this sample has a larger distance to the target distribution. And on the other hand, setting $\psi(x) = -x$ is also very easy to understand, i.e., updating samples with evenly distributed weights. We believe the choice of $\psi(x)$ is also an interesting research topic and we leave it as future work.

The results in terms of Inception Score (IS) (Salimans et al., 2016) and Frechet Inception Distance (FID) (Heusel et al., 2017) are presented in Table 2. For all experiments, we adopt the network structures and hyper-parameter setting from (Gulrajani et al., 2017), where WGANs-GP in our implementation achieves IS 7.71 ± 0.03 and FID 18.86 ± 0.13 on CIFAR-10. We use MaxGP and search the best regularization weight $\rho/2$ in $[0.01, 0.1, 1.0, 10.0]$. We use 200,000 iterations for better convergence and use $500k$ samples to evaluate IS and FID for preferable stability. We note that IS, though being popular, is not well explained (Zhou et al., 2018; Borji, 2019). And it is highly unstable during training. By contrast, FID is fairly stable. We include IS for better reference.

We plot the training curves in terms of FID in Figures 10. The training curves in terms of IS are provided in the Appendix (Figure 18). From the Figures and Table 2, we can clearly tell that all other LGANs instances consistently and remarkably outperform WGANs, while LGANs with WGANs loss metric shares a similar performance of WGANs. Different instances of LGANs have relatively similar final results, while the loss metrics $\phi(x) = \varphi(-x) = x + \sqrt{x^2 + 1}$ and $\phi(x) = \varphi(-x) = \exp(x)$ and achieve the best performances.

This is probably because LGANs with strictly convex loss metrics reduces the gradient of well-identified points towards zero, which means the benefit of further discriminating this sample is reduced and hence enables the discriminator to pay more attention to these ill-identified. And hence LGANs generally work better than WGANs and these instances with relatively strong convexity perform better.

The hinge loss and quadratic loss with a suitable regularization weight ρ turn out to also work pretty good. But we also find that if we use a too small α , e.g., $\alpha = 0.1$, its performance will significantly drop, which is consistent with our analysis.

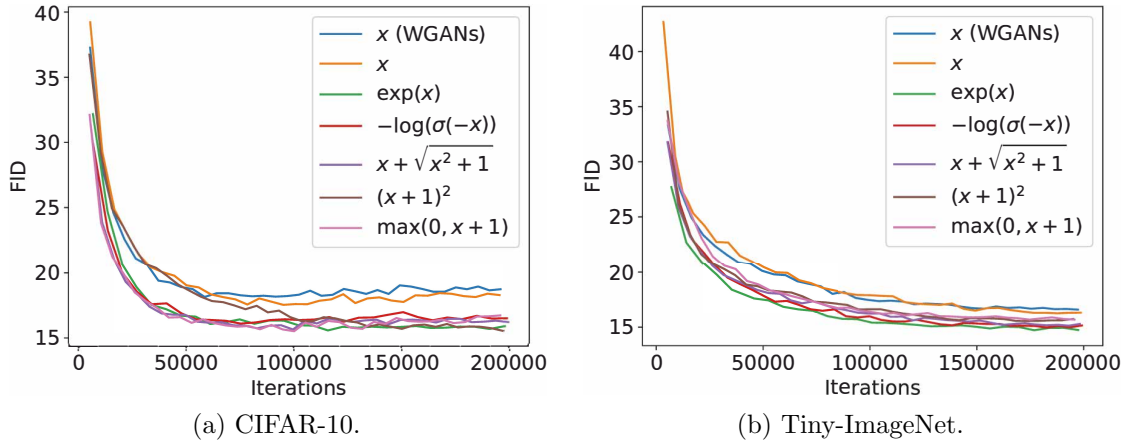


Figure 10: Training curves in terms of FID. WGANs and a set of instances of LGANs.

| Loss Metrics | CIFAR-10 | | Tiny-ImageNet | |
|----------------------|-----------------------------------|------------------------------------|-----------------------------------|------------------------------------|
| | IS | FID | IS | FID |
| x | 7.68 ± 0.03 | 18.35 ± 0.12 | 8.66 ± 0.04 | 16.47 ± 0.04 |
| $-\log(\sigma(-x))$ | 7.95 ± 0.04 | 16.47 ± 0.11 | 8.70 ± 0.04 | 15.05 ± 0.07 |
| $x + \sqrt{x^2 + 1}$ | 7.97 ± 0.03 | 16.03 ± 0.09 | 8.82 ± 0.03 | 15.11 ± 0.06 |
| $\exp(x)$ | 8.03 ± 0.03 | 15.64 ± 0.07 | 8.67 ± 0.04 | 14.90 ± 0.07 |
| $(x + 1)^2$ | 7.97 ± 0.04 | 15.90 ± 0.09 | 8.53 ± 0.04 | 15.72 ± 0.11 |
| $\max(0, x + 1)$ | 7.91 ± 0.04 | 16.52 ± 0.12 | 8.63 ± 0.04 | 15.75 ± 0.06 |

Table 2: The quantitative comparisons. WGANs loss metric and other instances of LGANs.

7. How Traditional GANs Work

This section is aimed to gain a more experienced understanding upon the training issues of unregularized GANs, and at the same time, to understand how unregularized GANs work in practice. We will first provide a more systematic study of its gradient issues, and then we will study the practical behavior of these gradient issues. And we will also explain why mode collapse is common in unregularized GANs.

We realize that the similar analysis apply to some other regularized GANs, whose $f^*(x)$ share the similar properties of unregularized GANs, i.e., only reflect local information and positively correlated with $\mathcal{P}_t(x)$ and negatively correlated with $\mathcal{P}_g(x)$, e.g., Fisher GANs. Hence, we more generally refer to these GANs as traditional GANs.

In the following, we will show that in traditional GANs, $\nabla_{f(x)}\psi(f(x))$ may lead to Type-I gradient vanishing, and $\nabla_x f(x)$ is involved with both Type-II gradient vanishing and faulty gradient direction, which is a generalized concept of gradient uninformativeness.

7.1 Type-I Gradient Vanishing

The well-known gradient vanishing issue (Goodfellow et al., 2014; Arjovsky and Bottou, 2017) mainly refers to the issue in the original GANs. It should be noted that, in terms of Eq. (8), the gradient vanishing issue in the original GANs⁶ mainly stems from the vanishing of the scalar term $\nabla_{f(x)}\psi(f(x))$, which we refer to as the Type-I gradient vanishing.

The occurrence of Type-I gradient vanishing, i.e., $\nabla_{f(x)}\psi(f(x)) = 0$, has two necessary conditions: (i) the existence of extreme point, i.e., $S = \{x \mid \nabla_x\psi(x) = 0\}$ and $S \neq \emptyset$; (ii) the accessibility of extreme point, i.e., $\{x \in S_g \mid f(x) \in S\} \neq \emptyset$.

In the original GANs, by switching to an alternative generator loss metric $\psi(x) = -\log \sigma(x)$, it avoids the accessibility of extreme points and hence solves the Type-I gradient vanishing. The Least-Squares GANs (Mao et al., 2017), with $\phi(x) = (x - \alpha)^2$ and $\psi(x) = (x - \gamma)^2$ and $\alpha \neq \gamma$, avoids the Type-I gradient vanishing via avoiding the accessibility of extreme points.

Wasserstein GANs (Arjovsky et al., 2017), with $\psi(x) = x$, avoids the existence of extreme points and thus avoids the Type-I gradient vanishing. LGANs penalizes the Lipschitz constant, forming bounding relationships, and hence avoids extreme points.

We will show in the next section that the vector term $\nabla_x f(x)$ may also be zero, which leads to another type of gradient vanishing that we call the Type-II gradient vanishing. Interestingly, the Least-Squares GANs (Mao et al., 2017), though avoids the Type-I gradient vanishing, still suffers from the Type-II gradient vanishing.

7.2 Type-II Gradient Vanishing and Faulty Gradient Direction

We here study the gradient issues arising from $\nabla_x f(x)$, from the perspective of the gradients of the optimal discriminative function at sample points, i.e., by analyzing $\nabla_x f^*(x)$.

6. In the original GANs, $f^*(x)$ for a fake sample in disjoint case is negative infinite. In practice, the values $f(x)$ of fake samples tend to be different, and thus it does not suffer the Type-II gradient vanishing.

Generally, if a sample x is at the local optimum of f^* , then it has $\nabla_x f^*(x) = 0$ and hence suffers from a substantive zero-gradient, which we refer to as the Type-II gradient vanishing. We broadly name gradients that do not guarantee convergence as faulty gradients. To highlight the importance of gradient direction, we refer to this issue as faulty gradient direction issue, which includes: (i) uninformative gradient; (ii) theoretically undefined gradient; (iii) unconverged Type-II gradient vanishing; (iv) local-greedy gradient.

As an important sub-case of faulty gradient direction issue, we also separately name the issue caused by uninformative gradient as the gradient uninformativeness issue.

Now we define and explain these different types of faulty gradients:

- Uninformative gradient: if the optimal discriminative function only reflects the local densities, when a generated sample is not surrounded by real samples, its gradient tells nothing about \mathcal{P}_t . Typical situation is that \mathcal{P}_g and \mathcal{P}_t are disjoint, which is common in practice according to Arjovsky and Bottou (2017);
- Theoretically undefined gradient: for generated sample x , if the optimal discriminative function is not fully defined in the surroundings of x , e.g., it is isolated and at the boundary (see the fake samples in the outside of \mathcal{S}_g in Figure 11). It suffers from a theoretically undefined gradient, whose behavior is undefined and depends on the training details, such as hyper-parameters and network structures;
- Unconverged Type-II gradient vanishing: for generated sample that theoretically suffers from Type-II gradient vanishing, despite the practical existence of Type-II gradient vanishing (see Figure 11a), it more commonly suffers from the unconverged version of Type-II gradient vanishing (see the fake samples in the central of the left region in Figure 11b), which usually behaves as random noisy gradient;
- Local-greedy gradient: when the optimal discriminative function only reflects the local densities, even if the gradient is well-defined and nonzero, the gradient update based on $\nabla_x f(x)$ is local-greedy, which turns out to be an intrinsic cause of mode collapse. See Section 7.5 for more details.

Samples that suffer from the uninformative gradient might at the same time suffer from theoretically undefined gradient: the uninformative gradient happens when the generated sample is not surrounded by real samples; if it is further not fully surrounded by any kind of (real or fake) samples, it also suffers the theoretically undefined gradient.

Meanwhile, theoretically undefined gradient is not a sub-issue of uninformative gradient: for sample at the boundary, it suffers theoretically undefined gradient, but its practical gradient might be somewhat informative, if there are some real samples in the surroundings.

If the variation of $f^*(x)$ in a region is too small, due to the precision limitation of the computing device, the practical neural network may not be able to capture the statistical variation. Then it may also behave as the Type-II gradient vanishing.

The faulty gradient direction issue is orthogonal to gradient vanishing: gradient vanishing is about the scale of the gradient (the overall scale or only the $\nabla_{f(x)}\psi(f(x))$ part), however, faulty gradient direction is mainly about the direction of the gradient.

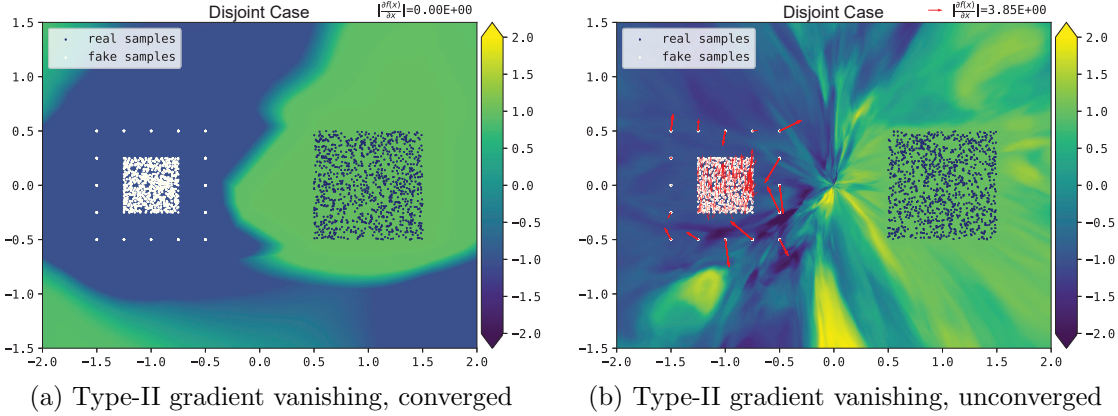


Figure 11: When \mathcal{S}_g and \mathcal{S}_t are disjoint: (i) Depending on the hyper-parameters and training states, samples inside \mathcal{S}_g suffer from the Type-II gradient vanishing if converged (11a), or otherwise suffer from faulty gradient that stems from unconverged Type-II gradient vanishing (11b). (ii) The gradients for samples that are isolated or at the boundary are theoretically undefined and uninformative, which in practice also behave as faulty gradients and appear as *pseudo random noises*.

Still one can consider the ideal case to understand that the two are indeed orthogonal, where \mathcal{P}_g and \mathcal{P}_t are totally overlapped and both consist of n discrete points but their probability mass over these points are different: its gradient direction is undefined and hence faulty and meaningless, but the gradient does not necessarily vanish.

7.3 The Practical Behaviors of These Gradient Issues

To study the practical behaviors of various gradient issues and understanding how GANs that theoretically has gradient issues works in practice. We conduct a set of experiments with various hyper-parameter settings. We use the Least-Squares GANs as a representative of traditional GANs in this experiment. The value surfaces and the gradients of generated samples under various situations are plotted in Figure 12.

These results show that the practical f highly depends on the hyper-parameter setting. Given limited capacity, the neural network tries to learn the best f which might lead to a simple value surface. When the neural network is capable of learning the (approximate) optimal f^* , how the actual f approaches f^* and how the theoretically undefined points behave highly depends on the optimization details and the characteristics of the network, which means the practical behavior of faulty gradient is hard to control and is controlled by hyper-parameters tuning.

According to Figure 12: (i) a low-capacity network tends to learn a simple surface; (ii) piecewise linear activation (e.g., ReLU) tends to result in simpler value surface, compared with highly nonlinear activation function (e.g., SELU, Klambauer et al. (2017)); (iii) Adam, compared with SGD, tends to learn a simpler surface; (iv) large learning rate (LR) tends to learn a simpler surface than small learning rate. For Adam, we set $\beta_1 = 0.0$ and $\beta_2 = 0.9$.

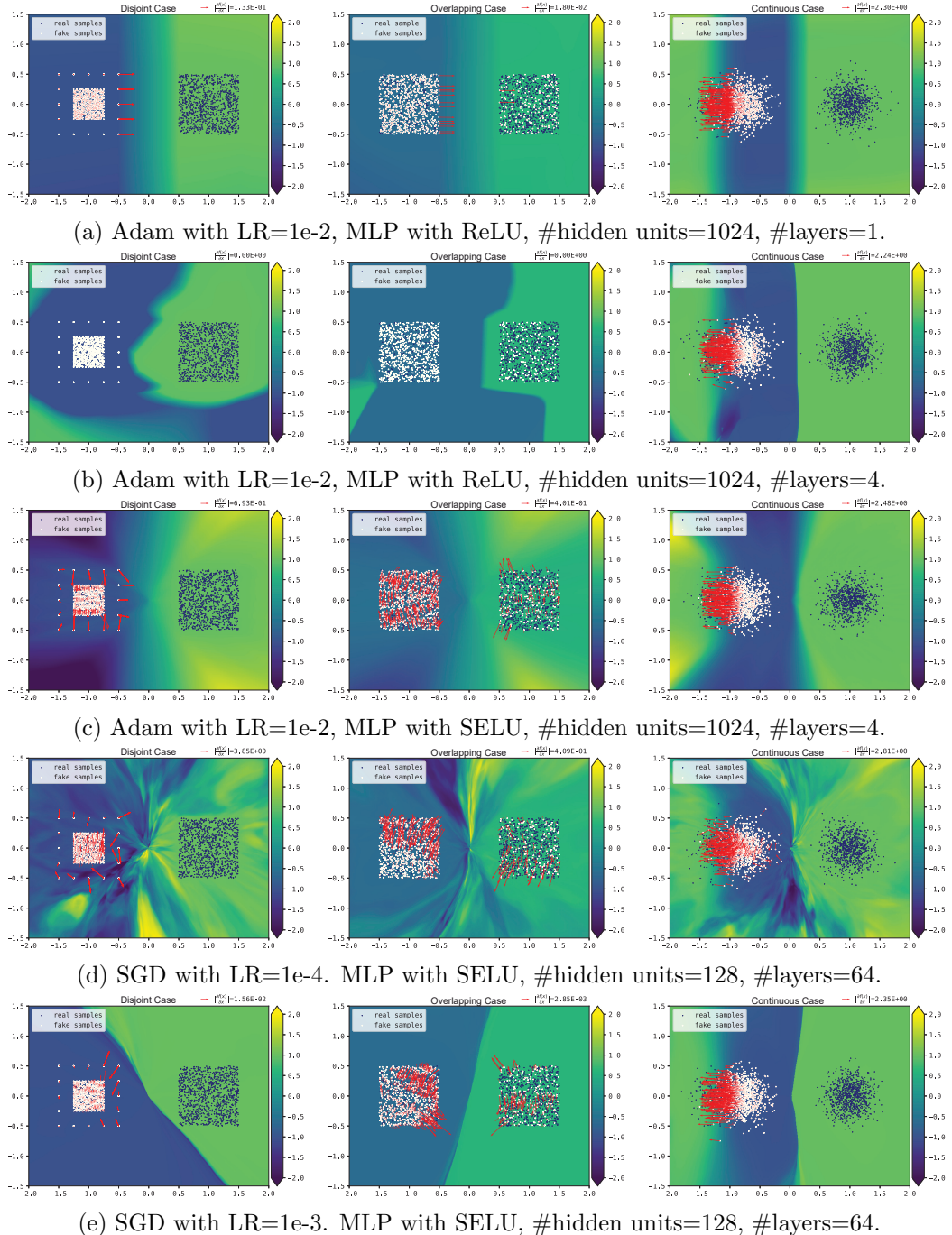


Figure 12: The practical f highly depends on the hyper-parameter setting. Some particular settings (e.g., Adam, ReLU, low capacity, large LR) lead to simple and smooth (or other favorable) value surfaces, where gradients generally point towards \mathcal{P}_t . Hyper-parameter setting that leads to a simple and smooth value surface is more likely to have successful training. These findings are basically consistent with the empirical success and failure of traditional GANs in common practice.

7.4 Explanation on the Empirical Success of Traditional GANs

Although traditional GANs do not have guarantee on its convergence, they have already achieved great success. The thing is that having no guarantee does not mean it cannot converge. It turns out extensive hyper-parameter tuning and a set of particular settings can increase the probability of its empirical success in training or convergence.

As shown in Figure 12, hyper-parameters, including network architecture, are important in influencing the value surface of f . Some typical settings (e.g., simplified neural network architecture, ReLU or leaky ReLU activation, relatively high learning rate, Adam optimizer, etc.) tend to form a relatively simple or smooth value surface, e.g., monotonically increasing from \mathcal{S}_g to \mathcal{S}_t , making the theoretically meaningless $\nabla_x f^*(x)$ much more meaningful.

That is, one can find these settings where $\nabla_x f^*(x)$ or $\nabla_x f(x)$ is more favourable (typically simple and smooth, or at least the increasing direction of the value surface is towards the real samples distribution), to enable traditional GANs to work or more likely to work.

For further verification, we have tried highly-nonlinear activation such as SWISH (Ramachandran et al., 2018) in the discriminator. It turns out traditional GANs are very likely to fail. By contrast, our proposed LGANs are compatible with highly-nonlinear activations.

Another important empirical technique is to delicately balance the generator and the discriminator or limit the capacity of the discriminator. This can be understood as it is trying to avoid the fatal optimal f^* and making the value surface not being overstretched.

Nevertheless, without any theoretical guarantee on its convergence, traditional GANs are practically hard to use, being unstable and sensitive to hyper-parameters and suffering from a possibility of model collapse. By contrast, WGANs and LGANs do not have such kind of training issues and can be much more easy to use, especially LGANs, which appears superior over WGANs due to its strictly convex properties.

7.5 The Cause of Mode Collapse

Mode collapse is a notorious issue in GANs' training, which refers to the phenomenon that the generator only learns to produce or imitate part(s) of \mathcal{P}_t , while missing some others.

A good deal of literature has tried to study the source of mode collapse (Che et al., 2017; Metz et al., 2017; Kodali et al., 2017; Arora et al., 2017) and/or measure the degree of mode collapse (Odena et al., 2017; Arora and Zhang, 2017).

The most recognized cause of mode collapse is that: if the generator is much stronger than the discriminator, particularly, when fix the discriminator and train the generator till optimum, it may learn to only produce the sample(s) in the local or global maximum(s) of $f(x)$ of the current discriminator.

This argument is true for most GANs (even for LGANs). However, from our perspective on $f^*(x)$ and its gradient, there actually exists a much more fundamental cause of mode collapse, i.e., the locality of $f^*(x)$ in traditional GANs and the locality of gradient operators.

Previously, we mainly discussed the issue of $\nabla_x f^*(x)$ in the cases where \mathcal{S}_g and \mathcal{S}_t are disjoint or being discrete. In the next, we extend our discussion to the overlapping and continuous cases, which reveals an intrinsic cause of mode collapse.

In the disjoint or discrete cases, we argue that in traditional GANs, the values of $f^*(x)$ on generated samples do not reflect any information about the location of other points of \mathcal{P}_t , which will lead to unfeasible $\nabla_x f^*(x)$ and thus nonconvergence.

In the overlapping and continuous case, things are actually different. For each generated sample x , $f^*(x)$ around x is well-defined and related to $\mathcal{P}_t(x)$, which means $\nabla_x f^*(x)$ is now informative and actually reflects the local variation of $f^*(x)$.

Optimizing the generator according to $\nabla_x f^*(x)$ will move the sample x following the direction of increasing $f^*(x)$. Because $f^*(x)$ is positively correlated with $\mathcal{P}_t(x)$ and negatively correlated with $\mathcal{P}_g(x)$, it in a sense means x is becoming more real. However, such a local-greedy property turns out to be a fundamental cause of mode collapse.

In traditional GANs, $f^*(x)$ is a function of local densities $\mathcal{P}_g(x)$ and $\mathcal{P}_t(x)$, which is local. And the gradient operator is also a local operator. As a result, $\nabla_x f^*(x)$ only reflects its local variations and cannot capture the statistic of \mathcal{P}_g and \mathcal{P}_t that is far from itself.

If $f^*(x)$ is well-defined in the surrounding area of x , $\nabla_x f^*(x)$ will move x towards the *nearby* location where the value of $f^*(x)$ is higher. It does not take the global statistics into account, hence will not be aware that there might be some place where samples are missing (i.e., there is a mode missing) and here the samples are too much (i.e., here is a mode collapse).

The typical result is that when fake samples get close to a mode of \mathcal{P}_t , they move towards the mode. And then get stuck there, due to the locality. Because they can not tell from $\nabla_x f^*(x)$ its current mode collapse state or the far way mode missing information. And there is no internal force to move them out of the mode collapse state. They just follow $\nabla_x f^*(x)$ and keep clustered together or vibrate around the mode; or once the entire surface is changing, they follow the entire surface move from one mode to another, or cycling in this manner. This is the practically observed behaviour of mode collapse.

Let's simulate some specific cases for a more intuitive sensation of this phenomenon. Let assume \mathcal{P}_t consists of two Gaussian distributions (A and B) that are distant from each other.

If the current \mathcal{P}_g is uniformly distributed over its restricted support which is close to real Gaussian A, clearly, $\nabla_x f(x)$ of all fake samples will point towards the center of Gaussian A.

If \mathcal{P}_g is a Gaussian with the same standard deviation as Gaussian A, $\nabla_x f(x)$ in the original GANs and Least-Squares GANs shows almost identical behaviors as the uniformly distributed case, which is illustrated in Figure 13. In Fisher GANs, if $\mu(x)$ is uniform, the case is even worse: a large amount of points that are relatively far from Gaussian A will move away from A. Although in our 1-D case, it is pointing towards B, but this does not necessarily hold in higher dimensions. The third column of Figure 12 simulates the above setting in the two dimensional case, and the samples tend to move towards the nearby mode.

As a summary, in the overlapping and continuous case, though $\nabla_x f^*(x)$ indeed carries information about \mathcal{P}_t , $\nabla_x f^*(x)$ based updating turns out to be a local-greedy strategy, which is still unfavorable and is a fundamental cause of mode collapse in traditional GANs.

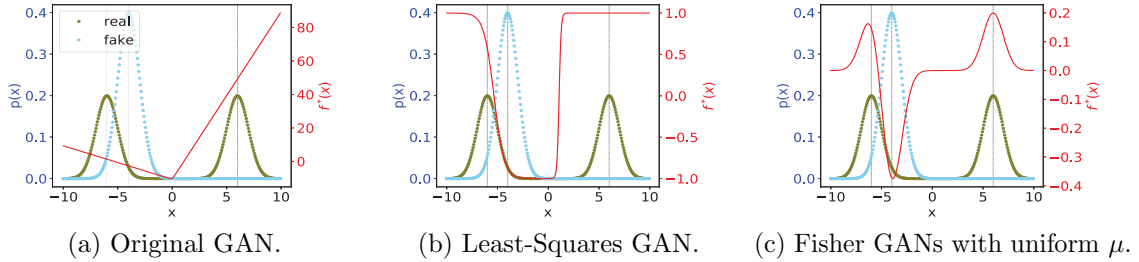


Figure 13: The source of mode collapse. In traditional GANs, $f^*(x)$ is a function of the local densities $\mathcal{P}_g(x)$ and $\mathcal{P}_t(x)$ and is usually an increasing function of $\mathcal{P}_t(x)$ and decreasing function of $\mathcal{P}_g(x)$. When fake samples get close to a mode of \mathcal{P}_t , they will follow $\nabla_x f^*(x)$ and move towards the mode, and then keep clustered together or vibrate around the mode; or once the entire surface is changing, they follow the entire surface move from one mode to another, or cycling in this way.

7.6 Adversarial Activation Maximization

Zhou et al. (2018) proposed the *adversarial activation maximization* understanding for the training of unregularized GANs, which appears to be another perspective because it is talking about the activation of a neuron, but its essence is basically the same as our value surface understanding.

Activation maximization is a traditional technique for visualizing or understanding the neuron(s) in pretrained neural networks. However, the maximized activation of a neuron by itself is not guaranteed to be a valid sample (i.e., not necessarily of high quality), and can be noise, which is also often regarded as a fake sample or adversarial example.

In unregularized GANs, the generator plays the role of doing activation maximization, while the discriminator plays the role of differentiating the fake or adversarial samples, preventing them from getting their desired high activation, and thus ensures the high-activation is achieved by high-quality samples that strongly confuse the discriminator.

With the adversarial training between the generator and discriminator, the adversarial activation maximization process helps solve the issue in vanilla activation maximization, and achieve valid high-activation and the generation of new or realistic samples.

Adversarial activation maximization is interesting, but we have to highlight that it is just another understanding. It does not change the fact that unregularized GANs do not guarantee its convergence. But, indeed, it helps understand how unregularized GANs work in practice and what are their limitations (i.e., the process may fail) from another perspective.

And actually, activation maximization and adversarial activation maximization can be easily understood from the value surface perspective, which means the two perspectives are, in a sense, equivalent, or the value surface perspective is more sophisticated:

- High-activation can be noise / adversarial sample:
 - $f(x') = f(x)$ does not imply $x' = x$;

- $f(x)$ is high for all $x \in \mathcal{S}_t$ does not imply: if $f(x')$ is high, then $x' \in \mathcal{S}_t$.
- The process may fail:
 - It is not guaranteed to have a path from x' to some $x \in \mathcal{S}_t$ with increasing $f(x)$.
- Adversarial training helps ensure high-quality:
 - If $x' \notin \mathcal{S}_t$ and the discriminator can tell the difference, then $f(x')$ will not be high.

8. The Envelope Theorem Perspective: the Essence of Convergence

Here, we explain the gradient issues from the perspective of the envelope theorem. The envelope theorem (Milgrom and Segal, 2002) is a classic result about the differentiation properties of a (constrained) optimization problem.

8.1 The Envelope Theorem

Let the parameter of the generator be θ and the parameter of discriminator be ϑ . $J_D(\theta, \vartheta) = \mathbb{E}_{z \sim \mathcal{P}_z}[\phi(f_\vartheta(g_\theta(z)))] + \mathbb{E}_{x \sim \mathcal{P}_t}[\varphi(f_\vartheta(x))]$. Consider the problem

$$J(\theta) = \arg \min_{\vartheta} J_D(\theta, \vartheta) \quad s.t. \quad s(\theta, \vartheta) \leq 0. \quad (28)$$

The Lagrangian dual problem is given by

$$L(\theta, \vartheta, \lambda) = J_D(\theta, \vartheta) + \lambda \cdot s(\theta, \vartheta), \quad (29)$$

where λ is the Lagrange multiplier.

Let ϑ^* and λ^* together be the solution that minimizes the objective function $L(\theta; \vartheta, \lambda)$.

According to the envelope theorem, if J and L are *continuously differentiable*, we have that

$$\frac{\partial J(\theta)}{\partial \theta} = \frac{\partial L(\theta, \vartheta, \lambda)}{\partial \theta} \Big|_{\vartheta=\vartheta^*, \lambda=\lambda^*} = \frac{\partial L(\theta; \vartheta^*, \lambda^*)}{\partial \theta} = \frac{\partial J_D(\theta; \vartheta^*)}{\partial \theta} + \lambda^* \cdot \frac{\partial s(\theta; \vartheta^*)}{\partial \theta}. \quad (30)$$

8.2 Unregularized GANs

As an illustrative sample, we first consider the following setting: let \mathcal{P}_g be a distribution on two points a and $1+a$ in \mathbb{R} with probability of p and $1-p$, respectively. And the target distribution is evenly distributed on points 0 and 1. Here a and p are the learnable parameters of the generator, and a currently equals 0, which means \mathcal{P}_g and \mathcal{P}_t are totally overlapped.

In this setting, we allow the generator to directly change the probability distribution indicated by p and also the location of samples indicated by a .

Note that $J_D(a, p, \vartheta) = p \cdot \phi(f_\vartheta(a)) + (1-p) \cdot \phi(f_\vartheta(1+a)) + 0.5 \cdot \varphi(f_\vartheta(0)) + 0.5 \cdot \varphi(f_\vartheta(1))$.

For unregularized GANs, we know that, theoretically, $f_{\vartheta^*}(x)$ is only defined on the two or four points 0 and 1, a and $1-a$. In any case, $\frac{\partial f_{\vartheta^*}(x)}{\partial x}$ is undefined for all points. And finite value of $f_{\vartheta^*}(x)$ requires $a=0$. If $a \neq 0$, then $|f_{\vartheta^*}(x)| = \infty$ for all these four points.

Now let's consider the gradient of J , applying the envelope theorem:

$$\begin{aligned}\frac{\partial J(a, p)}{\partial a} &= \frac{\partial J_D(a, p; \vartheta^*)}{\partial a} = p \frac{\partial \phi(f_{\vartheta^*}(a))}{\partial f_{\vartheta^*}(a)} \frac{\partial f_{\vartheta^*}(a)}{\partial a} + (1-p) \frac{\partial \phi(f_{\vartheta^*}(1+a))}{\partial f_{\vartheta^*}(1+a)} \frac{\partial f_{\vartheta^*}(1+a)}{\partial(1+a)}; \\ \frac{\partial J(a, p)}{\partial p} &= \frac{\partial J_D(a, p; \vartheta^*)}{\partial p} = \phi(f_{\vartheta^*}(a)) - \phi(f_{\vartheta^*}(1+a)).\end{aligned}\quad (31)$$

Because there is no constraint or regularization, we ignore the term $\lambda^* \cdot \frac{\partial s(a, p; \vartheta^*)}{\partial p}$.

The $\frac{\partial J(a, p)}{\partial p}$ means that: if $a = 0$, which leads to well-defined $f_{\vartheta^*}(x)$, p has a well-defined gradient; if $a \neq 0$, then the gradient of p is exceptional. However, evidenced by $\frac{\partial J(a, p)}{\partial a}$, its gradient for a is always undefined, because $\frac{\partial f_{\vartheta^*}(x)}{\partial x}$ is always undefined.

We understand the above analysis as:

- The undefined gradient with respect to a stems from the fact that $J(a, p)$ as a function of a is actually not continuously differentiable (by contrast, Wasserstein distance would be continuously differentiable), i.e., envelope theorem is actually inapplicable to the setting.
- The well-defined gradient with respect to the density or probability p is interesting, and it reveals that a fundamental limitation of the GANs framework, i.e., it is sample-based because the discriminator takes a sample as input. If GANs is somehow density-based or has direct access to the probability parameters, it might be applicable in more cases.
- In this prototype, p is an explicit parameter in the objective function, hence it might be optimized. However, in practice, the p is usually implicitly given by the different amounts of samples in different locations. Hence, the gradient from J , in practice, also can not pass to p . Because it needs to pass via $\frac{\partial f_{\vartheta^*}(x)}{\partial x} \cdot \frac{\partial x}{\partial p}$ and $\frac{\partial f_{\vartheta^*}(x)}{\partial x}$ is not well-defined.

As a summary, for unregularized GANs, it is common that the overall objective J (the one that is already fully optimized over the discriminator or f , playing the role as a distance metric between the real and fake distributions to guide the optimization of the generator) is not differentiable with respect to the location of samples, which leads to the undefined gradients. And unfortunately, in the current sample-based GANs formulation, where the discriminator takes a sample as input, the gradient must be passed via $\frac{\partial f_{\vartheta^*}(x)}{\partial x}$. The above two combined together makes GANs sometimes theoretically not optimizable.

So, given the fact the current GANs formulation is sample-based and the gradient must be passed via $\frac{\partial f_{\vartheta^*}(x)}{\partial x}$, we maybe should switch to sample-based distance metrics, e.g., optimal transport based metric like Wasserstein distance or these implicitly implied by LGANs.

For the fully overlapped case, J should also have well-defined gradients for the parameters that change the location of samples. However, the underlying objective of J is convex with respect to \mathcal{P}_g does not imply the model of J is convex with respect to the generator's parameter θ . And as a matter of fact, we have already known that the gradients from J with respect to samples in unregularized GANs only reflect the local information and tend to lead to model collapse. So, clearly, well-defined gradients or optimizable is not a sufficient condition for convergence. The key may lie in the (big) gap between sample-based optimization and density-based distance metric.

8.3 Wasserstein Distance with Compact Dual

Arjovsky et al. (2017) has already provided the envelope theorem based analysis for the KR duality of Wasserstein distance. Here, we will analyse our newfound compact dual of Wasserstein distance to gain a deeper understanding on the essence of convergence of GANs.

For Wasserstein distance with the compact dual, to make the analysis even simple, we consider the following case: let \mathcal{P}_g be a delta distribution at θ in \mathbb{R} with $\theta < 1$, while \mathcal{P}_t is a delta distribution at 1. Then $J_D(\theta, \vartheta) = f_\vartheta(1) - f_\vartheta(\theta)$ and the constraint is $f_\vartheta(1) - f_\vartheta(\theta) - (1 - \theta) \leq 0$. We know that for the optimal $f_{\vartheta^*}(x)$, it has $f_{\vartheta^*}(\theta) = f_{\vartheta^*}(1) - 1 + \theta$. Due to the free offset property of Wasserstein distance, we further assume $f(1) = 1$ without loss of generality. Then the problem is simplified as: $J_D(\theta, \vartheta) = 1 - f_\vartheta(\theta)$ with the constraint $f_\vartheta(\theta) - \theta \leq 0$.

Note that, $f_{\vartheta^*}(\theta)$ is only necessarily defined on θ and 1, and $\frac{\partial f_{\vartheta^*}(\theta)}{\partial x}$ is also undefined for all sample points.

The Lagrangian dual problem is given by

$$L(\theta, \vartheta, \lambda) = 1 - f_\vartheta(\theta) + \lambda \cdot (f_\vartheta(\theta) - \theta). \quad (32)$$

From the envelope theorem, we have

$$\begin{aligned} \frac{\partial J(\theta)}{\partial \theta} &= \frac{\partial L(\theta; \vartheta^*, \lambda^*)}{\partial \theta} = -\frac{\partial f_{\vartheta^*}(\theta)}{\partial \theta} + \lambda^* \cdot \frac{\partial(f_{\vartheta^*}(\theta) - \theta)}{\partial \theta} \\ &= -\frac{\partial f_{\vartheta^*}(\theta)}{\partial \theta} + (\lambda^* \cdot \frac{\partial f_{\vartheta^*}(\theta)}{\partial \theta} - \lambda^*) = (\lambda^* - 1) \cdot \frac{\partial f_{\vartheta^*}(\theta)}{\partial \theta} - \lambda^*. \end{aligned} \quad (33)$$

By first order optimality condition of the optimal ϑ^* and λ^* , we have:

$$\begin{aligned} \frac{\partial L}{\partial \vartheta^*} &= (\lambda^* - 1) \frac{\partial f_{\vartheta^*}(\theta)}{\partial \vartheta^*} = 0, \\ \frac{\partial L}{\partial \lambda^*} &= f_{\vartheta^*}(\theta) - \theta = 0. \end{aligned} \quad (34)$$

We can notice that $\lambda^* = 1$ is one of its solutions. Applying it to Eq. (33), we get $\frac{\partial J(\theta)}{\partial \theta} = 1$, which is reasonable and true, and more importantly, we notice that the sample gradient $\frac{\partial f_{\vartheta^*}(\theta)}{\partial \theta}$, though is still undefined, it is eliminated by the gradient from the constraint.

In summary, for Wasserstein distance with compact dual, because the parameter of the generator is also in the constraint(s). When applying the envelope theorem, it is necessary to consider the gradient from the constraint(s). And it seems the undefined gradient $\frac{\partial f_{\vartheta^*}(\theta)}{\partial \theta}$ will be somehow eliminated. And the actual gradient, which really takes effect, may come from the remaining part of the gradient from the constraint(s). See, by first order optimality condition Eq (34), it holds $f_{\vartheta^*}(\theta) = \theta$.

8.4 With Lipschitz Condition or Lipschitz Regularization

WGANS with Wasserstein distance in KR duality does not involve the parameters of the generator in the constraint of the optimization problem (has the Lipschitz condition). LGANs penalizes the Lipschitz constant, which also does not involve the parameters of the generator

in the constraints. So, as long as J is continuously differentiable, the envelope theorem is applicable and we have

$$\begin{aligned}\frac{\partial J(\theta; \vartheta^*)}{\partial \theta} &= \frac{\partial J_D(\theta; \vartheta^*)}{\partial \theta} \\ &= \frac{\partial \mathbb{E}_{z \sim \mathcal{P}_z} [\phi(f_{\vartheta^*}(g_\theta(z)))] + \mathbb{E}_{x \sim \mathcal{P}_t} [\psi(f_{\vartheta^*}(x))]}{\partial \theta} \\ &= \frac{\partial \mathbb{E}_{z \sim \mathcal{P}_z} [\phi(f_{\vartheta^*}(g_\theta(z)))]}{\partial \theta}.\end{aligned}\tag{35}$$

With the Lipschitz condition or penalizing the Lipschitz constant, the objective is intuitively continuously differentiable with respect to \mathcal{P}_g . If the generative function is continuous and locally Lipschitz with respect to its parameter θ , then the overall objective J should be continuously differentiable with respect to the generator's parameter θ .

In fact, we have shown in the paper that Lipschitz continuity with respect to Euclidean distance results in excellent gradient properties in terms of $\frac{\partial f_{\vartheta^*}(g_\theta(z))}{\partial g_\theta(z)}$. So, if the generator is continuously differentiable with respect to θ , i.e., if $\frac{\partial g_\theta(z)}{\partial \theta}$ is well-defined, then $\frac{\partial \phi(f_{\vartheta^*}(g_\theta(z)))}{\partial \theta}$ and hence Eq. (35) is well-defined, and is expected to well behave.

8.5 Sample-Based Distribution Estimation

In unregularized GANs, if $\mathcal{S}_g \cup \mathcal{S}_t$ does not cover the whole input space, $f^*(x)$ would be undefined outside $\mathcal{S}_g \cup \mathcal{S}_t$. As a result, the gradient for samples, which are isolated or at the boundary, can be problematic. This also leads to a more serious problem: it prevents samples in one region from adapting to other regions and consequently prevents \mathcal{P}_g from converging to \mathcal{P}_t .

From the above envelope theorem based analysis, one could notice that the sample-based distribution estimation (i.e., implicit density models, which GANs belong to) is quite different from explicit density estimation (where the distribution is directly parameterized).

When directly parameterizing the distribution (which is usually intractable), the density of sample points can be directly optimized, while in sample-based distribution estimation, to increase or decrease the density of a certain point, it requires modifying samples from being the support of one probability to another.

This is why cases with totally-overlapped distributions also suffer from the faulty gradient. Such a conclusion also reminds us that we need to be cautious when understanding or proving GANs at the distribution level, because with the discriminator taking a sample as input, GANs is actually sample-based.

8.5.1 THE CHOICE OF TARGET POINT OF GENERATOR IN THE LEAST-SQUARES GANs

The notion that GANs is sample-based also explains a weird phenomenon about the optimal target point of the generator in the Least-Squares GANs. Note that the generator loss metric of the Least-Squares GANs is $(x - \gamma)^2$ and the γ derived from the Pearson χ^2 divergence is 0 in the case $\alpha = -1$ and $\beta = 1$. But, in practice, $\gamma = 1$ usually works better than $\gamma = 0$.

In Least-Squares GANs, $f^*(x) \in [-1, 0]$ means $\mathcal{P}_g(x) \geq \mathcal{P}_t(x)$. If the target γ equals 0, samples from points where $\mathcal{P}_g(x) \geq \mathcal{P}_t(x)$ (i.e., where the current $f^*(x) \in [-1, 0]$) cannot be adapted to locations where $\mathcal{P}_g(x) \leq \mathcal{P}_t(x)$ (i.e., where $f^*(x) \in [0, 1]$). As a result, \mathcal{P}_g would never converge to \mathcal{P}_t . And γ actually needs to be the same as β to avoid this issue.

The arguments above can actually be more general: In sample-based optimization, if $f^*(x)$ is a monotonically increasing function of $\mathcal{P}_t(x)$ and a monotonically decreasing function of $\mathcal{P}_g(x)$, this issue is generally inevitable, and the target point has to equal to the maximum possible value of $f^*(x)$ to avoid the above mentioned problem.

9. Related Work

We have shown that Lipschitz regularization is able to ensure the convergence for a family of GANs objectives, which is not limited to the Wasserstein distance. For example, Lipschitz regularization is also introduced to the original GANs (Miyato et al., 2018; Kodali et al., 2017; Fedus et al., 2018), achieving improvements in the quality of generated samples. As a matter of fact, the original GANs loss metric $\phi(x) = \varphi(-x) = -\log(\sigma(-x))$ is a special case of our LGANs. Thus, our analysis explains why and how Lipschitz regularization works under the original GANs objective.

Farnia and Tse (2018) also provided some analysis on how the f -divergence would behave when combined with Lipschitz continuity condition, i.e., resulting in a new well-behaving distance metric. However, their analysis is limited to the symmetric f -divergence.

Fedus et al. (2018) argued that divergence is not the primary guide of the training of GANs. However, they thought that the original GANs with a non-saturating generator loss metric somehow works. According to our analysis, the original GANs and more generally all unregularized GANs have no guarantee on its convergence, no matter what generator loss metric it adopts. And we have also provided a reasonable explanation on how these traditional GANs, who do not guarantee its convergence, work in practice.

Unterthiner et al. (2018) provided some arguments on the unreliability/issues of $\nabla_x f^*(x)$ in traditional GANs, which motivates their proposal of Coulomb GANs. However, the arguments in their paper are not thorough. By contrast, we provided a systematic and thorough study over the gradient issues in traditional GANs. And we have also accordingly proposed a new solution, i.e., the Lipschitz regularized GANs, which shall be a strong rival to their proposed Coulomb GANs, with superior efficiency and sample quality.

Some work studies the suboptimal convergence of GANs (Mescheder et al., 2017, 2018; Arora et al., 2017; Liu et al., 2017; Farnia and Tse, 2018; Zhang et al., 2018), which is another important direction for theoretically understanding of GANs. Despite the fact that the behavior of suboptimal can be different from the one of optimal, we think it should, first of all, well-behave under the optimum condition.

Researchers found that applying Lipschitz continuity condition to the generator also benefits the quality of generated samples (Zhang et al., 2019; Odena et al., 2018). And Qi (2020) studied the Lipschitz condition from the perspective of loss-sensitive with a Lipschitz data

density assumption. However, these are actually different branches and not necessarily related. Their discussions or comparisons are hence out of the scope of this paper.

There exist generative models that do not use $\nabla_x f^*(x)$ as the primal guide of the generator's update. For example, Sanjabi et al. (2018) updates the generator according to the optimal transport plan. However, the sample quality of this branch of works is currently limited.

There are also GANs where the discriminator's input is not a single sample. For example, Li et al. (2017) requires a batch of samples, simulating the distribution. And Jolicoeur Martineau (2018) requires simultaneously inputting one real sample and one fake sample. Our analysis does not directly apply to their models, but the similar spirit, i.e., analysing whether the gradient flaw between the generator and the discriminator is effective, assuming the optimal discriminator, can be used to analyse their models.

10. Conclusion

In this paper, we studied the training instability issue of GANs from the perspective of the optimal discriminative function. By raising the concept of the gradient uninformative-ness issue, we showed that unregularized GANs, where there is no regularization in the discriminative function space, commonly does not guarantee its convergence, which can be a fundamental cause of its training instability.

We then developed Lipschitz regularized GANs as a general solution to the gradient uninformative-ness issue and showed its various favorable theoretical properties. Verifying these theoretical properties raises the requirement of strict Lipschitz regularization implementation. Thereupon, we studied the existing Lipschitz regularization implementations and found their underlying issues, and then naturally proposed max gradient norm penalty and its augmented Lagrangian version as alternatives. Then, we verified the theoretical properties of LGANs and showed its consistently superior performance over WGANs.

To provide a more comprehensive understanding of the training instability issue of GANs, we further studied the gradient issues of traditional GANs, with unregularized GANs as their representative, and these gradient issues' practical behaviors, from which we learn the mechanisms of how traditional GANs works in practice and found a fundamental cause of mode collapse, i.e., the locality of $f^*(x)$ and the gradients.

Finally, to reveal the essence to convergence guarantee of GANs, we studied the gradient flow between the generator and the discriminator with the help of the envelope theorem, and found that the key issue might lie in the sample-based nature of the current GANs framework because the discriminator takes a sample as input and the information interchange between the generator and the discriminator must be passed via $\nabla_x f^*(x)$.

Acknowledgements

This work is sponsored by APEX-YITU Joint Research Program. The authors thank the support of National Natural Science Foundation of China (61702327, 61772333, 61632017), Shanghai Sailing Program (17YF1428200). Zhiming Zhou personally thanks Jiadong Liang

and Dachao Lin for a lot of helpful discussions on the central theorems and proofs of LGANs. Zhiming Zhou personally thanks Yuxuan Song and Lantao Yu for their fruitful discussions on the initial idea of LGANs. Zhiming Zhou personally thanks Hongwei Wang and Weinan Zhang for their suggestions and helps on the writing and presentation. Zhiming Zhou personally thanks Yong Yu for his unreserved support all these years. Zhihua Zhang has been supported by Beijing Municipal Commission of Science and Technology under Grant No. 181100008918005 and by Beijing Academy of Artificial Intelligence (BAAI).

Appendix A. Proofs

A.1 Proof of the Compact Dual Form of Wasserstein Distance

We here provide a proof for our new dual form of Wasserstein distance, i.e., Eq. (4). We will still use $W_1(\mathcal{P}_g, \mathcal{P}_t)$ to denote the primal form of Wasserstein distance, while we will use $W_{\text{KR}}(\mathcal{P}_g, \mathcal{P}_t)$ to denote its Kantorovich-Rubinstein (KR) duality and use $W_{\text{KRC}}(\mathcal{P}_g, \mathcal{P}_t)$ to denote the proposed compact dual form.

Theorem 8 *Given $W_1(\mathcal{P}_g, \mathcal{P}_t) = W_{\text{KR}}(\mathcal{P}_g, \mathcal{P}_t)$, we have $W_1(\mathcal{P}_g, \mathcal{P}_t) = W_{\text{KRC}}(\mathcal{P}_g, \mathcal{P}_t)$.*

Proof

1. For any f that satisfies “ $f(x) - f(y) \leq d(x, y), \forall x, \forall y$ ”, it must satisfy “ $f(x) - f(y) \leq d(x, y), \forall x \in \mathcal{S}_t, \forall y \in \mathcal{S}_g$ ”. Thus, $W_{\text{KR}}(\mathcal{P}_g, \mathcal{P}_t) \leq W_{\text{KRC}}(\mathcal{P}_g, \mathcal{P}_t)$.
2.
 - Let $F_{\text{KRC}} = \{f \mid f(x) - f(y) \leq d(x, y), \forall x \in \mathcal{S}_g, \forall y \in \mathcal{S}_t\}$.
 - Let $A = \{(x, y) \mid x \in \mathcal{S}_g, y \in \mathcal{S}_t\}$ and $I_A = \begin{cases} 1, & (x, y) \in A; \\ 0, & \text{otherwise} \end{cases}$.
 - Let A^c denote the complementary set of A and define I_{A^c} accordingly.
 - $\forall \pi \in \Pi(\mathcal{P}_g, \mathcal{P}_t)$, we have the following:

$$\begin{aligned} W_{\text{KRC}}(\mathcal{P}_g, \mathcal{P}_t) &= \sup_{f \in F_{\text{KRC}}} \mathbb{E}_{x \sim \mathcal{P}_g} [f(x)] - \mathbb{E}_{x \sim \mathcal{P}_t} [f(x)] \\ &= \sup_{f \in F_{\text{KRC}}} \mathbb{E}_{(x,y) \sim \pi} [f(x) - f(y)] \\ &= \sup_{f \in F_{\text{KRC}}} \mathbb{E}_{(x,y) \sim \pi} [(f(x) - f(y)) I_A] + \mathbb{E}_{(x,y) \sim \pi} [(f(x) - f(y)) I_{A^c}] \\ &= \sup_{f \in F_{\text{KRC}}} \mathbb{E}_{(x,y) \sim \pi} [(f(x) - f(y)) I_A] \\ &\leq \mathbb{E}_{(x,y) \sim \pi} [d(x, y) I_A] \\ &\leq \mathbb{E}_{(x,y) \sim \pi} [d(x, y)]. \end{aligned}$$

- That is, $W_{\text{KRC}}(\mathcal{P}_g, \mathcal{P}_t) \leq \mathbb{E}_{(x,y) \sim \pi} [d(x, y)], \forall \pi \in \Pi(\mathcal{P}_g, \mathcal{P}_t)$.
 - Thereby, $W_{\text{KRC}}(\mathcal{P}_g, \mathcal{P}_t) \leq \inf_{\pi \in \Pi(\mathcal{P}_g, \mathcal{P}_t)} \mathbb{E}_{(x,y) \sim \pi} [d(x, y)] = W_1(\mathcal{P}_g, \mathcal{P}_t)$.
3. Combining (i) and (ii), we have $W_{\text{KR}}(\mathcal{P}_g, \mathcal{P}_t) \leq W_{\text{KRC}}(\mathcal{P}_g, \mathcal{P}_t) \leq W_1(\mathcal{P}_g, \mathcal{P}_t)$. Given $W_{\text{KR}}(\mathcal{P}_g, \mathcal{P}_t) = W_1(\mathcal{P}_g, \mathcal{P}_t)$, we have $W_{\text{KR}}(\mathcal{P}_g, \mathcal{P}_t) = W_{\text{KRC}}(\mathcal{P}_g, \mathcal{P}_t) = W_1(\mathcal{P}_g, \mathcal{P}_t)$.

■

A.2 Proof of Theorem 2

Let x, y be two random vectors such that $x \sim \mathcal{P}_g, y \sim \mathcal{P}_t$. Assume $\mathbb{E}_{x \sim \mathcal{P}_g} \|x\| < \infty$ and $\mathbb{E}_{y \sim \mathcal{P}_t} \|y\| < \infty$. Let $\mathfrak{G}(f) = \mathbb{E}_{x \sim \mathcal{P}_g} [\phi(f(x))] + \mathbb{E}_{y \sim \mathcal{P}_t} [\varphi(f(y))]$.

Lemma 9 Let ϕ and φ be two convex functions, whose domains are both \mathbb{R} . Assume f is subject to $k(f) \leq k_0$. If there is $a_0 \in \mathbb{R}$ such that $\phi'(a_0) + \varphi'(a_0) = 0$, then we have a lower bound for $\mathfrak{G}(f)$.

Proof

Since ϕ, φ are convex functions, we have

$$\begin{aligned}
\mathfrak{G}(f) &= \mathbb{E}_{x \sim \mathcal{P}_g}[\phi(f(x))] + \mathbb{E}_{y \sim \mathcal{P}_t}[\varphi(f(y))] \\
&\geq \mathbb{E}_{x \sim \mathcal{P}_g}[\phi'(a_0)(f(x) - a_0) + \phi(a_0)] + \mathbb{E}_{y \sim \mathcal{P}_t}[\varphi'(a_0)(f(y) - a_0) + \varphi(a_0)] \\
&= \phi'(a_0)\mathbb{E}_{x \sim \mathcal{P}_g}[f(x)] + \varphi'(a_0)\mathbb{E}_{y \sim \mathcal{P}_t}[f(y)] + C_0 \\
&= (\phi'(a_0) + \varphi'(a_0))\mathbb{E}_{x \sim \mathcal{P}_g}[f(x)] + \varphi'(a_0)(\mathbb{E}_{y \sim \mathcal{P}_t}[f(y)] - \mathbb{E}_{x \sim \mathcal{P}_g}[f(x)]) + C_0 \\
&= k(f)\varphi'(a_0)(\mathbb{E}_{y \sim \mathcal{P}_t}\left[\frac{f(y)}{k(f)}\right] - \mathbb{E}_{x \sim \mathcal{P}_g}\left[\frac{f(x)}{k(f)}\right]) + C_0 \\
&\geq -k(f)\varphi'(a_0)W_1(\mathcal{P}_g, \mathcal{P}_t) + C_0 \\
&\geq -k_0\varphi'(a_0)W_1(\mathcal{P}_g, \mathcal{P}_t) + C_0.
\end{aligned} \tag{36}$$

Therefore, we get the lower bound. ■

Lemma 10 Let ϕ and φ be two convex functions, whose domains are both \mathbb{R} . Assume f is subject to $k(f) \leq k_0$.

- If there exists $a_1 \in \mathbb{R}$ such that $\phi'(a_1) + \varphi'(a_1) > 0$, then we have: if $f(0) \rightarrow +\infty$, then $\mathfrak{G}(f) \rightarrow +\infty$;
- If there exists $a_2 \in \mathbb{R}$ such that $\phi'(a_2) + \varphi'(a_2) < 0$, then we have: if $f(0) \rightarrow -\infty$, then $\mathfrak{G}(f) \rightarrow +\infty$.

Proof

Since ϕ, φ are convex functions, we have

$$\begin{aligned}
\mathfrak{G}(f) &= \mathbb{E}_{x \sim \mathcal{P}_g}[\phi(f(x))] + \mathbb{E}_{y \sim \mathcal{P}_t}[\varphi(f(y))] \\
&\geq \mathbb{E}_{x \sim \mathcal{P}_g}[\phi'(a_1)(f(x) - a_1) + \phi(a_1)] + \mathbb{E}_{y \sim \mathcal{P}_t}[\varphi'(a_1)(f(y) - a_1) + \varphi(a_1)] \\
&= \phi'(a_1)\mathbb{E}_{x \sim \mathcal{P}_g}[f(x)] + \varphi'(a_1)\mathbb{E}_{y \sim \mathcal{P}_t}[f(y)] + C_1 \\
&= (\phi'(a_1) + \varphi'(a_1))\mathbb{E}_{x \sim \mathcal{P}_g}[f(x)] + \varphi'(a_1)(\mathbb{E}_{y \sim \mathcal{P}_t}[f(y)] - \mathbb{E}_{x \sim \mathcal{P}_g}[f(x)]) + C_1 \\
&= (\phi'(a_1) + \varphi'(a_1))\mathbb{E}_{x \sim \mathcal{P}_g}[f(x)] + k(f)\varphi'(a_1)(\mathbb{E}_{y \sim \mathcal{P}_t}\left[\frac{f(y)}{k(f)}\right] - \mathbb{E}_{x \sim \mathcal{P}_g}\left[\frac{f(x)}{k(f)}\right]) + C_1 \\
&\geq (\phi'(a_1) + \varphi'(a_1))\mathbb{E}_{x \sim \mathcal{P}_g}[f(x)] - k(f)\varphi'(a_1)W_1(\mathcal{P}_g, \mathcal{P}_t) + C_1 \\
&\geq (\phi'(a_1) + \varphi'(a_1))(f(0) - k_0\mathbb{E}_{x \sim \mathcal{P}_g}\|x\|) - k_0\varphi'W_1(\mathcal{P}_g, \mathcal{P}_t) + C_1.
\end{aligned}$$

Thus, if $f(0) \rightarrow +\infty$, then $\mathfrak{G}(f) \rightarrow +\infty$. And we can prove the other case symmetrically. ■

Lemma 11 Let ϕ and φ be two convex functions, whose domains are both \mathbb{R} . If ϕ and φ further satisfy the following properties:

- $\phi' \geq 0$ and $\varphi' \leq 0$;
- There exist $a_0, a_1, a_2 \in \mathbb{R}$ such that

$$\phi'(a_0) + \varphi'(a_0) = 0, \quad (37)$$

$$\phi'(a_1) + \varphi'(a_1) > 0, \quad (38)$$

$$\phi'(a_2) + \varphi'(a_2) < 0. \quad (39)$$

Then we have $\mathfrak{G}(f) = \mathbb{E}_{x \sim \mathcal{P}_t}[\phi(f(x))] + \mathbb{E}_{y \sim \mathcal{P}_g}[\varphi(f(y))]$, where f is subject to $k(f) \leq k_0$, has global minima.

That is, $\exists f^*$ such that

- $k(f^*) \leq k_0$;
- $\forall f$ s.t. $k(f) \leq k_0$, we have $\mathfrak{G}(f^*) \leq \mathfrak{G}(f)$.

Proof

According to Lemma 9, $\mathfrak{G}(f)$ has a lower bound, which means $\inf(\mathfrak{G}(f)) > -\infty$. Thus we can get a series of functions $\{f_n\}_{n=1}^\infty$ such that $\lim_{n \rightarrow \infty} \mathfrak{G}(f_n) = \inf(\mathfrak{G}(f))$.

Suppose that $\{r_i\}_{i=1}^\infty$ is the sequence of all rational points in $\text{dom}(f)$. According to Lemma 10, for any $x \in \mathbb{R}$, $\{f_n(x) \mid n \in \mathbb{R}\}$ is bounded. By Bolzano-Weierstrass theorem, there is a subsequence $\{f_{1,n}\}_{n=1}^\infty \subseteq \{f_n\}_{n=1}^\infty$ such that $\{f_{1,n}(r_1)\}_{n=1}^\infty$ converges. And there is a subsequence $\{f_{2,n}\}_{n=1}^\infty \subseteq \{f_{1,n}\}_{n=1}^\infty$ such that $\{f_{2,n}(r_2)\}_{n=1}^\infty$ converges. As for r_i , there is a subsequence $\{f_{i,n}\}_{n=1}^\infty \subseteq \{f_{i-1,n}\}_{n=1}^\infty$ such that $\{f_{i,n}(r_i)\}_{n=1}^\infty$ converges. Then the sequence $\{f_{m,n}\}_{n=1}^\infty$ will converge at $\{r_i\}_{i=1}^m$.

Furthermore, for all $x \in \text{dom}(f)$, $\forall \epsilon > 0$, $\exists r \in \{r_i\}_{n=1}^\infty$ such that $\|x - r\| \leq \frac{\epsilon}{10k_0}$. Then

$$\begin{aligned} & \lim_{m,l,n \rightarrow \infty} |f_{m,n}(x) - f_{l,n}(x)| \\ & \leq \lim_{m,l,n \rightarrow \infty} (|f_{m,n}(x) - f_{m,n}(r)| + |f_{m,n}(r) - f_{l,n}(r)| + |f_{l,n}(r) - f_{l,n}(x)|) \\ & \leq \lim_{m,l,n \rightarrow \infty} \left(\frac{\epsilon}{10} + \frac{\epsilon}{10} + |f_{m,n}(r) - f_{l,n}(r)| \right) = \frac{\epsilon}{5}. \end{aligned} \quad (40)$$

Let $\epsilon \rightarrow 0$, then we get $\lim_{m,l,n \rightarrow \infty} |f_{m,n}(x) - f_{l,n}(x)| = 0$. So, we claim that $\{\{f_{m,n}\}_{n=1}^\infty\}_{m=1}^\infty$ converges at x . Then let $g_m = \lim_{n \rightarrow \infty} f_{m,n}$ and assume $\{g_m\}_{m=1}^\infty$ converges to g .

According to Lemma 10, we know that $\exists C'$ such that $|g_m(0)| \leq C'$, $\forall m \in \mathbb{N}$. Furthermore, because $\phi' \geq 0$ and $\varphi' \leq 0$, we have

$$\begin{aligned} \phi(g_m(x)) & \geq \phi(g_m(0) - k_0\|x\|) \geq \phi(-C' - k_0\|x\|) \\ & \geq \phi'(a_0)(-C' - k_0\|x\| - a_0) + \phi(a_0) \\ & = -k_0\phi'(a_0)\|x\| + C'' \end{aligned} \quad (41)$$

That is, $\phi(g_m(x)) + k_0\phi'(a_0)\|x\| - C'' \geq 0$.

By Fatou's Lemma,

$$\begin{aligned} \mathbb{E}_{x \sim \mathcal{P}_g} [\phi(g(x)) + k_0\phi'(a_0)\|x\| - C''] &= \mathbb{E}_{x \sim \mathcal{P}_g} \lim_{m \rightarrow \infty} [\phi(g_m(x)) + k_0\phi'(a_0)\|x\| - C''] \\ &\leq \liminf_{m \rightarrow \infty} \mathbb{E}_{x \sim \mathcal{P}_g} [\phi(g_m(x)) + k_0\phi'(a_0)\|x\| - C''] \quad (42) \\ &= \liminf_{m \rightarrow \infty} \mathbb{E}_{x \sim \mathcal{P}_g} [\phi(g_m(x))] + \mathbb{E}_{x \sim \mathcal{P}_g} [k_0\phi'(a_0)\|x\| - C''] \end{aligned}$$

It means $\mathbb{E}_{x \sim \mathcal{P}_g} [\phi(g(x))] \leq \liminf_{m \rightarrow \infty} \mathbb{E}_{x \sim \mathcal{P}_g} [\phi(g_m(x))]$.

Similarly, we have $\mathbb{E}_{y \sim \mathcal{P}_t} [\varphi(g(y))] \leq \liminf_{m \rightarrow \infty} \mathbb{E}_{y \sim \mathcal{P}_t} [\varphi(g_m(y))]$.

Note that for any $x, y \in \text{dom}(g)$, $|g(x) - g(y)| \leq \lim_{n \rightarrow \infty} (|g(x) - g_m(x)| + |g_m(x) - g_m(y)| + |g_m(y) - g(y)|) \leq k_0\|x - y\|$. That is, $k(g) \leq k_0$.

Combining these inequalities, we have

$$\begin{aligned} \mathfrak{G}(g) &= \mathbb{E}_{x \sim \mathcal{P}_g} [\phi(g(x))] + \mathbb{E}_{y \sim \mathcal{P}_t} [\varphi(g(y))] \\ &\leq \liminf_{m \rightarrow \infty} \mathbb{E}_{x \sim \mathcal{P}_g} [\phi(g_m(x))] + \liminf_{m \rightarrow \infty} \mathbb{E}_{y \sim \mathcal{P}_t} [\varphi(g_m(y))] \\ &\leq \liminf_{m \rightarrow \infty} (\mathbb{E}_{x \sim \mathcal{P}_g} [\phi(g_m(x))] + \mathbb{E}_{y \sim \mathcal{P}_t} [\varphi(g_m(y))]) \quad (43) \\ &= \inf_{k(f) \leq k_0} \mathfrak{G}(f) \end{aligned}$$

■

Lemma 12 $\mathfrak{T}(f) = \mathbb{E}_{x \sim \mathcal{P}_g} [f(x)] - \mathbb{E}_{y \sim \mathcal{P}_t} [f(y)]$, where f is subject to $k(f) \leq k_0$, has global minima.

Proof It is easy to find that for any $C \in \mathbb{R}$, $\mathfrak{T}(f + C) = \mathfrak{T}(f)$. Similar to the previous lemma, we can get a series of functions $\{f_n\}_{n=1}^{\infty}$ such that $\lim_{n \rightarrow \infty} \mathfrak{T}(f_n) = \inf(\mathfrak{T}(f))$. Without loss of generality, we assume that $f_n(0) = 0, \forall n \in \mathbb{N}^+$. Because $k(f_n) \leq k_0$, we can claim that for any $x \in \mathbb{R}$, $\{f_n(x) | n \in \mathbb{R}\}$ is bounded. Then we can imitate the method used in Lemma 11 and find the optimal function f^* such that $\mathfrak{T}(f^*) = \inf_{k(f) \leq k_0} \mathfrak{T}(f)$. ■

Lemma 13 Let ϕ and φ be two convex functions, whose domains are both \mathbb{R} . If we further suppose that the support sets \mathcal{S}_g and \mathcal{S}_t are bounded. Then if ϕ and φ satisfy the following properties:

- $\phi' \geq 0$ and $\varphi' \leq 0$;
- There is $a_0 \in \mathbb{R}$ such that $\phi'(a_0) + \varphi'(a_0) = 0$.

We have $\mathfrak{G}(f) = \mathbb{E}_{x \sim \mathcal{P}_g} [\phi(f(x))] + \mathbb{E}_{y \sim \mathcal{P}_t} [\varphi(f(y))]$, where f is subject to $k(f) \leq k_0$, has global minima.

That is, $\exists f^*$ such that

- $k(f^*) \leq k_0$
- $\forall f \text{ s.t. } k(f) \leq k_0, \text{ we have } \mathfrak{G}(f^*) \leq \mathfrak{G}(f).$

Proof We have proved most conditions in previous lemmas. And we only have to consider the condition that:

- for any $x \in \mathbb{R}$, $\phi'(x) + \varphi'(x) \geq 0$ and there exists a_1 such that $\phi'(a_1) + \varphi'(a_1) > 0$;
- for any $x \in \mathbb{R}$, $\phi'(x) + \varphi'(x) \leq 0$ and there exists a_2 such that $\phi'(a_2) + \varphi'(a_2) < 0$.

Without loss of generality, we assume that $\phi'(x) + \varphi'(x) \geq 0$ for all x and there exists a_1 such that $\phi'(a_1) + \varphi'(a_1) > 0$. Then we know $\forall x \leq a_0$, $\phi'(x) + \varphi'(x) = 0$, which leads to $\forall x \leq a_0$, $\phi'(x) = -\varphi'(x)$. Thus, for any $x \leq a_0$, $0 \leq \phi''(x) = -\varphi''(x) \leq 0$, which means $\forall x \leq a_0$, $\phi(x) = -\varphi(x) = tx$, $t \geq 0$.

Similar to the previous lemmas, we can get a series of functions $\{f_n\}_{n=1}^\infty$ such that $\lim_{n \rightarrow \infty} \mathfrak{G}(f_n) = \inf(\mathfrak{G}(f))$. Actually we can assume that for all $n \in \mathbb{N}^+$, there is $f_n(0) \in [-C, C]$, where C is a constant. In fact, it is not difficult to find $f_n(0) \leq C$ with Lemma 10. On the other hand, when $C > k_0 \cdot \text{diam}(\mathcal{S}_t \cup \mathcal{S}_g) + a_0$, then: if $f(0) < -C$, we have $f(x) < a_0$ for all $x \in \mathcal{S}_g \cup \mathcal{S}_t$. In this case, $\mathfrak{G}(f) = \mathfrak{G}(f - f(0) - C)$. This is the reason we can assume $f_n(0) \in [-C, C]$. Because $k(f_n) \leq k_0$, we can assert that for any $x \in \mathbb{R}$, $\{f_n(x) | n \in \mathbb{R}\}$ is bounded. So we can imitate the method used in Lemma 11 and find the optimal function f^* such that $\mathfrak{G}(f^*) = \inf_{k(f) \leq k_0} \mathfrak{G}(f)$. ■

Lemma 14 (Theorem 2, Existence) *Under the same assumption of Lemma 13, we have $\mathfrak{F}(f) = \mathbb{E}_{x \sim \mathcal{P}_g}[\phi(f(x))] + \mathbb{E}_{y \sim \mathcal{P}_t}[\varphi(f(y))] + \frac{\rho}{2}k(f)^\alpha$ with $\rho > 0$ and $\alpha > 1$ has global minima.*

Proof When $k(f) = \infty$, it is trivial that $\mathfrak{F}(f) = \infty$. And when $k(f) < \infty$, combining Lemma 9, we have $\mathfrak{F}(f) = \mathfrak{G}(f) + \frac{\rho}{2}k(f)^\alpha \geq -k(f)\varphi'(a_0)W_1(\mathcal{P}_t, \mathcal{P}_g) + \frac{\rho}{2}k(f)^\alpha$. When $\rho > 0$ and $\alpha > 1$, the right term is a convex function about $k(f)$, it has a lower bound. So we can find a sequence $\{f_n\}_{n=1}^\infty$ such that $\lim_{n \rightarrow \infty} \mathfrak{F}(f_n) = \inf_{f \in \text{dom } \mathfrak{F}} \mathfrak{F}(f)$. It is no doubt that there exists a constant C such that $k(f_n) \leq C$ for all f_n . Then it is not difficult to show for any point x , $\{f_n(x)\}$ is bounded. So we can imitate the method used in main theorem to find the sequence $\{g_n\}$ such that $\{g_n\} \subseteq \{f_n\}$ and $\{g_n\}_{n=1}^\infty$ converge at every point x . Suppose $\lim_{n \rightarrow \infty} g_n = g$, then by Fatou's Lemma, we have $\mathfrak{G}(g) \leq \underline{\lim}_{n \rightarrow \infty} \mathfrak{G}(g_n)$.

Next, We prove that $k(g) \leq \underline{\lim}_{n \rightarrow \infty} k(g_n)$. If the claim holds, then $\mathfrak{F}(g) = \mathfrak{G}(g) + \frac{\rho}{2}k(g)^\alpha \leq \underline{\lim}_{n \rightarrow \infty} \mathfrak{G}(g_n) + \underline{\lim}_{n \rightarrow \infty} \frac{\rho}{2}k(g_n)^\alpha \leq \underline{\lim}_{n \rightarrow \infty} (\mathfrak{G}(g_n) + \frac{\rho}{2}k(g_n)^\alpha) = \inf \mathfrak{F}(f)$. Thus, the global minima exists. In fact, if $k(g) > \underline{\lim}_{n \rightarrow \infty} k(g_n)$, then there exist x, y such that $\frac{|g(x)-g(y)|}{\|x-y\|} \geq \underline{\lim}_{n \rightarrow \infty} k(g_n) + \epsilon \geq \underline{\lim}_{n \rightarrow \infty} \frac{|g_n(x)-g_n(y)|}{\|x-y\|} + \epsilon$. i.e. $|g(x)-g(y)| \geq \underline{\lim}_{n \rightarrow \infty} |g_n(x)-g_n(y)| + \epsilon \|x-y\| = |g(x)-g(y)| + \epsilon \|x-y\| > |g(x)-g(y)|$. The contradiction tells us that $k(g) \leq \underline{\lim}_{n \rightarrow \infty} k(g_n)$. ■

Lemma 15 (Theorem 2, Uniqueness) *Let ϕ and φ be two convex functions, whose domains are both \mathbb{R} . If ϕ or φ is strictly convex, then the minimizer of $\mathfrak{F}(f) = \mathbb{E}_{x \sim \mathcal{P}_g}[\phi(f(x))] + \mathbb{E}_{y \sim \mathcal{P}_t}[\varphi(f(y))] + \frac{\rho}{2}k(f)^\alpha$ with $\rho > 0$ and $\alpha > 1$ is unique (on the support of $\mathcal{S}_g \cup \mathcal{S}_t$).*

Proof Without loss of generality, we assume that ϕ is strictly convex. By the strict convexity of ϕ , we have $\forall x, y \in \mathbb{R}$, $\phi(\frac{x+y}{2}) < \frac{1}{2}(\phi(x) + \phi(y))$. Assume f_1 and f_2 are two different minimizers of $\mathfrak{F}(f)$.

First, we have

$$\begin{aligned} k\left(\frac{f_1 + f_2}{2}\right) &= \sup_{x,y} \frac{\frac{f_1(x) + f_2(x)}{2} - \frac{f_1(y) + f_2(y)}{2}}{\|x - y\|} \\ &\leq \sup_{x,y} \frac{1}{2} \frac{|f_1(x) - f_1(y)| + |f_2(x) - f_2(y)|}{\|x - y\|} \\ &\leq \frac{1}{2} \left(\sup_{x,y} \frac{|f_1(x) - f_1(y)|}{\|x - y\|} + \sup_{x,y} \frac{|f_2(x) - f_2(y)|}{\|x - y\|} \right) \\ &= \left(\frac{k(f_1) + k(f_2)}{2} \right). \end{aligned} \tag{44}$$

And given $\rho > 0$ and $\alpha > 1$, we further have

$$\begin{aligned} \frac{\rho}{2}k\left(\frac{f_1 + f_2}{2}\right)^\alpha &\leq \frac{\rho}{2} \left(\frac{k(f_1) + k(f_2)}{2} \right)^\alpha \\ &\leq \frac{\rho}{2} \left(\frac{k(f_1)^\alpha + k(f_2)^\alpha}{2} \right). \end{aligned} \tag{45}$$

Let $\mathfrak{G}(f_1) = \mathfrak{G}(f_2) = \inf \mathfrak{G}(f)$. Then we have

$$\begin{aligned} \mathfrak{G}\left(\frac{f_1 + f_2}{2}\right) &= \mathbb{E}_{x \sim \mathcal{P}_g} \phi\left(\frac{f_1 + f_2}{2}\right) + \mathbb{E}_{y \sim \mathcal{P}_t} \varphi\left(\frac{f_1 + f_2}{2}\right) + \frac{\rho}{2}k\left(\frac{f_1 + f_2}{2}\right)^\alpha \\ &< \mathbb{E}_{x \sim \mathcal{P}_g} \left(\frac{\phi(f_1) + \phi(f_2)}{2} \right) + \mathbb{E}_{y \sim \mathcal{P}_t} \varphi\left(\frac{f_1 + f_2}{2}\right) + \frac{\rho}{2}k\left(\frac{f_1 + f_2}{2}\right)^\alpha \\ &\leq \mathbb{E}_{x \sim \mathcal{P}_g} \left(\frac{\phi(f_1) + \phi(f_2)}{2} \right) + \mathbb{E}_{y \sim \mathcal{P}_t} \left(\frac{\varphi(f_1) + \varphi(f_2)}{2} \right) + \frac{\rho}{2}k\left(\frac{f_1 + f_2}{2}\right)^\alpha \\ &\leq \mathbb{E}_{x \sim \mathcal{P}_g} \left(\frac{\phi(f_1) + \phi(f_2)}{2} \right) + \mathbb{E}_{y \sim \mathcal{P}_t} \left(\frac{\varphi(f_1) + \varphi(f_2)}{2} \right) + \frac{\rho}{2} \left(\frac{k(f_1)^\alpha + k(f_2)^\alpha}{2} \right) \\ &= \frac{1}{2}(\mathfrak{G}(f_1) + \mathfrak{G}(f_2)) = \inf \mathfrak{G}(f) \end{aligned} \tag{46}$$

We get a contradiction $\mathfrak{G}\left(\frac{f_1 + f_2}{2}\right) < \inf \mathfrak{G}(f)$, which implies that the minimizer of $\mathfrak{G}(f)$ is unique. \blacksquare

A.3 Proof of Theorem 3

Let $J_D = \mathbb{E}_{x \sim \mathcal{P}_g}[\phi(f(x))] + \mathbb{E}_{x \sim \mathcal{P}_t}[\varphi(f(x))]$. Let $\mathring{J}_D(x) = \mathcal{P}_g(x)\phi(f(x)) + \mathcal{P}_t(x)\varphi(f(x))$. Clearly, $J_D = \int_{\mathbb{R}^n} \mathring{J}_D(x) dx$. Let $J_D^*(k) = \min_{f \in \mathcal{F}_{\mathbf{k}\text{-Lip}}} J_D = \min_{f \in \mathcal{F}_{1\text{-Lip}}, b} \mathbb{E}_{x \sim \mathcal{P}_g}[\phi(k \cdot f(x) + b)] + \mathbb{E}_{x \sim \mathcal{P}_t}[\varphi(k \cdot f(x) + b)]$.

Let $k(f)$ denote the Lipschitz constant of f . Define $J = J_D + \frac{\rho}{2} \cdot k(f)^2$ and $f^* = \arg \min_f [J_D + \frac{\rho}{2} \cdot k(f)^2]$.

Lemma 16 *It holds $\frac{\partial \dot{J}_D(x)}{\partial f^*(x)} = 0$ for all x , if and only if, $k(f^*) = 0$.*

Proof

(i) If $\frac{\partial \dot{J}_D(x)}{\partial f^*(x)} = 0$ holds for all x , then $k(f^*) = 0$.

For the optimal f^* , it holds that $\frac{\partial J}{\partial k(f^*)} = \frac{\partial J_D^*}{\partial k(f^*)} + 2\frac{\rho}{2} \cdot k(f^*) = 0$.

$\frac{\partial \dot{J}_D(x)}{\partial f^*(x)} = 0$ for all x implies $\frac{\partial J_D^*}{\partial k(f^*)} = 0$. Thus we conclude that $k(f^*) = 0$.

(ii) If $k(f^*) = 0$, then $\frac{\partial \dot{J}_D(x)}{\partial f^*(x)} = 0$ holds for all x .

For the optimal f^* , it holds that $\frac{\partial J}{\partial k(f^*)} = \frac{\partial J_D^*}{\partial k(f^*)} + 2\frac{\rho}{2} \cdot k(f^*) = 0$.

$k(f^*) = 0$ implies $\frac{\partial J_D^*}{\partial k(f^*)} = 0$. $k(f^*) = 0$ also implies $\forall x, y, f^*(x) = f^*(y)$.

Given $\forall x, y, f^*(x) = f^*(y)$, if there exists some point x such that $\frac{\partial \dot{J}_D(x)}{\partial f^*(x)} \neq 0$, then it is obvious that $\frac{\partial J_D^*}{\partial k(f^*)} \neq 0$.

It is contradictory to $\frac{\partial J_D^*}{\partial k(f^*)} = 0$. Thus we have $\forall x, \frac{\partial \dot{J}_D(x)}{\partial f^*(x)} = 0$. ■

Lemma 17 *If $\forall x, y, f^*(x) = f^*(y)$, then $\mathcal{P}_t = \mathcal{P}_g$.*

Proof $\forall x, y, f^*(x) = f^*(y)$ implies $k(f^*) = 0$. According to Lemma 16, for all x it holds $\frac{\partial \dot{J}_D(x)}{\partial f^*(x)} = 0$, i.e., $\mathcal{P}_g(x) \frac{\partial \phi(f^*(x))}{\partial f^*(x)} + \mathcal{P}_t(x) \frac{\partial \varphi(f^*(x))}{\partial f^*(x)} = 0$. Thus, $\frac{\mathcal{P}_g(x)}{\mathcal{P}_t(x)} = -\frac{\frac{\partial \varphi(f^*(x))}{\partial f^*(x)}}{\frac{\partial \phi(f^*(x))}{\partial f^*(x)}}$. That is, $\frac{\mathcal{P}_g(x)}{\mathcal{P}_t(x)}$ has a constant value, which straightforwardly implies $\mathcal{P}_t = \mathcal{P}_g$. ■

Proof [Proof of Theorem 3]

(a): Let k be the Lipschitz constant of f^* . Consider x with $\frac{\partial \dot{J}_D(x)}{\partial f^*(x)} \neq 0$. Define $k(x) = \sup_y \frac{|f(y) - f(x)|}{\|y - x\|}$.

(i) If $\forall \delta$ s.t. $\forall \epsilon$ there exist $z, w \in B(x, \epsilon)$ such that $\frac{|f^*(z) - f^*(w)|}{\|z - w\|} \geq k - \delta$, which means there exists t such that $f'(t) \geq k - \delta$, because $\frac{|f^*(z) - f^*(w)|}{\|z - w\|} = \frac{\int_w^z f^{*\prime}(t) dt}{\|z - w\|}$. Let $\epsilon \rightarrow 0$, we have $t \rightarrow x$. Then $|f''(t)| \rightarrow |f''(x)|$. Let $\delta \rightarrow 0$, we have $(k - \delta) \rightarrow k$. Assume f^* is smooth, we have that $|f'(x)| = k$, which means there exists a y such that $|f^*(y) - f^*(x)| = k\|y - x\|$.

(ii) Assume that $\exists \delta$ s.t. $\exists \epsilon$ and for all $z, w \in B(x, \epsilon)$, $\frac{|f^*(z) - f^*(w)|}{\|z - w\|} < k - \delta$. Consider the following condition, for all δ_2 and $\epsilon_2 \in (0, \epsilon/2)$, $\exists y \in B(x, \epsilon_2)$, such that $k(y) > k - \delta_2$. Then

there exists a sequence of $\{y_n\}_{n=1}^\infty$ s.t. $\lim_{n \rightarrow \infty} \frac{|f(y) - f(y_n)|}{\|y - y_n\|} = k(y)$. Then there exists a y' such that $\frac{|f(y) - f(y')|}{\|y - y'\|} \geq k - \delta_2$. According to the assumption, we have $\|y - y'\| \geq \frac{\epsilon}{2}$. Then $k(x) \geq \frac{|f^*(x) - f^*(y)|}{\|x - y\|} \geq \frac{|f^*(y) - f^*(y')| - |f^*(x) - f^*(y)|}{\|x - y\| + \|y - y'\|} \geq \frac{|f^*(y) - f^*(y')| - k\|x - y\|}{\|x - y\| + \|y - y'\|} \geq (k - \delta_2) \frac{\|y - y'\|}{\|x - y\| + \|y - y'\|} - k \frac{\|x - y\|}{\|x - y\| + \|y - y'\|} \geq (1 - \frac{\epsilon_2}{\epsilon_2 + \|y - y'\|})(k - \delta_2) - k \frac{\epsilon_2}{\|y - y'\|} \geq (1 - \frac{\epsilon_2}{\epsilon_2 + \|y - y'\|})(k - \delta_2) - k \frac{\epsilon_2}{\|y - y'\|}$. Let $\epsilon_2 \rightarrow 0$ and $\delta_2 \rightarrow 0$. We get $k(x) = k$, which means there exists a y such that $|f^*(y) - f^*(x)| = k\|y - x\|$.

(iii) Now we can assume $\exists \delta_2$ s.t. $\exists \epsilon_2$ and for all $y \in B(x, \epsilon_2)$, such that $k(y) \leq k - \delta_2$. If $\frac{\partial \hat{J}_D(x)}{\partial f^*(x)} \neq 0$, without loss of generality, we can assume $\frac{\partial \hat{J}_D(x)}{\partial f^*(x)} > 0$. Then, for all $y \in B(x, \epsilon_2)$, we have $\frac{\partial \hat{J}_D(y)}{\partial f^*(y)} > 0$, as long as ϵ_2 is small enough. Now we change the value of $f^*(y)$ for $y \in B(x, \epsilon_2)$. Let $g(y) = \begin{cases} f^*(y) - \frac{\epsilon_2}{N}(1 - \frac{\|x - y\|}{\epsilon_2}), & y \in B(x, \epsilon_2); \\ f^*(y) & \text{otherwise.} \end{cases}$. Because $\frac{\partial \hat{J}_D(y)}{\partial f^*(y)} > 0$,

$\forall y \in B(x, \epsilon_2)$, when N is sufficiently large, it is not difficult to show $J_D(g) < J_D(f^*)$. We next verify that $\|g\|_{Lip} \leq k$. For any y, z , if $y, z \notin B(x, \epsilon_2)$, then $\frac{|g(y) - g(z)|}{\|y - z\|} = \frac{|f^*(y) - f^*(z)|}{\|y - z\|} < k$. If $y \in B(x, \epsilon_2)$, $z \notin B(x, \epsilon_2)$, then $\frac{|g(y) - g(z)|}{\|y - z\|} \leq \frac{|(f^*(y) - f^*(z)) + \frac{\epsilon_2}{N}(1 - \frac{\|x - y\|}{\epsilon_2})|}{\|y - z\|} \leq \frac{|f^*(y) - f^*(z)|}{\|y - z\|} + \frac{\frac{\epsilon_2}{N}(1 - \frac{\|x - y\|}{\epsilon_2})}{\|y - z\|} = \frac{|(f^*(y) - f^*(z))| + \frac{1}{N}}{\|y - z\|} \leq k(y) + \frac{1}{N} \leq k - \delta_2 + \frac{1}{N} < k$ (when $N \gg \frac{1}{\delta_2}$). If $y, z \in B(x, \epsilon)$, then $\frac{|g(y) - g(z)|}{\|y - z\|} \leq \frac{|f^*(y) - f^*(z)| + |\frac{\epsilon_2}{N}(1 - \frac{\|x - y\|}{\epsilon_2}) - \frac{\epsilon_2}{N}(1 - \frac{\|x - z\|}{\epsilon_2})|}{\|y - z\|} = \frac{|f^*(y) - f^*(z)|}{\|y - z\|} + \frac{\frac{\epsilon_2}{N}(\frac{\|x - y\| - \|x - z\|}{\epsilon_2})}{\|y - z\|} \leq \frac{|f^*(y) - f^*(z)|}{\|y - z\|} + \frac{1}{N} \frac{\|y - z\|}{\|y - z\|} = \frac{|f^*(y) - f^*(z)|}{\|y - z\|} + \frac{1}{N} \leq k - \delta_2 + \frac{1}{N} < k$ (when $N \gg \frac{1}{\delta_2}$). So, we have $\|g\|_{Lip} \leq k$. But we have $J_D(g) < J_D(f^*)$. The contradiction tells us that there must exist a y such that $|f^*(y) - f^*(x)| = k\|y - x\|$.

(b): For $x \in \mathcal{S}_t \cup \mathcal{S}_g - \mathcal{S}_t \cap \mathcal{S}_g$, assuming $\mathcal{P}_g(x) \neq 0$ and $\mathcal{P}_t(x) = 0$, we have $\frac{\partial \hat{J}_D(x)}{\partial f^*(x)} = \mathcal{P}_g(x) \frac{\partial \phi(f^*(x))}{\partial f^*(x)} + \mathcal{P}_t(x) \frac{\partial \varphi(f^*(x))}{\partial f^*(x)} = \mathcal{P}_g(x) \frac{\partial \phi(f^*(x))}{\partial f^*(x)} > 0$, because $\mathcal{P}_g(x) > 0$ and $\frac{\partial \phi(f^*(x))}{\partial f^*(x)} > 0$. Then according to (a), there must exist a y such that $|f^*(y) - f^*(x)| = k(f^*) \cdot \|y - x\|$. The other situation can be proved in the same way.

(c): According to Lemma 17, in the situation that $\mathcal{P}_t \neq \mathcal{P}_g$, for the optimal f^* , there must exist at least one pair of points x and y such that $y \neq x$ and $f^*(x) \neq f^*(y)$. It also implies that $k(f^*) > 0$. Then according to Lemma 16, there exists a point x such that $\frac{\partial \hat{J}_D(x)}{\partial f^*(x)} \neq 0$. According to (a), there exists y with $y \neq x$ satisfying that $|f^*(y) - f^*(x)| = k(f^*) \cdot \|y - x\|$.

(d): In Nash equilibrium state, it holds that, for any $x \in \mathcal{S}_t \cup \mathcal{S}_g$, $\frac{\partial J}{\partial k(f)} = \frac{\partial J_D^*}{\partial k(f)} + 2\frac{\rho}{2} \cdot k(f) = 0$ and $\frac{\partial \hat{J}_D(x)}{\partial f(x)} \frac{\partial f(x)}{\partial x} = 0$. We claim that in the Nash equilibrium state, the Lipschitz constant $k(f)$ must be 0. If $k(f) \neq 0$, according to Lemma 16, there must exist a point \hat{x} such that $\frac{\partial \hat{J}_D(\hat{x})}{\partial f(\hat{x})} \neq 0$. And according to (a), it must hold that $\exists \hat{y}$ fitting $|f(\hat{y}) - f(\hat{x})| = k(f) \cdot \|\hat{x} - \hat{y}\|$.

According to Theorem 5, we have $\left\| \frac{\partial f(\hat{x})}{\partial \hat{x}} \right\| = k(f) \neq 0$. This is contradictory to that $\frac{\partial \hat{J}_D(\hat{x})}{\partial f(\hat{x})} \frac{\partial f(\hat{x})}{\partial \hat{x}} = 0$. Thus $k(f) = 0$. That is, $\forall x \in \mathcal{S}_t \cup \mathcal{S}_g$, $\frac{\partial f(x)}{\partial x} = 0$, which means $\forall x, y, f(x) = f(y)$. According to Lemma 17, $\forall x, y, f(x) = f(y)$ implies $\mathcal{P}_t = \mathcal{P}_g$. Thus $\mathcal{P}_t = \mathcal{P}_g$ is the only Nash equilibrium in our system. \blacksquare

Remark 18 For the Wasserstein distance, $\nabla_{f^*(x)} \hat{J}_D(x) = 0$ if and only if $\mathcal{P}_t(x) = \mathcal{P}_g(x)$. For the Wasserstein distance, penalizing the Lipschitz constant also benefits: at the convergence state, it will hold $\frac{\partial f^*(x)}{\partial x} = 0$ for all x .

A.4 Proof of Theorem 4

Lemma 19 Let k be the Lipschitz constant of f . If $f(a) - f(b) = k\|a - b\|$ and $f(b) - f(c) = k\|b - c\|$, then $f(a) - f(c) = k\|a - c\|$ and $(a, f(a)), (b, f(b)), (c, f(c))$ lies in the same line.

Proof $f(a) - f(c) = f(a) - f(b) + f(b) - f(c) = k\|a - b\| + k\|b - c\| \geq k\|a - c\|$. Because the Lipschitz constant of f is k , we have $f(a) - f(c) \leq k\|a - c\|$. Thus $f(a) - f(c) = k\|a - c\|$. Because the triangle equality holds, we have a, b, c is in the same line. Furthermore, because $f(a) - f(b) = k\|a - b\|$, $f(b) - f(c) = k\|b - c\|$ and $f(a) - f(c) = k\|a - c\|$, we have $(a, f(a)), (b, f(b)), (c, f(c))$ lies in the same line. \blacksquare

Lemma 20 For any x with $\frac{\partial \hat{J}_D(x)}{\partial f^*(x)} > 0$, there exists a y with $\frac{\partial \hat{J}_D(x)}{\partial f^*(x)} < 0$ such that $f^*(y) - f^*(x) = k(f^*)\|y - x\|$.

For any y with $\frac{\partial \hat{J}_D(y)}{\partial f^*(y)} < 0$, there exists a x with $\frac{\partial \hat{J}_D(x)}{\partial f^*(x)} > 0$ such that $f^*(y) - f^*(x) = k(f^*)\|y - x\|$.

Proof Consider x with $\frac{\partial \hat{J}_D(x)}{\partial f^*(x)} > 0$. According to Theorem 3, there exists y such that $|f^*(y) - f^*(x)| = k(f^*)\|y - x\|$. Assume that for every y that holds $|f^*(y) - f^*(x)| = k(f^*)\|y - x\|$, it has $\frac{\partial \hat{J}_D(y)}{\partial f^*(y)} \geq 0$. Consider the set $S(x) = \{y \mid f^*(y) - f^*(x) = k(f^*)\|y - x\|\}$. Note that, according to Lemma 19, any z that holds $f^*(z) - f^*(y) = k(f^*)\|z - y\|$ for any $y \in S(x)$ will also be in $S(x)$. Similar to the proof of (a) in Theorem 3, we can decrease the value of $f^*(y)$ for all $y \in S(x)$ to construct a better f . By contradiction, we have that there must exist a y with $\frac{\partial \hat{J}_D(x)}{\partial f^*(x)} < 0$ such that $|f^*(y) - f^*(x)| = k(f^*)\|y - x\|$. Given the fact $\frac{\partial \hat{J}_D(x)}{\partial f^*(x)} > 0$ and $\frac{\partial \hat{J}_D(x)}{\partial f^*(x)} < 0$, we can conclude that $f^*(y) > f^*(x)$ and $f^*(y) - f^*(x) = k(f^*)\|y - x\|$. Otherwise, if $f^*(x) - f^*(y) = k(f^*)\|y - x\|$, then we can construct a better f by decreasing $f^*(x)$ and increasing $f^*(y)$ which does not break the k -Lipschitz constraint. The other case can be proved similarly. \blacksquare

Lemma 21 For any x , if $\frac{\partial \hat{J}_D(x)}{\partial f(x)} > 0$, then $\mathcal{P}_g(x) > 0$. For any y , if $\frac{\partial \hat{J}_D(y)}{\partial f(y)} < 0$, then $\mathcal{P}_t(y) > 0$.

Proof $\frac{\partial \hat{J}_D(x)}{\partial f(x)} = \mathcal{P}_g(x) \frac{\partial \phi(f(x))}{\partial f(x)} + \mathcal{P}_t(x) \frac{\partial \varphi(f(x))}{\partial f(x)}$. And we know $\phi'(x) > 0$ and $\varphi'(x) < 0$. Naturally, $\frac{\partial \hat{J}_D(x)}{\partial f(x)} > 0$ implies $\mathcal{P}_g(x) > 0$. Similarly, $\frac{\partial \hat{J}_D(y)}{\partial f(y)} < 0$ implies $\mathcal{P}_t(y) > 0$. \blacksquare

Proof [Proof of Theorem 4]

For any $x \in \mathcal{S}_g$, if $\frac{\partial \hat{J}_D(x)}{\partial f^*(x)} > 0$, according to Lemma 20, there exists a y with $\frac{\partial \hat{J}_D(x)}{\partial f^*(x)} < 0$ such that $f^*(y) - f^*(x) = k(f^*)\|y - x\|$. According to Lemma 21, we have $\mathcal{P}_t(y) > 0$. That is, there is a $y \in \mathcal{S}_t$ such that $f^*(y) - f^*(x) = k(f^*)\|y - x\|$. We can prove the other case symmetrically. \blacksquare

Remark 22 $\frac{\partial \hat{J}_D(x)}{\partial f^*(x)} < 0$ for some $x \in \mathcal{S}_g$ means x is at the overlapping region of \mathcal{S}_t and \mathcal{S}_g . It can be regarded as a $y \in \mathcal{S}_t$, and one can apply the other rule which guarantees that there exists an $x' \in \mathcal{S}_g$ that bounds this point.

A.5 Proof of Theorem 5 and the Necessity of Euclidean Distance

In this section, we will prove Theorem 5, i.e., Lipschitz continuity with l_2 -norm (Euclidean Distance) can guarantee that the gradient is directly pointing towards some sample, and at the same time, demonstrate that the other norms do not have this property.

Let (x, y) be such that $y \neq x$, and we define $x_t = x + t \cdot (y - x)$ with $t \in [0, 1]$.

Lemma 23 If $f(x)$ is k -Lipschitz with respect to $\|\cdot\|_p$ and $f(y) - f(x) = k\|y - x\|_p$, then $f(x_t) = f(x) + t \cdot k\|y - x\|_p$

Proof As we know $f(x)$ is k -Lipschitz, with the property of norms, we have

$$\begin{aligned} f(y) - f(x) &= f(y) - f(x_t) + f(x_t) - f(x) \\ &\leq f(y) - f(x_t) + k\|x_t - x\|_p = f(y) - f(x_t) + t \cdot k\|y - x\|_p \\ &\leq k\|y - x_t\|_p + t \cdot k\|y - x\|_p = k \cdot (1-t)\|y - x\|_p + t \cdot k\|y - x\|_p \\ &= k\|y - x\|_p. \end{aligned} \tag{47}$$

$f(y) - f(x) = k\|y - x\|_p$ implies all the inequalities are equalities. Therefore, $f(x_t) = f(x) + t \cdot k\|y - x\|_p$. \blacksquare

Lemma 24 Let v be the unit vector $\frac{y-x}{\|y-x\|_2}$. If $f(x_t) = f(x) + t \cdot k\|y - x\|_2$, then $\frac{\partial f(x_t)}{\partial v}$ equals k .

Proof

$$\begin{aligned} \frac{\partial f(x_t)}{\partial v} &= \lim_{h \rightarrow 0} \frac{f(x_t + hv) - f(x_t)}{h} = \lim_{h \rightarrow 0} \frac{f(x_t + h \frac{y-x}{\|y-x\|_2}) - f(x_t)}{h} \\ &= \lim_{h \rightarrow 0} \frac{f(x_t + \frac{h}{\|y-x\|_2}) - f(x_t)}{h} = \lim_{h \rightarrow 0} \frac{\frac{h}{\|y-x\|_2} \cdot k\|y - x\|_2}{h} = k. \end{aligned}$$

■

Proof [Proof of Theorem 5] Assume $p = 2$. According to (Adler and Lunz, 2018), if $f(x)$ is k -Lipschitz with respect to $\|\cdot\|_2$ and $f(x)$ is differentiable at x_t , then $\|\nabla f(x_t)\|_2 \leq k$. Let v be the unit vector $\frac{y-x}{\|y-x\|_2}$. We have

$$k^2 = k \frac{\partial f(x_t)}{\partial v} = k \langle v, \nabla f(x_t) \rangle = \langle kv, \nabla f(x_t) \rangle \leq \|kv\|_2 \|\nabla f(x_t)\|_2 = k^2. \quad (48)$$

Because the equality holds only when $\nabla f(x_t) = kv = k \frac{y-x}{\|y-x\|_2}$, we have that $\nabla f(x_t) = k \frac{y-x}{\|y-x\|_2}$. ■

Above proof utilizes the property that $\|\nabla f(x_t)\|_2 \leq k$, which is derived from that $f(x)$ is k -Lipschitz with respect to $\|\cdot\|_2$. However, other norms do not satisfy this property. Specifically, according to the theory in (Adler and Lunz, 2018): if a differentiable function f is k -Lipschitz with respect to norm $\|\cdot\|_p$, then the Lipschitz continuity actually implies a bound on the dual norm of gradients, i.e., $\|\nabla f\|_q \leq k$. Here $\|\cdot\|_q$ is the dual norm of $\|\cdot\|_p$, which satisfies $\frac{1}{p} + \frac{1}{q} = 1$. As we could notice, a norm is equal to its dual norm if and only if $p = 2$. Switching to l_p -norm with $p \neq 2$, it is actually bounding the l_q -norm of the gradients. However, bounding the l_q -norm of the gradients does not guarantee the gradient direction at fake samples point towards real samples. A counter-example is provided as follows.

Consider a function $g(x, y) = x + y$ on \mathbb{R}^2 . We have for all $(x_1, y_1), (x_2, y_2)$, there is $g(x_1, y_1) - g(x_2, y_2) = (x_1 - x_2) + (y_1 - y_2) \leq |x_1 - x_2| + |y_1 - y_2| = \|(x_1, y_1) - (x_2, y_2)\|_1$, which means g is a 1-Lipschitz function with respect to l_1 -norm. According to the above, the dual norm of ∇g is bounded, with $\|\nabla g\|_\infty \leq 1$; one could also verify that ∇g is equal to $(1, 1)$ at every point in \mathbb{R}^2 with $\|\nabla g\|_\infty = 1$. However, selecting two points $A = (0, 0)$ and $B = (2, 1)$, we have $g(A) - g(B) = \|A - B\|_1$, but we can notice that $\nabla g(A) = (1, 1)$, which is **not directly** pointing towards B .

Note that different norms will induce different gradients with different properties (Adler and Lunz, 2018). We here expect the gradient directly points towards a real sample.

Appendix B. Experiment Details and More Results

We use multilayer perceptrons (MLPs) for all toy experiments and use a Resnet architecture (He et al., 2016) that is similar to the one used in (Gulrajani et al., 2017) for all other real data (high dimensional, images) experiments. See the code for the detailed architectures.

We use Adam optimizer with $\beta_1 = 0.0$ and $\beta_2 = 0.9$, and the learning rate is 0.0002, which linear decays to zero in 200,000 iterations. We use 5 discriminator updates per generator update. For all experiments that involve regularization and hence have a hyper-parameter ρ , we search the best regularization weight $\frac{\rho}{2}$ in $[0.01, 0.1, 1.0, 10.0]$.

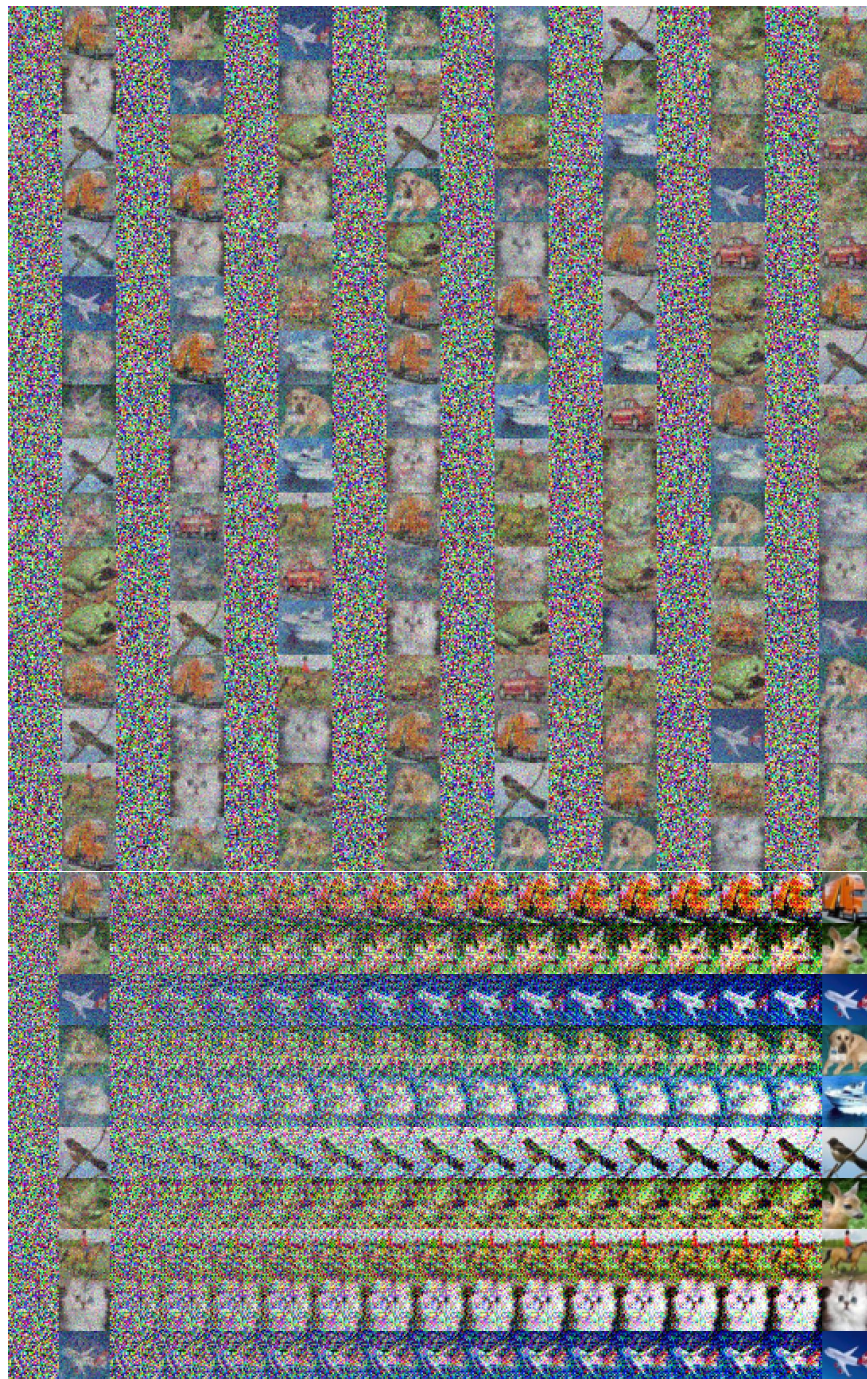


Figure 14: Verifying $\nabla_x f^*(x)$ in LGANs points towards real samples. Here, \mathcal{P}_t consists of ten images and \mathcal{P}_g is Gaussian noise. Up: Each odd column are $x \in \mathcal{S}_g$ and the nearby column are their gradients $\nabla_x f^*(x)$. Down: the leftmost in each row is $x \in \mathcal{S}_g$, the second are their gradients $\nabla_x f^*(x)$, the interiors are $x + \epsilon \cdot \nabla_x f^*(x)$ with increasing ϵ , and the rightmost is the nearest $y \in \mathcal{S}_t$.



Figure 15: Random samples of LGANs with different loss metrics on Oxford 102.



Figure 16: Random samples of LGANs with different loss metrics on CIFAR-10.

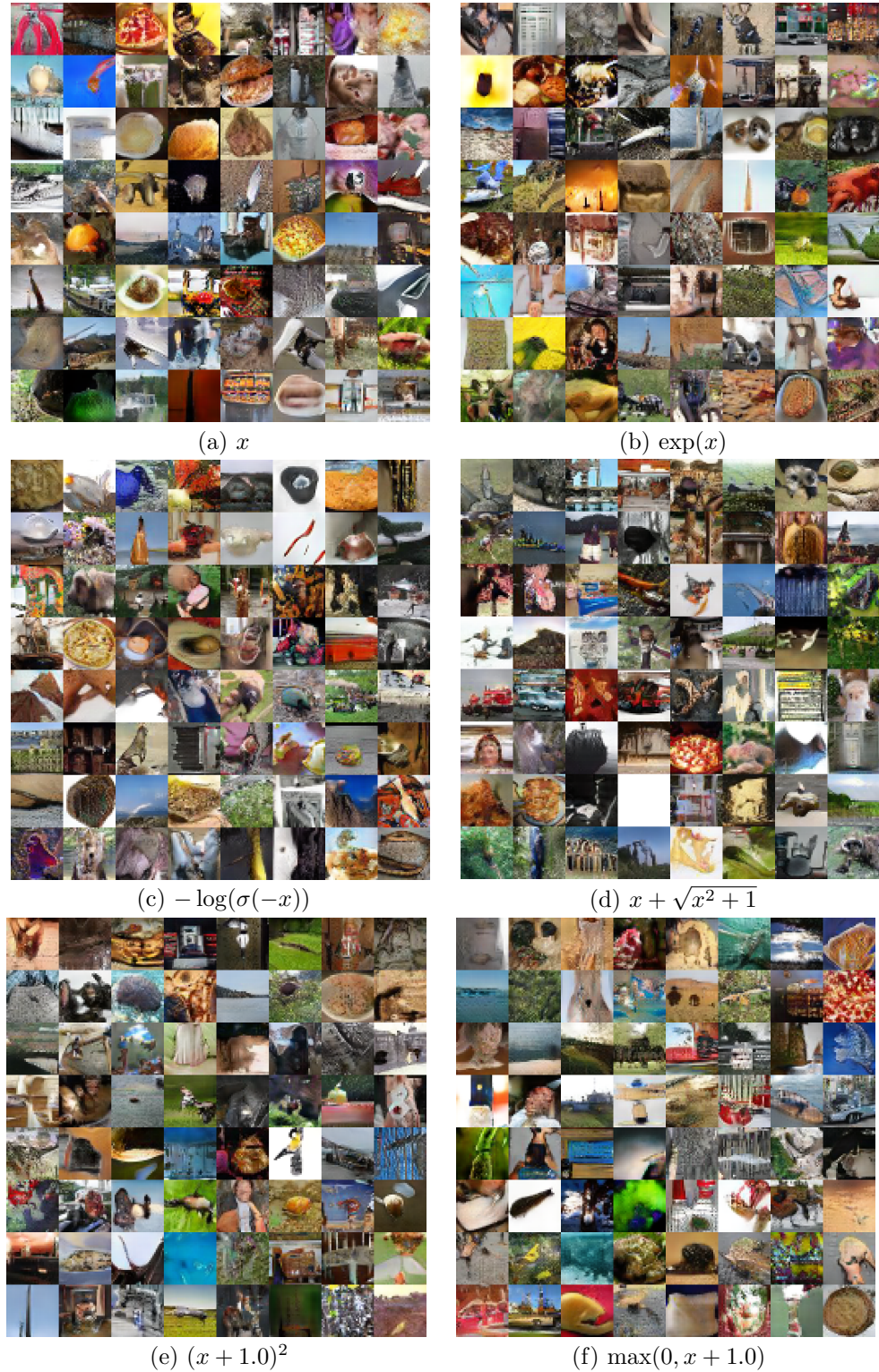


Figure 17: Random samples of LGANs with different loss metrics on Tiny-ImageNet.

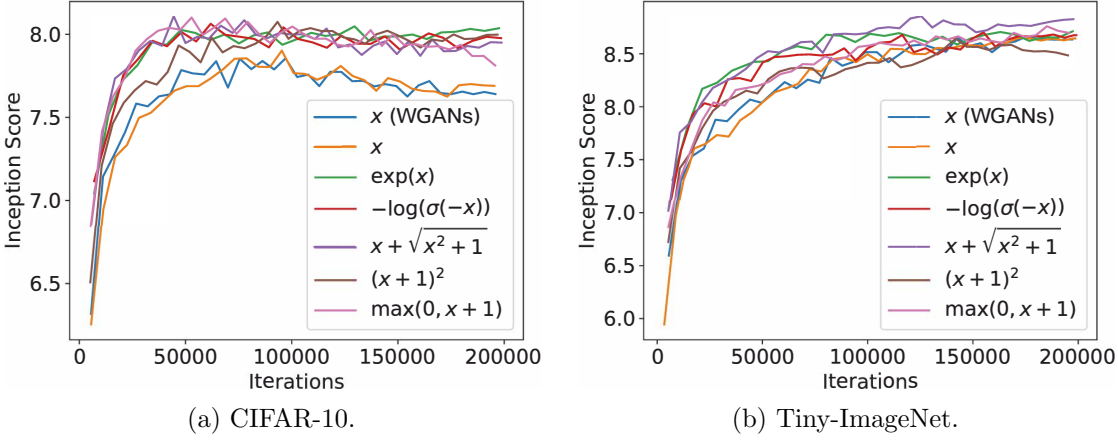


Figure 18: Training curves in terms of IS. WGANs and a set of instances of LGANs.

For all experiments that are aimed for a contrast test, we only change the necessary part(s), saying the objectives or loss metrics or the implementations of Lipschitz regularization, and keep the rest identical or as the same as possible. Please check more details in our codes.

We provide an extra experiment for verifying $\nabla_x f^*(x)$ in LGANs under a more complex setting, where \mathcal{P}_g is a Gaussian distribution, in Figure 14. As an extra experiment, we provide the visual results of LGANs on Oxford 102 in Figure 15. We provide the visual results of LGANs in Figure 16 and Figure 17 for CIFAR-10 and Tiny-ImageNet, respectively. We provide the training curve of LGANs in terms of Inception Score in Figure 18.

References

- Jonas Adler and Sebastian Lunz. Banach Wasserstein GAN. In *Advances in Neural Information Processing Systems (NeurIPS)*, pages 6754–6763, 2018.
- Martin Arjovsky and Léon Bottou. Towards principled methods for training generative adversarial networks. In *International Conference on Learning Representations (ICLR)*, 2017.
- Martin Arjovsky, Soumith Chintala, and Léon Bottou. Wasserstein generative adversarial networks. In *International Conference on Machine Learning (ICML)*, pages 214–223, 2017.
- Sanjeev Arora and Yi Zhang. Do GANs actually learn the distribution? an empirical study. *arXiv preprint arXiv:1706.08224*, 2017.
- Sanjeev Arora, Rong Ge, Yingyu Liang, Tengyu Ma, and Yi Zhang. Generalization and equilibrium in generative adversarial nets. In *International Conference on Machine Learning (ICML)*, pages 224–232, 2017.

- Marc G Bellemare, Ivo Danihelka, Will Dabney, Shakir Mohamed, Balaji Lakshminarayanan, Stephan Hoyer, and Rémi Munos. The Cramer distance as a solution to biased Wasserstein gradients. *arXiv preprint arXiv:1705.10743*, 2017.
- Ali Borji. Pros and cons of GAN evaluation measures. *Computer Vision and Image Understanding (CVIU)*, 179:41–65, 2019.
- Tong Che, Yanran Li, Athul Paul Jacob, Yoshua Bengio, and Wenjie Li. Mode regularized generative adversarial networks. In *International Conference on Learning Representations (ICLR)*, 2017.
- Farzan Farnia and David Tse. A convex duality framework for GANs. In *Advances in Neural Information Processing Systems (NeurIPS)*, pages 5248–5258, 2018.
- William Fedus, Mihaela Rosca, Balaji Lakshminarayanan, Andrew M Dai, Shakir Mohamed, and Ian Goodfellow. Many paths to equilibrium: GANs do not need to decrease a divergence at every step. In *International Conference on Learning Representations (ICLR)*, 2018.
- Ian Goodfellow. Nips 2016 tutorial: Generative adversarial networks. *arXiv preprint arXiv:1701.00160*, 2016.
- Ian Goodfellow, Jean Pouget-Abadie, Mehdi Mirza, Bing Xu, David Warde-Farley, Sherjil Ozair, Aaron Courville, and Yoshua Bengio. Generative adversarial nets. In *Advances in Neural Information Processing Systems (NeurIPS)*, pages 2672–2680, 2014.
- Ishaan Gulrajani, Faruk Ahmed, Martin Arjovsky, Vincent Dumoulin, and Aaron C Courville. Improved training of Wasserstein GANs. In *Advances in Neural Information Processing Systems (NeurIPS)*, pages 5767–5777, 2017.
- Kaiming He, Xiangyu Zhang, Shaoqing Ren, and Jian Sun. Deep residual learning for image recognition. In *IEEE Conference on Computer Vision and Pattern Recognition (CVPR)*, pages 770–778, 2016.
- Martin Heusel, Hubert Ramsauer, Thomas Unterthiner, Bernhard Nessler, and Sepp Hochreiter. GANs trained by a two time-scale update rule converge to a local nash equilibrium. In *Advances in Neural Information Processing Systems (NeurIPS)*, pages 6626–6637, 2017.
- Alexia Jolicoeur Martineau. The relativistic discriminator: a key element missing from standard GAN. In *International Conference on Learning Representations (ICLR)*, 2018.
- Tero Karras, Timo Aila, Samuli Laine, and Jaakko Lehtinen. Progressive growing of GANs for improved quality, stability, and variation. In *International Conference on Learning Representations (ICLR)*, 2018.
- Diederik P Kingma and Jimmy Ba. Adam: A method for stochastic optimization. In *International Conference on Learning Representations (ICLR)*, 2015.
- Günter Klambauer, Thomas Unterthiner, Andreas Mayr, and Sepp Hochreiter. Self-normalizing neural networks. In *Advances in Neural Information Processing Systems (NeurIPS)*, pages 971–980, 2017.

- Naveen Kodali, Jacob Abernethy, James Hays, and Zsolt Kira. On convergence and stability of GANs. *arXiv preprint arXiv:1705.07215*, 2017.
- Chengtao Li, David Alvarez-Melis, Keyulu Xu, Stefanie Jegelka, and Suvrit Sra. Distributional adversarial networks. *arXiv preprint arXiv:1706.09549*, 2017.
- Jae Hyun Lim and Jong Chul Ye. Geometric GAN. *arXiv preprint arXiv:1705.02894*, 2017.
- Shuang Liu, Olivier Bousquet, and Kamalika Chaudhuri. Approximation and convergence properties of generative adversarial learning. In *Advances in Neural Information Processing Systems (NeurIPS)*, pages 5545–5553, 2017.
- Xudong Mao, Qing Li, Haoran Xie, Raymond YK Lau, Zhen Wang, and Stephen Paul Smolley. Least squares generative adversarial networks. In *IEEE International Conference on Computer Vision (ICCV)*, pages 2794–2802, 2017.
- Lars Mescheder, Sebastian Nowozin, and Andreas Geiger. The numerics of GANs. In *Advances in Neural Information Processing Systems (NeurIPS)*, pages 1825–1835, 2017.
- Lars Mescheder, Andreas Geiger, and Sebastian Nowozin. Which training methods for GANs do actually converge? In *International Conference on Machine Learning (ICML)*, pages 3478–3487, 2018.
- Luke Metz, Ben Poole, David Pfau, and Jascha Sohl-Dickstein. Unrolled generative adversarial networks. In *International Conference on Learning Representations (ICLR)*, 2017.
- Paul Milgrom and Ilya Segal. Envelope theorems for arbitrary choice sets. *Econometrica*, 70(2):583–601, 2002.
- Takeru Miyato, Toshiki Kataoka, Masanori Koyama, and Yuichi Yoshida. Spectral normalization for generative adversarial networks. In *International Conference on Learning Representations (ICLR)*, 2018.
- Youssef Mroueh and Tom Sercu. Fisher GAN. In *Advances in Neural Information Processing Systems (NeurIPS)*, pages 2513–2523, 2017.
- Youssef Mroueh, Chun-Liang Li, Tom Sercu, Anant Raj, and Yu Cheng. Sobolev GAN. In *International Conference on Learning Representations (ICLR)*, 2018.
- Augustus Odena, Christopher Olah, and Jonathon Shlens. Conditional image synthesis with auxiliary classifier GANs. In *International Conference on Machine Learning (ICML)*, pages 2642–2651, 2017.
- Augustus Odena, Jacob Buckman, Catherine Olsson, Tom Brown, Christopher Olah, Colin Raffel, and Ian Goodfellow. Is generator conditioning causally related to GAN performance? In *International Conference on Machine Learning (ICML)*, pages 3849–3858, 2018.
- Henning Petzka, Asja Fischer, and Denis Lukovnikov. On the regularization of Wasserstein GANs. In *International Conference on Learning Representations (ICLR)*, 2018.

- Guo-Jun Qi. Loss-sensitive generative adversarial networks on Lipschitz densities. *International Journal of Computer Vision (IJCV)*, 128(5):1118–1140, 2020.
- Prajit Ramachandran, Barret Zoph, and Quoc V Le. Searching for activation functions. In *International Conference on Learning Representations (ICLR)*, 2018.
- Sashank J Reddi, Satyen Kale, and Sanjiv Kumar. On the convergence of adam and beyond. In *International Conference on Learning Representations (ICLR)*, 2018.
- Tim Salimans, Ian Goodfellow, Wojciech Zaremba, Vicki Cheung, Alec Radford, and Xi Chen. Improved techniques for training GANs. In *Advances in Neural Information Processing Systems (NeurIPS)*, pages 2234–2242, 2016.
- Maziar Sanjabi, Jimmy Ba, Meisam Razaviyayn, and Jason D Lee. On the convergence and robustness of training GANs with regularized optimal transport. In *Advances in Neural Information Processing Systems (NeurIPS)*, pages 7091–7101, 2018.
- Vivien Seguy, Bharath Bhushan Damodaran, Remi Flamary, Nicolas Courty, Antoine Rolet, and Mathieu Blondel. Large scale optimal transport and mapping estimation. In *International Conference on Learning Representations (ICLR)*, 2018.
- Thomas Unterthiner, Bernhard Nessler, Calvin Seward, Günter Klambauer, Martin Heusel, Hubert Ramsauer, and Sepp Hochreiter. Coulomb GANs: Provably optimal nash equilibria via potential fields. In *International Conference on Learning Representations (ICLR)*, 2018.
- Cédric Villani. *Optimal transport: old and new*, volume 338. Springer Science & Business Media, 2008.
- Yuichi Yoshida and Takeru Miyato. Spectral norm regularization for improving the generalizability of deep learning. *arXiv preprint arXiv:1705.10941*, 2017.
- Han Zhang, Ian Goodfellow, Dimitris Metaxas, and Augustus Odena. Self-attention generative adversarial networks. In *International Conference on Machine Learning (ICML)*, pages 7354–7363. PMLR, 2019.
- Pengchuan Zhang, Qiang Liu, Dengyong Zhou, Tao Xu, and Xiaodong He. On the discrimination-generalization tradeoff in GANs. In *International Conference on Learning Representations (ICLR)*, 2018.
- Junbo Zhao, Michael Mathieu, and Yann LeCun. Energy-based generative adversarial network. In *International Conference on Learning Representations (ICLR)*, 2017.
- Zhiming Zhou, Han Cai, Shu Rong, Yuxuan Song, Kan Ren, Weinan Zhang, Jun Wang, and Yong Yu. Activation maximization generative adversarial nets. In *International Conference on Learning Representations (ICLR)*, 2018.
- Zhiming Zhou, Jiadong Liang, Yuxuan Song, Lantao Yu, Hongwei Wang, Weinan Zhang, Yong Yu, and Zhihua Zhang. Lipschitz generative adversarial nets. In *International Conference on Machine Learning (ICML)*, pages 7584–7593, 2019a.

Zhiming Zhou, Qingru Zhang, Guansong Lu, Hongwei Wang, Weinan Zhang, and Yong Yu. Adashift: Decorrelation and convergence of adaptive learning rate methods. In *International Conference on Learning Representations (ICLR)*, 2019b.

Fangyu Zou, Li Shen, Zequn Jie, Weizhong Zhang, and Wei Liu. A sufficient condition for convergences of adam and rmsprop. In *IEEE Conference on Computer Vision and Pattern Recognition (CVPR)*, pages 11127–11135, 2019.